# APPLICATION OF DENSITY MATRIX THEORY TO DYNAMICAL PROBLEMS IN THE NUCLEAR MAGNETIC RESONANCE OF $I > 1/2$ SPIN SYSTEMS DISPLAYING ORIENTATIONAL ANISOTROPY

short title: Theoretical NMR of Anisotropic I > 1/2 Spin Systems

by

Timothy R.J. Dinesen
Department of Chemistry
McGill University
Montréal, CANADA

National Library
of Canada

Acquisitions and
Bibliographic Services Branch

395 Wellington Street
Ottawa, Ontario
K1A 0N4

Bibliothèque nationale
du Canada

Direction des acquisitions et
des services bibliographiques

395, rue Wellington
Ottawa (Ontario)
K1A 0N4

*Your file Votre référence*

*Our file Notre référence*

ISBN 0-612-19719-0

# ABSTRACT

Density matrix theory is used to arrive at theoretical representations of pulsed Nuclear Magnetic Resonance experiments performed on two diverse systems, both giving evidence of orientational anisotropy. The first case examines the Multiple Quantum Filtered line shape of $^{23}$Na ($I$=3/2), as recently observed in some biological tissues. Relaxation is accounted for by use of Redfield theory, and the production of a second rank tensor contribution to the line shape is shown to be directly attributable to the presence of a non-vanishing electric quadrupole coupling constant. The derived equations of motion for $I$=3/2 can be applied to a general pulse sequence and a specific solution to the Double Quantum Filtered experiment is discussed. The second case seeks to account for the response signal of both $o$-$D_2$ (with rotational angular momentum $J$=0 and nuclear spin $I$=2) and $p$-$D_2$ (with $J$=1 and $I$=1) in NMR experiments consisting of two-pulse sequences. The predicted solid echo amplitude for both the $I$=1 and $I$=2 contributions is expressed as a function of the mole fraction, the pulse parameters, the time between the two pulses, the average spin-pair dipolar field and the average inhomogeneous field. The properties of solid hydrogen are discussed within the context of the two pulse solid echo experiment. For the $I$=2 fraction, the positions of the expected satellite echoes are determined, while failure to observe them in solid $D_2$ is discussed in terms of the relative magnitudes of the intramolecular coupling terms and the inhomogeneous field.

# RÉSUMÉ

La théorie de la matrice de densité est utilisée pour obtenir une representation théoretique de la Resonance Magnétique Nucléaire (RMN) effectuée sur deux systemes differents, les deux menant à dencé de l'"anisotropy orientational". Le premier cas examine la "Multiple Quantum Filtered" (MQF) ligne en forme de $^{23}$Na ($I$=3/2) tel qu'observé recemment dans certains tissus biologiques. On peut remenquer la relaxation en utilisant la théorie de Redfield. La production de la contribution d'un tenseur de deuxième ranq à la forme de la ligne est demontée être directment attributable à la presence d'une constante de copulation quadrupole electrique qui ne disparant pas. Les equations des mouvements dèrivées pour $I$=3/2 peuvent être appliquées a une sequence general de pouls et une solution specifiques pour l'expérience DQF est discutée. Le deuxiéme cas recherche le signal réponse de $o$-$D_2$ (avec impulsion angulaire rotationalle $J$=0 et le spin angulaire $I$=2) et $p$-$D_2$ (avec $J$=1 et $I$=1) dans les expériences RMN consistant dans une sequence à deux pouls. L'amplitude prevue de l'echo solide pur les contributions de $I$=1 et $I$=2 est exprimée par une fraction molaire, les parametres du pouls, l'intervalle entre les deux pouls, le champs moyen dipolaire de la pair de spin et le champs non-homogéne magnétique. Les propriétés de l'hydrogene solide sont discutées dans le contexte de l'expérience de l'echo solide. Pour la fraction $I$=2, les positions prevues pour les echos satellites sont déterminées ainsi que l'impossibilté de les observer en $D_2$ solide est discuteés en termes des granduers relative des constantes de copulation intramoléculaire et du champs non-homogéne magnétique.

# ACKNOWLEDGEMENT

This thesis would not have been written without the support and guidance of Professor B.C. Sanctuary.

Many thanks are also due Professor Horst Meyer of Duke University for the tireless collaborative efforts put forth in the solid $D_2$ work. The helpful discussions and experimental results provided by Dr. Joe Tauskela are also gratefully acknowledged.

Past and present members of the "Multipole Think Tank" have provided less tangible, though no less significant support.

The generous financial support of the Natural Sciences and Engineering Research Council (NSERC), McGill University and the Walter Sumner Foundation is also recognized.

# TABLE OF CONTENTS

PART 1

**PART 2**

**PART 3**

# LIST OF FIGURES

# LIST OF TABLES

# GENERAL INTRODUCTION

In the realm of chemical spectroscopy, modern Nuclear Magnetic Resonance is without equal. Arguably, the most significant technical advance in this field has been the introduction of Fourier transform methods. Traditional continuous wave techniques have been supplanted by the use of tuned radio frequency pulses, thus permitting the development of a plethora of experiments, each designed to probe the microscopic dynamics of nuclear spins and to enhance understanding of molecular structure. With the advent of superconductor magnet technology and fast data archival systems came such a high degree of spectroscopic resolution that the imagination of the experimentalist became the most obvious limitation.

Part of the continuing appeal of NMR is due to its adaptability, allowing a wide range of studies on diverse samples. Due to the fact that the energy separation between the non-degenerate angular momentum states is small relative to thermal background, the various interactions between spin bearing nuclei can be resolved. Some theoretical understanding of the physical properties of the system permits direct relation of the resonant line shapes and amplitudes to such phenomena as chemical exchange, molecular dynamics, crystal and molecular structure through interpretation of the various correlation times and relaxation rates. A thoughtfully designed NMR experiment can be an invaluable attribute to a greater research regimen.

Recent burgeoning experimental applications have provided a wealth of information on physical, chemical and biological systems and, at once, have betrayed the lack of comprehensive theoretical developments that can adequately explain these results. This difficulty is exacerbated for studies on nuclei of $I > 1/2$. Recognizing the potential value in studying nuclei other than the proton, investigators have given increasing attention to this class of nuclei. The familiar vector model used for the visualization of nuclear magnetization of $I = 1/2$ nuclei does not provide an adequate description of the dynamics of these higher spin magnitudes, as the number of quantum mechanical states required to span a spin space scale as $2I+1$. Such nuclei also bear nuclear electric quadrupole moments that couple to electric field gradients around the nucleus, inducing rapid relaxation and the requisite line broadening. On one hand, these nuclei provide unique probes into the dynamics and physical environs of both ions in solution and molecules in a rigid lattice. On the other hand, it can be a formidable task to extract physically meaningful information from the higher dimensional theoretical space in which nuclear dynamics are cast and relate it to an experimental line shape, especially one that is broad and featureless. This thesis was written as a partial address to these considerations.

Of the wide variety of theoretical approaches to NMR experiments, a true distinction can be made between those that seek to describe structure and those describing dynamics. One field of rapid development concerns itself with the structural elucidation of macromolecules. The general philosophy of this pursuit is to treat the vast number of correlations between all spin bearing nuclei in the macromolecule ( generally only H and $^{13}C$ ) as one body of information. Clever combinatorial algorithms are then applied in the hope of finding a molecular structure that is consistent with the information content of the experiments. In contrast, a careful account of the dynamics of the individual spins requires some knowledge of the physical environment which inevitably form the coherence pathways through which energy is transferred. For these purposes, it is convenient to envisage a statistical mixture of nuclear spins which require consideration of all possible multiquantum coherences amongst all possible nuclear spin levels, to mathematically treat this statistical mixture as a spin density operator and subsequently account for the dynamical evolution of the density operator by solving the quantum Liouville equation of motion.

Described in this thesis are theoretical treatments of two regimes of experimental NMR, presented in the framework of density matrix theory. The physical and practical differences between the two sets of experiments will be obvious, but it is the strength of density matrix theory that will allow discussion of all relevant experimental results within the context of one theoretical construct. While the theoretical formulations were conceived with the experimental results in mind, new theoretical results were obtained that will allow simulation of more general NMR experiments. PART 1 of this thesis gives a short review of those theoretical aspects of angular momentum, spherical tensors and density operators required to pursue a theoretical treatment of the experiments described herein.

In PART 2, the relaxation of an $I = 3/2$ spin system in an anisotropic environment characterized by a finite residual quadrupolar splitting, $\omega_q$, is modeled by analytically solving for the density operator from Redfield's relaxation theory. The resulting equations are cast into the multipole basis in order to describe the tensorial components of the spin density matrix. Included in the relaxation matrix are off-diagonal elements, $J_1$ and $J_2$, which accounts for anisotropic systems with $\omega_q$ values less than the width of the resonant line. With the Wigner rotation matrices simulating hard pulses, the response to an arbitrary pulse sequence can be determined. An analytical expression for the response to the double quantum filtered (DQF) pulse sequence $\pi/2 - \tau/2 - \pi - \tau/2 - \theta - \delta - \theta - AQ$ for $6 = \pi/2$ is presented, explicitly showing the formation of a second rank tensor owing only to the presence of a finite $\omega_q$. This second rank tensor displays asymptotic behavior when the (reduced) quadrupole splitting is equal to either of the off-diagonal spectral densities $J_2$ and $J_1$. Line shape simulations for $\omega_q$ values of less than a line width reproduce the general features of some recently reported $^{23}$Na DQF line shapes from biological systems. Distinct relaxation dynamics govern each of the tensorial components of the resonant signal revealing the influence of the experimental variables on the line shape.

In PART 3, density matrix theory is used to calculate the response signal of both $o$-$D_2$ (with rotational angular momentum $J=0$ and nuclear spin $I=2$) and $p$-$D_2$ (with $J=1$ and $I=1$) in NMR experiments consisting of two-pulse sequences. The closed form method previously applied to the NMR "solid echo" of $o$-$H_2$ (with $J=1$ and $I=1$) has been extended to the deuterium system arriving at a detailed account of the dipolar interactions between like and unlike spins in a hcp lattice of concentration $X(J=1)$. The predicted solid echo amplitude for both the $I=1$ and $I=2$ contributions is expressed as a function of the mole fraction $X$, the pulse parameters (the angle $\beta$ and relative phase $\varphi$), the time $\tau$ between the two pulses, the average spin-pair dipolar field $\overline{\delta_{jk}}$ and the average inhomogeneous field $\overline{\alpha_j}$. Agreement is good between the theoretical predictions and the experiments in which the solid echo amplitude is recorded as a function of the experimentally controllable parameters $\beta$, $\varphi$ and $\tau$. For the $I=2$ fraction, the positions of the expected satellite echoes are determined, while failure to observe them in solid $D_2$ is discussed in terms of the relative magnitudes of the intramolecular coupling terms and $\overline{\alpha_j}$.

# PART 1

# GENERAL THEORY

## Chapter 1. ANGULAR MOMENTUM AND SPIN

### *Angular Momentum Operators and Single Spin Basis States*

Consider a single isolated particle described by the three Cartesian co-ordinates $x$, $y$, and $z$ and their conjugate momenta $p_x$, $p_y$ and $p_z$. The associated classical angular momentum about some origin is defined by the vector equation

$$\boldsymbol{L} = \boldsymbol{r} \times \boldsymbol{p} \qquad [1.1.1]$$

where $\boldsymbol{r}$ is the vector from the origin to the particle and $\boldsymbol{p}$ is its momentum. The corresponding quantum mechanical operator is formed by replacing the classical momentum by its operator representation $-i\hbar\nabla$, forming from [1.1.1]

$$\boldsymbol{L} = -i\hbar(\boldsymbol{r} \times \nabla) \qquad [1.1.2].$$

Assignment of the relevant quantum numbers is not arbitrary, rather it follows as a natural consequence of the system. Considering only integral values of the angular momentum, one method for deriving the quantum numbers is to solve the equation of motion given by the time dependent Schrödinger equation

$$\mathcal{H}(t)\Psi = E\Psi = i\hbar\frac{\partial \Psi}{\partial t} \qquad [1.1.3],$$

where $\mathcal{H}(t)$ is the Hamiltonian or total energy operator of the particle, for the wavefunctions describing the three-dimensional rigid rotator. Introducing the square of the angular momentum *(1)*

$$L^2 = L_x^2 + L_y^2 + L_z^2 = -\hbar^2\left[\frac{1}{\sin\theta}\frac{\partial}{\partial\theta}\left(\sin\theta\frac{\partial}{\partial\theta}\right)+\frac{1}{\sin^2\theta}\frac{\partial^2}{\partial\phi^2}\right] \qquad [1.1.4]$$

leads to an explicit representation of the angular momentum algebra. Assuming that an eigenvalue equation of the form [1.1.3] is to be solved i.e.

$$L^2\Psi = \hbar^2(l')^2\Psi \qquad [1.1.5]$$

suggests that $\Psi$ is separable into its angular components

$$\Psi(\theta,\phi) = \Theta(\theta)\Phi(\phi) \qquad [1.1.6]$$

such that

$$\frac{1}{\Phi(\phi)}\frac{\partial^2\Phi(\phi)}{\partial\phi^2} = -m^2 \qquad [1.1.7]$$

yields Legendre's equation, with $x = \cos\theta$ and $\Theta(\theta) \equiv P(x)$

$$\left(1-x^2\right)\frac{d^2P(x)}{dx^2} - 2x\frac{dP(x)}{dx} + \left[(l')^2 - \frac{m^2}{1-x^2}\right]P(x) = 0 \qquad [1.1.8].$$

Boundary conditions and convergence require that $(l')^2 = l(l+1)$, $-l \le m \le l$ and that both $l$ and $m$ are integers. Of course, the eigenfunctions of $L^2$ are the spherical harmonics *(2)*

$$Y_{lm}(\theta,\phi) = \sqrt{\frac{2l+1}{4\pi}\frac{(l-m)!}{(l+m)!}}\frac{(-1)^m}{2^l l!}\left(1-x^2\right)^{m/2}\frac{\partial^{l+m}}{\partial x^{l+m}}\left(x^2-1\right)^l e^{im\phi} \qquad [1.1.9]$$

and are thus representations of the abstract Dirac quantum state $|lm\rangle$ *(3)*

$$Y_{lm}(\theta,\phi) = \langle\theta\phi|lm\rangle \qquad [1.1.10].$$

Given the differential forms of $L_z$ and the shift operators

$$L_z = -i\hbar\frac{\partial}{\partial\phi} \qquad [1.1.11]$$

$$L_\pm = L_x \pm iL_y = \hbar e^{\pm i\phi}\left[\pm\frac{\partial}{\partial\theta} + i\cot\frac{\partial}{\partial\phi}\right] \qquad [1.1.12]$$

leads to the explicit representation of the angular momentum algebra in the $Y_{lm}(\theta,\phi)$ basis

$$L_{\pm}Y_{lm}(\theta,\phi) = \hbar\sqrt{l(l+1) - m(m\pm 1)}\,Y_{lm}(\theta,\phi)$$
$$L_z Y_{lm}(\theta,\phi) = \hbar m Y_{lm}(\theta,\phi) \qquad [1.1.13]$$

with orthonormalization

$$\int_0^{2\pi}\int_0^{\pi} Y^*_{lm}(\theta,\phi)Y_{l'm'}(\theta,\phi)\sin\theta\, d\theta\, d\phi = \delta_{ll'}\delta_{mm'} \qquad [1.1.14].$$

This arbitrary selection of $L_z$ as an eigenoperator means that $L_x$ and $L_y$ are not, by virtue of the uncertainty relation, signifying the non-commutativity of the components of the angular momentum.

Though consistent, this procedure for obtaining angular momentum quantum numbers is not completely satisfactory as it negates the possibility of half-integer values of $l$. That is to say, functions of the type $Y_{\frac{1}{2}m}(\theta,\phi)$ are not single valued and the eigenvalue conditions in [1.1.13] are not followed. While it may be sufficient to discard half-integer values of $l$ as regards the description of the quantum rigid rotator, no such argument may be made for the case of intrinsic spin $\boldsymbol{I}$, since the existence of a wavefunction (that is, a function of the co-ordinates in the position representation) is not required *a priori*.

Spin angular momentum operators $\boldsymbol{I}$ do not have representations as differential operators, rather they follow the more fundamental commutation relations given equivalently by

$$\boldsymbol{I}\times\boldsymbol{I} = i\hbar\boldsymbol{I}$$

or

$$\left[I_x, I_y\right] = i\hbar I_z \text{ (and cyclic permutations)} \qquad [1.1.15]$$

which determine all properties of angular momentum, including operators not defined by [1.1.2].

Considering, then, the spin angular momentum, it is convenient to re-define the shift operators

$$I_{\pm} = I_x \pm iI_y \qquad [1.1.16]$$

and the square of the total spin angular momentum

$$I^2 = I \cdot I = I_x^2 + I_y^2 + I_z^2 = \left(I_+I_- + I_-I_+\right)/2 + I_z^2 \qquad [1.1.17]$$

which commutes with all components $I_x$, $I_y$ and $I_z$. A set of basis states for the representation of these operators may be chosen as the normalized simultaneous eigenvectors, $|IM\rangle$, of $I^2$ and one of the Cartesian components (again, $I_z$ is conventionally and arbitrarily selected). Following the notation of Dirac *(3)*, the ket vector $|\gamma IM\rangle$ is labeled by the quantum numbers $I$ and $M$, related to the eigenvalues of $I^2$ and $I_z$ by

$$\begin{gathered} I_z|\gamma IM\rangle = \hbar M|\gamma IM\rangle \\ I^2|\gamma IM\rangle = \hbar^2 I(I+1)|\gamma IM\rangle \end{gathered} \qquad [1.1.18]$$

and the set of all other spin independent quantum numbers, $\gamma$ , needed to fully specify the state (neglected hereafter). The intrinsic spin is labeled such that $I$ = 1/2, 1, 3/2,... and it follows from [1.1.18] and [1.1.15] that for any fixed value of $I$ there exist $2I$+1 possible values of $M$, namely $M = -I, -I+1, \ldots, 0, I-1, I$.

The complete set of ket or state vectors $|II\rangle, \ldots, |I-I\rangle$ can be understood to span an abstract vector space. A dual vector space is defined by the dual bra vectors $\langle IM|$ standing in one to one correspondence with the associated ket vectors. Together these follow the orthonormality relation

$$\langle I'M'|IM\rangle = \delta_{I'I}\delta_{M'M} \qquad [1.1.19a]$$

and closure

$$\sum_M |IM\rangle\langle IM| = 1 \qquad [1.1.19b]$$

forming a complete basis for a (2*I*+1) dimensional Hilbert space. There also exists a set of projection operators such that for any vector in this space, $|\beta\rangle$, associated with some other property of the system

$$|\beta\rangle = \sum_M |IM\rangle\langle IM|\beta\rangle = \sum_M b_M |IM\rangle \qquad [1.1.20]$$

where the components $b_M$ of this vector are complex numbers. Eigenvalues of $I_\pm$ can be determined with the definition of the scalar product [1.1.19]

$$I_\pm|IM\rangle = \hbar\exp(\pm i\varphi)\sqrt{I(I+1)-M(M\pm1)}|IM\pm1\rangle \qquad [1.1.21]$$

where $\varphi$ is some arbitrary phase. The widely accepted convention of Condon and Shortley *(4)* is used to fix $\varphi = 0$ and define the relative phases of the states $|IM\rangle$ of different $M$

$$|I-M\rangle = (-1)^M|IM\rangle^* \qquad [1.1.22]$$

where the asterisk indicates the complex conjugate.

### *Multispin Basis States*

In classical mechanics the addition of dynamically independent angular momenta is carried out according to the laws of vector addition. Addition of quantum mechanical angular momenta is considerably more involved. Consider two spins defined by independent angular momentum operators $I_1$ and $I_2$. As always, the commutation relations for each $I_i$ are [1.1.15] and it is left to construct the eigenkets and determine the corresponding eigenvalues of the total angular momentum

$$\boldsymbol{I} = \boldsymbol{I}_1 + \boldsymbol{I}_2 \qquad [1.1.23]$$

for fixed values of $I_1$ and $I_2$. One component of $\boldsymbol{I}$ can be specified simultaneously with $I^2$ and because $I_1^2$ and $I_2^2$ are scalars, they also commute with $I^2$. However, since $[I^2, I_{1z}] = 2[I_1 \cdot I_2, I_{1z}] \neq 0$, and $[I^2, I_{2z}] \neq 0$, $I_{1z}$ and $I_{2z}$ cannot be specified simultaneously with the square of the total angular momentum operator. What results is two complete sets of compatible angular momentum observables: the already described set associated with the product of the individual angular momenta $\left\{I_1^2, I_{1z}, I_2^2, I_{2z}\right\}$ and the coupled set $\left\{I^2, I_z, I_1^2, I_2^2\right\}$ yet to be determined. ( It isn't possible to completely describe any system in terms of the angular momentum variables alone. In this development it is convenient to ignore these further observables owing to the Hamiltonian as they are expected to commute with the angular momentum operators. Hence, all other quantum numbers required to specify the kets are ignored since they do not change throughout this derivation.) The former set satisfy ($i$ = 1 or 2)

$$\hbar^2\left(I_i^2 - I_i\left(I_i+1\right)\right)\left|I_1M_1I_2M_2\right\rangle = 0$$
$$\hbar\left(I_{1z} - M_i\right)\left|I_1M_1I_2M_2\right\rangle = 0 \qquad [1.1.24]$$

as expected from [1.1.18]. The eigenkets of the latter set are defined by

$$\hbar^2\left(I^2 - I(I+1)\right)\left|I_1I_2IM\right\rangle = 0$$
$$\hbar\left(I_z - M\right)\left|I_1I_2IM\right\rangle = 0$$
$$\hbar^2\left(I_i^2 - I_i\left(I_i+1\right)\right)\left|I_1I_2IM\right\rangle = 0 \qquad [1.1.25]$$

and the orthonormality condition

$$\left\langle I_1'I_2'I'M'\middle|I_1I_2IM\right\rangle = \delta_{II'}\delta_{MM'}\delta_{I_1I_1'}\delta_{I_2I_2'} \qquad [1.1.26]$$

An orthogonal $\left(2I_1+1\right)\left(2I_2+1\right)$-dimensional subspace of the Hilbert space for the composite spin is formed from the discrete product $\left|I_1M_1\right\rangle\otimes\left|I_2M_2\right\rangle \equiv \left|I_1M_1I_2M_2\right\rangle \equiv \left|I_1M_1\right\rangle\left|I_2M_2\right\rangle$. Spanning each subspace are the kets $\left|I_1M_1I_2M_2\right\rangle$ following the closure

$$\sum_{M_1M_2}\left|I_1M_1I_2M_2\right\rangle\left\langle I_1M_1I_2M_2\right| = 1 \qquad [1.1.27]$$

and these undetermined kets may then be written in terms of the known kets

$$\left|I_1I_2IM\right\rangle = \sum_{M_1M_2}\left\langle I_1M_1I_2M_2\middle|I_1I_2IM\right\rangle\left|I_1M_1I_2M_2\right\rangle \qquad [1.1.28]$$

The unitary transformation is determined by the real valued Clebsch-Gordan (C-G) coefficient, *(6)* related to the Wigner 3-$j$ symbol through *(5)*

$$\langle I_1M_1I_2M_2|I_1I_2IM\rangle = (-1)^{I_1-I_2+I}(-1)^{I-M}\sqrt{2I+1}\begin{pmatrix} I_1 & I_2 & I \\ M_1 & M_2 & -M \end{pmatrix} \quad [1.1.29].$$

The completeness relations [1.1.26] and [1.1.27] then imply

$$\sum_{IM}(2I+1)\begin{pmatrix} I_1 & I_2 & I \\ M_1 & M_2 & M \end{pmatrix}\begin{pmatrix} I_1 & I_2 & I \\ M_1' & M_2' & M \end{pmatrix} = \delta_{M_1M_1'}\delta_{M_2M_2'}$$

$$\sum_{M_1M_2}\begin{pmatrix} I_1 & I_2 & I \\ M_1 & M_2 & M \end{pmatrix}\begin{pmatrix} I_1 & I_2 & I' \\ M_1 & M_2 & M' \end{pmatrix} = (2I+1)^{-1}\delta_{II'}\delta_{MM'} \quad [1.1.30].$$

The 3-*j* symbol vanishes unless the triangle inequality $I_1 + I_2 \geq I \geq |I_1 - I_2|$ and conservation of angular momentum $M = M_1 + M_2$ are satisfied. There is, therefore, only one state for each value of $I$ and $M$ verified by the fact that the dimensionality of the state sub-space has been preserved

$$\sum_{I=|I_1-I_2|}^{I_1+I_2}(2I+1) = (2I_1+1)(2I_2+1) \quad [1.1.31].$$

Some symmetry properties of the 3-*j* coefficient will be of future use: they are symmetric under a cyclic permutation of the columns

$$\begin{pmatrix} I_1 & I_2 & I_3 \\ M_1 & M_2 & M_3 \end{pmatrix} = \begin{pmatrix} I_3 & I_1 & I_2 \\ M_3 & M_1 & M_2 \end{pmatrix} = \begin{pmatrix} I_2 & I_3 & I_1 \\ M_2 & M_3 & M_1 \end{pmatrix} \quad [1.1.32a],$$

non-cyclic permutations are multiplied by a phase

$$\begin{pmatrix} I_1 & I_2 & I_3 \\ M_1 & M_2 & M_3 \end{pmatrix} = (-1)^{I_1+I_2+I_3}\begin{pmatrix} I_2 & I_1 & I_3 \\ M_2 & M_1 & M_3 \end{pmatrix} \quad [1.1.32b],$$

similarly if all magnetic quantum numbers are inverted

$$\begin{pmatrix} I_1 & I_2 & I_3 \\ -M_1 & -M_2 & -M_3 \end{pmatrix} = (-1)^{I_1+I_2+I_3}\begin{pmatrix} I_1 & I_2 & I_3 \\ M_1 & M_2 & M_3 \end{pmatrix} \quad [1.1.32c].$$

When the coupling of three or more product eigenstates to give a resultant state defined by a total angular momentum must be considered, a further difficulty arises from the fact that there is no unique representation of such higher direct products *(7)* i.e. of

$|I_1M_1\rangle \otimes |I_2M_2\rangle \otimes \ldots \otimes |I_nM_n\rangle$. A coupling scheme must be specified followed by construction of a complete set of orthonormal basis states for a Hilbert subspace, by successive C-G coupling between pairs of $|I_iM_i\rangle$ states, as per [1.1.28]. *(8)* For three spin angular momenta $I_1$, $I_2$ and $I_3$, there exist two distinct coupling schemes: coupling of $I_1$ and $I_2$ and subsequently $I_3$ with the resultant $I_{12}$ and the coupling of $I_1$ with the resultant $I_{23}$ of $I_2$ and $I_3$. Both the $|((I_1I_2)I_{12}I_3)IM\rangle$ and $|(I_1(I_2I_3)I_{23})IM\rangle$ bases give equivalent representations of any three spin operator and are related by a unitary transformation involving the matrix of 6-*j* symbols. *(5)* Coupling four $I_i$'s leads to a 9-*j* symbol.*(5)* These 6-*j* and higher "recoupling coefficients" can be reduced to sums of products of 3-*j* symbols and have been used to construct complete orthonormal bases for *n* spins following various coupling schemes. *(6)*

*Representation of Finite Rotations*

A right hand positive rotation through an angle $\theta$ may be regarded as the sum of a series of *n* successive rotations through angles $\theta / n$. Defining the infinitesimal rotation angle $\delta\theta = \lim_{n\to\infty} (\theta / n)$, the finite rotation $R_k(\theta)$ about some axis *k* in terms of *n* infinitesimal rotations is

$$R_k(\theta) = \lim_{n\to\infty} \left(R_k(\theta / n)\right)^n = \lim_{\delta\theta\to 0} \left(R_k(\delta\theta)\right)^{\theta/\delta\theta} \qquad [1.1.33].$$

The $2I+1$ eigenstates $|IM\rangle$ of fixed *I* are of significance at this point, in that they span an irreducible representation $D^{(I)}$ of the infinite rotation group $R_3$, *(9)* such that

$$R_k(\theta) = \exp\left(\frac{i\theta}{\hbar} I_k\right) \qquad [1.1.34]$$

for *k*=*x*, *y*, *z*. An arbitrary "passive" rotation operator $D(\alpha, \beta, \gamma)$ is conveniently described by rotations about these axes subtented by the Euler angles $\alpha$, $\beta$, $\gamma$

$$\mathrm{D}(\alpha,\beta,\gamma)=\exp\left(\frac{i\gamma}{\hbar}I_z\right)\exp\left(\frac{i\beta}{\hbar}I_y\right)\exp\left(\frac{i\alpha}{\hbar}I_z\right) \qquad [1.1.35]$$

which has the effect on a function of rotating the coodinate system through right handed positive rotations. Other authors *(10, 11)* write

$$D(\alpha,\beta,\gamma)=\exp\left(-\frac{i\alpha}{\hbar}I_z\right)\exp\left(-\frac{i\beta}{\hbar}I_y\right)\exp\left(-\frac{i\gamma}{\hbar}I_z\right)$$

which is an "active" rotation of functions by positive angles $\alpha,\beta,\gamma$ with respect to some fixed coordinate system.

A basis state transforms under a rotation by

$$D(\alpha,\beta,\gamma)|IM\rangle=\sum_{M'}\mathcal{D}^{(I)}_{M'M}(\alpha,\beta,\gamma)|IM'\rangle \qquad [1.1.36].$$

With the orthonormailty condition of the basis functions [1.1.19], an expression for the Wigner rotation matrix is readily found *(6)*

$$\begin{aligned}\mathcal{D}^{(I)}_{M'M}(\alpha,\beta,\gamma)&=\langle IM'|D(\alpha,\beta,\gamma)|IM\rangle\\&=\exp(iM\alpha+iM'\gamma)\langle IM'|\exp(i\beta\, I_y)|IM\rangle \qquad [1.1.37],\end{aligned}$$

where the fact that the vectors $|IM\rangle$ and $|IM'\rangle$ are eigenstates of $I_z$ has been exploited. Futher, it is typical to identify the remaining matrix element in [1.1.37] as the reduced Wigner rotation matrix element

$$d^{(I)}_{M'M}(\beta)=\langle IM'|\exp(i\beta I_y)|IM\rangle=\mathcal{D}^{(I)}_{M'M}(0,\beta,0) \qquad [1.1.38].$$

There exists an infinite number of representations $D^{(I)}$ of the infinite rotation group $R_3$ (hence the name), each of dimension $2I+1$ (deduced from [1.1.37]) for all positive half integer values of $I$. A number of methods have been used for the non-trivial evaluation of the $d^{(I)}_{M'M}(\beta)$, including use of Wigner monomials *(5, 12)*, boson operators *(13)* and second order differential equations in $\beta$. *(14)* While half integer representations of the angular momentum may not be expressed as differential operators in configuration space, the general form of the rotation is derived from the corresponding transformations of the $|IM\rangle$. One explicit form is *(6)*

$$d^{(I)}_{M'M}(\beta) = \sqrt{(I+M')!(I-M')!(I+M)!(I-M)!} \times \sum_{s} \frac{(-1)^{M'-M+s}\left(\cos\frac{\beta}{2}\right)^{2I+M-M'-2s}\left(\sin\frac{\beta}{2}\right)^{M'-M+2s}}{(I+M-s)!\,s!\,(M'-M+s)!\,(I-M'-s)!} \qquad [1.1.38]$$

where $s$ runs over all integral values leading to non-negative factorials. From this is recovered the explicit form of the transformation of states [1.1.36], under finite rotations.

It is not difficult to conceive that any two rotations may be expressed as a single rotation about a suitably chosen axis, from which it follows that any series of rotations may be expressed as a single rotation about some axis.

$$D(\alpha',\beta',\gamma')D(\alpha'',\beta'',\gamma'') \equiv D(\alpha,\beta,\gamma) \qquad [1.1.39].$$

As representations of the infinite rotation group $R_3$, it is worth stating the group properties of the $\mathcal{D}^{(I)}$: there exists a unit element $\mathcal{D}^{(I)}(000)$, an inverse $\mathcal{D}^{(I)\,-1}(\alpha,\beta,\gamma)$ $= \mathcal{D}^{(I)}(-\alpha,-\beta,-\gamma) = \left[\mathcal{D}^{(I)}(\alpha,\beta,\gamma)\right]^{\dagger}$ ( $\dagger$ is the normal operator adjoint) and associativity holds; $\mathcal{D}^{(I)}(1)\left[\mathcal{D}^{(I)}(2)\mathcal{D}^{(I)}(3)\right] = \left[\mathcal{D}^{(I)}(1)\mathcal{D}^{(I)}(2)\right]\mathcal{D}^{(I)}(3)$. It remains, however, to express the closure [1.1.39] in terms of the irreducible representations. To do this we must appeal to the methods used to describe the coupling of angular momenta employed earlier. It was tacitly stated that the $2I+1$ eigenfunctions of $I_z$ and $I^2$, $|IM\rangle$, span a $D^{(I)}$. For $I = I_1 + I_2$, simultaneous eigenfunctions of $I_z$ and $I^2$ must be built from linear combinations of the $(2I_1+1)(2I_2+1)$, $|I_1M_1\rangle|I_2M_2\rangle$ product states vis [1.1.28]. Equivalently, for two sets of functions, one spanning one representation of a group $\Gamma^{(1)}$ and the other spanning a second $\Gamma^{(2)}$, the direct product spans the representation $\Gamma^{(1)} \otimes \Gamma^{(2)}$, which is, in general, reducible. Perhaps intuitively, it should be expected that

$$\mathcal{D}^{(I_1)} \otimes \mathcal{D}^{(I_2)} = \mathcal{D}^{(I_1+I_2)} + \mathcal{D}^{(I_1+I_2-1)} + \ldots + \mathcal{D}^{|I_1-I_2|} \qquad [1.1.40]$$

as is well known for the group $R_3$. Considering the effect of the total angular momentum rotation operator

$$\exp\left[\frac{i\gamma}{\hbar}\left(I_{1z}+I_{2z}\right)\right]\exp\left[\frac{i\beta}{\hbar}\left(I_{1y}+I_{2y}\right)\right]\exp\left[\frac{i\alpha}{\hbar}\left(I_{1z}+I_{2z}\right)\right]$$

$$=\exp\left[\frac{i\gamma}{\hbar}I_{1z}\right]\exp\left[\frac{i\gamma}{\hbar}I_{2z}\right]\exp\left[\frac{i\beta}{\hbar}I_{1y}\right]\exp\left[\frac{i\beta}{\hbar}I_{2y}\right]\exp\left[\frac{i\alpha}{\hbar}I_{1z}\right]\exp\left[\frac{i\alpha}{\hbar}I_{2z}\right] \qquad [1.1.41]$$

(note that $e^{(A+B)} = e^{A}e^{B}$ IFF $[A,B]=0$) on both sides of [1.1.28] and taking matrix elements over the relevant values of $M = M_1 + M_2$ and $M' = M_1' + M_2'$ yields the C-G reduction of the representation

$$\mathcal{D}^{(I_1)}_{M_1' M_1}\mathcal{D}^{(I_2)}_{M_2' M_2} = \sum_{IM'M}\left\langle I_1 M_1' I_2 M_2' \middle| I_1 I_2 I M'\right\rangle\left\langle I_1 M_1 I_2 M_2 \middle| I_1 I_2 I M\right\rangle \mathcal{D}^{(I)}_{M'M}$$

$$= \sum_{IM'M}(-1)^{-(M'+M)}(2I+1)\begin{pmatrix} I_1 & I_2 & I \\ M_1' & M_2' & -M' \end{pmatrix}\begin{pmatrix} I_1 & I_2 & I \\ M_1 & M_2 & -M \end{pmatrix}\mathcal{D}^{(I)}_{M'M} \qquad [1.1.42a].$$

and the inverse

$$\frac{\mathcal{D}^{(I)*}_{M'M}}{(2I+1)}\delta_{II'} = \sum_{\substack{M_1' M_2' \\ M_1 M_2}}\begin{pmatrix} I_1 & I_2 & I \\ M_1' & M_2' & M' \end{pmatrix}\mathcal{D}^{(I_1)}_{M_1' M_1}\mathcal{D}^{(I_2)}_{M_2' M_2}\begin{pmatrix} I_1 & I_2 & I \\ M_1 & M_2 & M \end{pmatrix} \qquad [1.1.42b]$$

where

$$\mathcal{D}^{(I)*}_{M'M}(\omega) = (-1)^{M'-M}\mathcal{D}^{(I)}_{-M'-M}(\omega) \qquad [1.1.42c].$$

### *Angular Momentum Operators Constitute a Lie Algebra*

The group $R_3$ is an example of a continuous group in that the operators of the group $D(\alpha,\beta,\gamma)$ are functions of continuously varying angles. Only because $R_3$ is continuous do the infinitesimal transformations have any meaning. Generally, a set of infinitesimal transformations $O_i$ derived from a continuous group can be written as

$$O_i = 1 + \sum_j \delta a_j P_j \qquad [1.1.43]$$

where $\delta a_j$ is some infintesimal change in some relevant variable and the $P_j$ are generators. The $O_i$ themselves form a group and obey the general commutation relation

$$\left[P_j, P_k\right] = \sum_l c(j,k,l) P_l \qquad [1.1.44].$$

These elements $P_{j,k,l}$ of the group and their commutation relationships constitute a general Lie algebra. Angular momentum operators are the generators of the infinitesimal rotation operators

$$R(\delta\theta) = 1 - \frac{i}{\hbar}\delta\theta \cdot I \qquad [1.1.45]$$

which, together with the structure constants, $c(j,k,l) = i\hbar$, also form a Lie algebra, from which the structure of the theory of angular momentum, based on this underlying symmetry, is obtained.

# Chapter 2. TENSOR OPERATORS

## *Construction of Single Spin Operators*

So far it has been shown that the angular momentum eigenvectors behave simply under the infinite group of coordinate rotations *vis* [1.1.36] and in fact, form basis sets for the irreducible representations $D^{(I)}$ of $R_3$. It remains to consider the transformation properties of operators subject to such rotations. To this end, an irreducible tensor operator of rank $k$ is defined as a set of $2k+1$ operators $\mathcal{T}^{(k)q}(I)$ which transform under coordinate rotations according to

$$D(\alpha,\beta,\gamma)\,\mathcal{T}^{(k)q}(I)D^{-1}(\alpha,\beta,\gamma) = \sum_{q'=-k}^{k}\mathcal{D}^{(k)}_{q'q}(\alpha,\beta,\gamma)\,\mathcal{T}^{(k)q'}(I) \qquad [1.2.1]$$

with the tensor components $q$ and $q'$ having the allowed $2k+1$ values running from $-k$ to $k$. These tensor operators are irreducible in the sense that there is no subset or linear combination of $\mathcal{T}^{(k)q}(I)$, for a given $k$, that transform separately amonst themselves under a rotation. Using the implications of the unitary transformation [1.2.1] and arguments similar to those employed for the determination of the eigenvalues $I$ and $M$ in state space, the analogous angular momentum eigenvalues in this operator space are found in terms of $k$ and $q$

$$\left[I,\left[I,\mathcal{T}^{(k)q}(I)\right]\right] = k(k+1)\,\mathcal{T}^{(k)q}(I)$$

$$\left[I_z,\mathcal{T}^{(k)q}(I)\right] = q\,\mathcal{T}^{(k)q}(I)$$

$$\left[I_\pm,\mathcal{T}^{(k)q}(I)\right] = \sqrt{(k\mp q)(k\pm q+1)}\,\mathcal{T}^{(k)q\pm 1}(I) \qquad [1.2.2].$$

As operators, the $\mathcal{T}^{(k)q}(I)$ are constructed differently for different spin magnitudes, but being tensors, are rotationally invariant regardless of the spin. Since rotations are viewed on a sphere, and anticipating applications to problems in NMR, a spherical basis is a natural selection for the construction of the $2k+1$ components of a tensor of rank $k$. One such spherical basis is selected such that

$$e^{(1)0} = iz$$

$$e^{(1)\pm 1} = \mp \,{}^{i}\!\big/\!_{\sqrt{2}}\,(x \pm iy) \qquad [1.2.3]$$

in terms of the Cartesian basis vectors. Generalization of the coordinate system in three dimensions in terms of these three unit vectors is given by the Clebsch-Gordan expansion

$$e^{(k)q} = \sum_{q_1 q_2} \langle k_1 q_1 k_2 q_2 | k_1 k_2 k q \rangle e^{(k_1)q_1} e^{(k_2)q_2} \qquad [1.2.4]$$

in a manner exactly analogous to [1.1.28]. The quantities $e^{(k)q}$ are the $k^{th}$ rank basis tensors from which the spherical tensor components (which are really Cartesian scalar operators) are obtained by a $k$-fold dot product

$$[I]^{(k)q} = [I]^{(k)} \odot^{k} e^{(k)q} \qquad [1.2.5]$$

where, for example, $A \odot^{2} B = \sum_{ij} A_{ij} B_{ji} = A{:}B$. The $e^{(k)q}$ obey the normalization

$$e^{(k)q} \odot^{k} e^{(k)}_{q'} = \delta_{qq'} \qquad [1.2.6]$$

with phase determined by the original selection in [1.2.3]

$$e^{(k)q*} = e^{(k)}_{q} = (-1)^{k-q} e^{(k)-q} \qquad [1.2.7].$$

Normalized $\mathcal{T}^{(k)}(I)$ are constructed from the $[I]^{(k)}$ *(15, 16)*

$$\mathcal{T}^{(k)}(I) = \sqrt{\frac{(2k+1)}{[I]^{(k)} \odot^{k} [I]^{(k)}}}\,[I]^{(k)} \qquad [1.2.8]$$

in such a way that

$$\mathcal{T}^{(k)}(I) \odot^{k} \mathcal{T}^{(k)}(I) = (2k+1) \qquad [1.2.9].$$

The normalization constant determined by the scalar $[I]^{(k)} \cdot {}^{k}[I]^{(k)}$ is given by *(13, 17)*

$$[I]^{(k)} \odot^{k} [I]^{(k)} = \frac{(k!)^2 (2I+k+1)!}{2^k (2I+1)(2k)!(2I-k)!} \qquad [1.2.10].$$

Individual spherical tensor components are again built from the tensor operators by the $k$-fold contraction given in [1.2.5].

As might be expected, higher rank spherical tensor operators can be built directly by the repeated Clebsch-Gordan coupling exploited in [1.2.4] and [1.1.28]. For example, the five $q$ components of the second rank $\mathcal{T}^{(2)}(I)$ can be constructed from the predetermined vector operators $\mathcal{T}^{(1)}(I)$

$$\mathcal{T}^{(1)0}(I) = \sqrt{\frac{3}{I(I+1)}}\, iI_z$$

$$\mathcal{T}^{(1)\pm 1}(I) = \sqrt{\frac{3}{2I(I+1)}}\left(\mp iI_\pm\right)$$

$$\mathcal{T}^{(2)q}(I) = \sum_{q_1 q_2} (-1)^{2-q}\sqrt{5}\begin{pmatrix} 1 & 1 & 2 \\ q_1 & q_2 & -q \end{pmatrix}\mathcal{T}^{(1)q_1}(I)\,\mathcal{T}^{(1)q_2}(I) \qquad [1.2.11]$$

*Transformation Properties of Single Spin Operators*

Just as the state space basis vectors $|I\,M\rangle$ evolve in a quantum mechanical system, the $\mathcal{T}^{(k)q}(I)$ determined by the quantum numbers $k$ and $q$ can also be mixed through coupling terms in the Hamiltonian. Both the set of so called multipole operators $\left\{\mathcal{T}^{(k)q}(I)\right\}$ and the $\{|IM\rangle\langle IM'|\}$ span the same operator space and the unitary transformation relating the two is given by the now familiar Clebsch-Gordan coupling coefficient

$$\mathcal{T}^{(k)q}(I) = \sum_{MM'} \langle IM|\mathcal{T}^{(k)q}(I)|IM'\rangle |IM\rangle\langle IM'| \qquad [1.2.12].$$

A most useful property of tensor operators is exploited by the well known Wigner-Eckart theorem *(18)*, which enables the factorization of matrix elements between any two angular momentum states into two parts

$$\langle IM|\mathcal{T}^{(k)q}(I)|IM'\rangle = (-1)^{I-M}\begin{pmatrix} I & k & I \\ -M & q & M' \end{pmatrix}\left\langle I\middle\|\mathcal{T}^{(k)}(I)\middle\|I\right\rangle \qquad [1.2.13].$$

The geometrical term is so named because of its dependence upon the spatial quantum numbers $q, M$ and $M'$, while the physical term $\left\langle I\middle\|\mathcal{T}^{(k)}(I)\middle\|I\right\rangle$, known as the reduced marix element, is dependent only upon the tensor rank and spin magnitude and has been evaluated in the multipole basis *(6, 8)*

$$\left\langle I\middle\|\mathcal{T}^{(k)}(I)\middle\|I\right\rangle = (i)^k\sqrt{(2I+1)(2k+1)} \qquad [1.2.14].$$

Hence, the expansion of the multipole operator in terms of the more common $\{|IM\rangle\langle IM'|\}$ basis is

$$\mathcal{T}^{(k)q}(I) = (i)^k\sqrt{(2I+1)(2k+1)}\sum_{MM'}(-1)^{I-M}\begin{pmatrix} I & k & I \\ -M & q & M' \end{pmatrix}|IM\rangle\langle IM'| \qquad [1.2.15a].$$

From the symmetry properties of the *3-j* symbol [1.1.32], the inverse of [1.2.15a] is found to be

$$|IM\rangle\langle IM'| = (-1)^{I-M}\sqrt{(2I+1)}\sum_{MM'} -(i)^k\sqrt{(2k+1)}\begin{pmatrix} I & k & I \\ -M & q & M' \end{pmatrix}\mathcal{T}^{(k)q}(I) \qquad [1.2.15b].$$

Specified by the properties of the *3-j* symbol are restrictions to which the quantum numbers $k$ and $q$ are subject. Meeting the conditions of the triangle inequality, $k$ has allowed values $k$ = 0, 1, 2, ..., $2I$ while the condition that $q + M' - M = 0$ provides for integer values of $q$ ranging from $-k$ to $k$. In this way the spherical tensor or multipole operator basis is a natural selection for the description of multiquantum NMR experiments. The tensorial or multipole rank is designated by $k$ (dipole, quadrupole, octupole etc.) and since $q = \Delta M$, a labeled multipole component represents a $q$-quantum coherence. The number of multipole operators for a given spin $I$ is then

$$\sum_{k=0}^{2I}(2k+1)=(2I+1)^2 \qquad [1.2.16]$$

each obeying the adjoint relation

$$\mathcal{T}^{(k)q}(I)^{\dagger}=\mathcal{T}^{(k)}_{q}(I)=(-1)^{k-q}\,\mathcal{T}^{(k)-q}(I) \qquad [1.2.17]$$

and the orthonormality condition defined by the quantum mechanical trace

$$\mathrm{tr}\left\{\mathcal{T}^{(k)q}(I)^{\dagger}\mathcal{T}^{(k')q'}(I)\right\}\equiv\left\langle\left\langle\mathcal{T}^{(k)q}(I)\middle|\mathcal{T}^{(k')q'}(I)\right\rangle\right\rangle=(2I+1)\delta_{kk'}\delta_{qq'} \qquad [1.2.18].$$

These $(2I+1)^2$ operators are closed under commutation *(18)*

$$\left[\mathcal{T}^{(l)m}(I),\mathcal{T}^{(k)q}(I)\right]=2\sum_{k'q'}\phi(klk')\left\langle\left\langle\mathcal{T}^{(k')q'}(I)\middle|\mathcal{T}^{(l)m}(I)\middle|\mathcal{T}^{(k)q}(I)\right\rangle\right\rangle\mathcal{T}^{(k')q'}(I) \qquad [1.2.19]$$

where, from the Wigner-Eckart theorem

$$\left\langle\left\langle\mathcal{T}^{(k')q'}(I)\middle|\mathcal{T}^{(l)m}(I)\middle|\mathcal{T}^{(k)q}(I)\right\rangle\right\rangle=\mathrm{tr}\left\{\mathcal{T}^{(k')q'}(I)^{\dagger}\mathcal{T}^{(l)m}(I)\,\mathcal{T}^{(k)q}(I)\right\} \qquad [1.2.20]$$

$$=(-1)^{k+q'+2I}(i)^{k+l+k'}\left[(2I+1)(2k+1)(2k'+1)(2l+1)\right]^{1/2}\begin{Bmatrix}I & I & k\\ l & k' & I\end{Bmatrix}\begin{pmatrix}k' & l & k\\ -q' & m & q\end{pmatrix}$$

$$=(-1)^{k-q}\begin{pmatrix}k' & l & k\\ -q' & m & q\end{pmatrix}\left\langle\left\langle\mathcal{T}^{(k')}(I)\middle\|\mathcal{T}^{(l)}(I)\middle\|\mathcal{T}^{(k)}(I)\right\rangle\right\rangle$$

for which {...} is the *6-j* recoupling coefficient *(6)* and $\phi(klk')=1$ if $k+l+k'$ is odd and zero otherwise.

For completeness sake, mention should be made of the construction of multipole operators for n-spin systems *(20)*, even though they will not be utilized in this thesis. For two spins $I_1$ and $I_2$, a two-spin multipole operator basis $T^{(k)q}(k_1 k_2)$ can be constructed from the direct product basis $\mathcal{T}^{(k_1)q_1}(I_1)\otimes\mathcal{T}^{(k_2)q_2}(I_2)\equiv\mathcal{T}^{(k_1)q_1}(I_1)\,\mathcal{T}^{(k_2)q_2}(I_2)$ that spans the two-spin operator basis, but it is over-complete in the sense that it is not irreducible under rotations generated by the total angular momentum $I=I_1+I_2$. A complete irreducible operator basis is obtained by the operator analogue of [1.1.28]

$$T^{(k)q}\left(k_1\,k_2\right)=\left[\left(2I_1+1\right)\left(2I_2+1\right)\right]^{1/2}\sum_{q_1\,q_2}(-1)^{k_1-k_2+k}(-1)^{k-q}\sqrt{2k+1}\times\begin{pmatrix}k_1 & k_2 & k\\ q_1 & q_2 & -q\end{pmatrix}\mathcal{T}^{(k_1)q_1}\left(I_1\right)\mathcal{T}^{(k_2)q_2}\left(I_2\right) \quad [1.2.20].$$

For $n > 2$ a complete operator basis is the uncoupled direct product of the irreducible single spin operators $\mathcal{T}^{(k_1)q_1}\left(I_1\right)\otimes\mathcal{T}^{(k_2)q_2}\left(I_2\right)\otimes\ldots\otimes\mathcal{T}^{(k_n)q_n}\left(I_n\right)$. Given the selection of a suitable coupling scheme, a complete irreducible spherical tensor basis can be evolved by repeated C-G coupling via [1.2.20]. Various properties of these multipole, multispin operators have been presented elsewhere *(20)*.

# Chapter 3. DENSITY MATRIX FORMALISM OF NMR

Applications of quantum mechanics are generally concerned with those states of systems that can be represented by state vectors. Indeed, within the context of NMR experiments, the dynamics of single spins can be interpreted within the context of the motion of the classical magnetization vectors, represented by the phenomenological Bloch equations. *(21)* However, for coupled systems or, more generally, for systems that have no more than a certain probability of being defined by a precise dynamical state vector, it is necessary to appeal to density matrix techniques. *(22, 23, 24)* First applied to the description of statistical concepts in quantum mechanics by von Neumann *(24)*, the density matrix is best suited to determine the average response of a macroscopic system.

In this chapter will be given an account of those aspects of density matrix formalism that are relevant to problems in NMR. The concepts presented previously will be extended to account for the behaviour of an ensemble of spins. Just as the spin operators presented in the previous sections can be constructed in a number of equivalent ways, so too can the dynamics of spin systems be calculated using different techniques. Numerical methods can be derived to treat spin dynamical calculations exactly, making such considerations moot. However, in many cases, accuracy comes at the expense of physical insight. Judicious selection of both the representation of the spin system and method by which the time evolution is determined is done to facilitate interpretation of the results of a particular NMR experiment. Observable transverse magnetization can then be resolved into its component contributions by considering some physical interpretation of the system.

### *Matrix Form of the Density Operator*

In order to define the form of the density operator of a quantum mechanical system, the time-dependent Schrödinger equation [1.1.3] is re-written

$$\mathcal{H}(t)\left|\Psi^{(i)}(t)\right\rangle = -i\hbar\frac{\partial\left|\Psi^{(i)}(t)\right\rangle}{\partial t} \qquad [1.3.1].$$

The $i$th dynamical state of the statistical quantum system is interpreted as an ensemble of the complete set of $n$ stationary basis states $\{|u_n\rangle\}$ of the Hamiltonian

$$\left|\Psi^{(i)}(t)\right\rangle = \sum_n c_n^{(i)}(t)\left|u_n\right\rangle \qquad [1.3.2]$$

expanded through the time-dependent coefficients $c_n^{(i)}(t)$. For an ensemble in thermal equilibrium, the density operator is determined by the probability $p_i$ that it will be observed in one of several normalized states $\left|\Psi^{(i)}(t)\right\rangle$, such that

$$\rho(t) = \sum_i \rho_i(t)\left|\Psi^{(i)}(t)\right\rangle\left\langle\Psi^{(i)}(t)\right| = \sum_i \rho_i(t)\sum_m\sum_n c_m^{(i)}(t)\,c_n^{(i)}(t)^*\left|u_m\right\rangle\left\langle u_n\right| \qquad [1.3.3].$$

Physical insight is gained by considering the matrix representation of the density operator in the orthonormal basis $\{|u_n\rangle\}$. Given any two generalized mixed states

$$\begin{aligned}\left\langle\Psi^{(r)}(t)\right|\rho(t)\left|\Psi^{(s)}(t)\right\rangle &= \sum_i \rho_i(t)\sum_m\sum_n c_m^{(i)}(t)\,c_n^{(i)}(t)^*\left\langle\Psi^{(r)}(t)\middle|u_m\right\rangle\left\langle u_n\middle|\Psi^{(s)}(t)\right\rangle\\ &= \overline{c^{(r)}(t)\,c^{(s)}(t)^*}\end{aligned} \qquad [1.3.4]$$

where $\sum_i \rho_i(t) = 1$ and the bar denotes the ensemble average. By virtue of [1.3.1], the $\left|\Psi^{(i)}(t)\right\rangle$ form an eigenvector basis of the Hamiltonian. Interaction with an electromagnetic field can cause transitions between states, providing a distinction between two types of matrix elements. If this interaction is weak enough so that the $\left|\Psi^{(i)}(t)\right\rangle$ are not appreciably changed, the operator representing this transition is $\left|\Psi^{(r)}(t)\right\rangle\left\langle\Psi^{(s)}(t)\right|$

bearing an associated phase $\exp\left(-\frac{i}{\hbar}(E_r - E_s)t\right)$. A "coherent superposition" of states is thought of as those members of the ensemble that are correlated with respect to time dependence and phase and is represented by the off-diagonal matrix element

$$\rho_{rs}(t) = \left\langle \Psi^{(r)}(t) \middle| \rho(t) \middle| \Psi^{(s)}(t) \right\rangle = \overline{c^{(r)}(t)\, c^{(s)}(t)^{*}} \qquad [1.3.5].$$

The diagonal elements are not influenced by the relative phases between the members of the ensemble, so that for a statistically significant number of particles, the matrix element

$$\rho_{rr}(t) = \left\langle \Psi^{(r)}(t) \middle| \rho(t) \middle| \Psi^{(r)}(t) \right\rangle = \overline{c^{(r)}(t)^{2}} \qquad [1.3.6]$$

can be interpreted as the population of particles in a particular state. In the random phase approximation, the density matrix of a system in thermal equilibrium with an external reservior ( a canonical ensemble ), containing no inherent time dependence, consists solely of the diagonal elements bearing the populations of the eigenstates given by the Boltzmann distribution

$$\overline{c^{(r)}(t)^{2}} = \frac{e^{-E^{(r)}/kT}}{\sum\limits_{r} e^{-E^{(r)}/kT}} \qquad [1.3.7].$$

and the trace of the density matrix is equal to unity

$$tr\{\rho(t)\} = \sum_{i} \rho_{ii}(t) = \sum_{i} \overline{c^{(i)}(t)^{2}} = 1 \qquad [1.3.8].$$

Of particular significance is the expectation value $\langle \mathcal{Q} \rangle$ of some arbitrary observable operator $\mathcal{Q}$, expressed in terms of $\rho(t)$ in the Schrödinger representation

$$\langle \mathcal{Q} \rangle = \sum_{i} \rho_i(t) \left\langle \Psi^{(i)}(t) \middle| \mathcal{Q} \middle| \Psi^{(i)}(t) \right\rangle$$

$$= \sum_{i} \rho_i(t) \sum_{m} \sum_{n} c_m^{(i)}(t)^{*}\, c_n^{(i)}(t) \left\langle u_m \middle| \mathcal{Q} \middle| u_n \right\rangle \qquad [1.3.9].$$

$$= \sum_{m} \sum_{n} \rho_{nm}(t)\, \mathcal{Q}_{mn} \equiv tr\{\mathcal{Q}\rho(t)\}$$

Finding the expectation value can be done equivalently in the Heisenberg representation by evaluating the trace of the product $\{\mathcal{Q}(t)\ \rho(0)\}$. This reflects one of the most powerful attributes of the density matrix theory, as the trace is independent of the representation used to give the form of the density matrix.

An idealized "pure" state is one in which all particles in the ensemble are in the same state and can be equally represented by the same normalized state function. For such a situation the exactly defined $\left|\Psi^{(i)}(t)\right\rangle$ represents a statistically significant number of simultaneously prepared particles. As an average of many identical single particle states, the pure state itself can be thought of as a single particle state, even though dispersion free states are not likely to be realized in practice. *(25)* The density matrix of a pure state is idempotent i.e. $\rho^2 = \rho$, and its matrix elements are projection operators akin to those introduced in [1.1.20]. From these considerations

$$tr\left\{\rho^2(t)\right\} \le 1 \qquad [1.3.10]$$

with the equality holding for pure states.

*Time Evolution of the Density Matrix*

The equation of motion for the density matrix follows directly from the Schrödinger equation for each statistical state

$$\left|\Psi^{(i)}(t)\right\rangle = \mathcal{U}(t)\left|\Psi^{(i)}(0)\right\rangle$$

$$i\hbar\frac{\partial \mathcal{U}(t)}{\partial t} = \mathcal{H}(t)\,\mathcal{U}(t); \qquad \mathcal{U}(0) = 1 \qquad [1.3.11]$$

which, when combined with [1.3.3], yields the quantum Liouville or von Neumann equation

$$i\hbar\frac{\partial\rho(t)}{\partial t}=\left[\mathcal{H}(t),\rho(t)\right]=\mathcal{L}(t)\,\rho(t)\qquad[1.3.12]$$

with time evolution of the density operator suitably determined by the unitary transformation

$$\rho(t)=\mathcal{U}(t)\,\rho(0)\mathcal{U}(t)^{\dagger}\qquad[1.3.13].$$

If the Hamiltonian is time-dependent wherein $\left[\mathcal{H}(t),\mathcal{H}(t')\right]\neq 0$ for $t\neq t'$, one formal solution for $\mathcal{U}(t)$ is the Feynman-Dyson expansion *(26)*

$$\mathcal{U}(t)=T\exp\left(-\tfrac{i}{\hbar}\int_0^t\mathcal{H}(t')\,dt'\right)\qquad[1.3.14].$$

A long expansion of nested commutators of $\mathcal{H}(t)$ at different $t$ is contained in the time ordering operator $T$. This series is normally truncated in order to facilitate evaluation, with the consequence that $\mathcal{U}(t)$ loses its unitary properties, such as preserving the trace of a quantum mechanical operator. Other methods, such as the Magnus expansion *(27)*, have been employed to expand $\mathcal{U}(t)$ in terms of Hermitian operators

$$\mathcal{U}(t)=\exp\left(\Omega(t)\right);\qquad\Omega(0)=0$$

$$\Omega(t)=\sum_{i=0}^{\infty}\Omega^{(i)}(t)\qquad[1.3.15]$$

however, only $\Omega^{(0)}(t)=-\frac{i}{\hbar}\int_0^t\mathcal{H}(t_1)dt_1$ is readily and generally calculable.

Selecting a suitable representation, such as a rotating frame, provides a means by which the Hamiltonian might be made time-independent within finite time segments. In this case the evolution of the density matrix can be expressed by a sequence of unitary transformations of the form

$$\rho(t)=\exp\left(-\tfrac{i}{\hbar}\mathcal{H}t\right)\rho(0)\exp\left(\tfrac{i}{\hbar}\mathcal{H}t\right)\qquad[1.3.16a]$$

$$\rho(t+\tau_1+\tau_2)=\exp\left(-\tfrac{i}{\hbar}\mathcal{H}_2\tau_2\right)\exp\left(-\tfrac{i}{\hbar}\mathcal{H}_1\tau_1\right)\rho(t)\exp\left(\tfrac{i}{\hbar}\mathcal{H}_1\tau_1\right)\exp\left(\tfrac{i}{\hbar}\mathcal{H}_2\tau_2\right)\qquad[1.3.16b]$$

defined by the propagators $\mathcal{U}(\tau_n)=e^{-\frac{i}{\hbar}\mathcal{H}_n\tau_n}$. This form applies to any sequence of intervals $\tau_n$ in which time-independent average Hamiltonians can be defined and is particularly useful for the representation of pulsed NMR experiments.

The formal solution to the quantum Liouville equation [1.3.12] for time-independent Hamiltonians is the unitary transformation [1.3.13]. Of interest is the solution of any matrix element of $\rho$ of the trace of some observable [1.3.9]. Two general methods are made use of in this thesis. The first is obtained by expanding [1.3.16a] as a Taylor series in time around $t$=0 giving the multiple commutator expansion known as the Baker-Campbell-Hausdorff fomula *(28)*

$$\rho(t)=\rho(0)+\left(-\tfrac{i}{\hbar}t\right)\left[\mathcal{H},\rho(0)\right]+\tfrac{1}{2!}\left(-\tfrac{i}{\hbar}t\right)^2\left[\mathcal{H},\left[\mathcal{H},\rho(0)\right]\right]+\cdots \qquad [1.3.17].$$

Also referred to as the exponential operator method, this treatment is easily handled for cases where the series quickly converges and the multiple commutators terminate. For example, under conditions allowing application of the high-temperature approximation, truncation of [1.3.17] to include only the first few terms is accurate and the series forms a useful perturbative result. This expansion is also convenient for the treatment of relatively simple two-pulse experiments.

As an alternative to the evaluation of $\rho(t)$ in terms of a series of nested commutators [1.3.17], the density matrix and the Hamiltonian can be expanded into a complete orthonormal basis set of operators $\left\{\chi^{(i)}\right\}\equiv\left\{\left|\Psi^{(i)}\right\rangle\left\langle\Psi^{(i)}\right|\right\}$. *(29)* Applying the evaluation of observables [1.3.9] to an adapted form of the expansion of $\rho(t)$ [1.3.3] gives

$$\rho(t)=\sum_i \rho_i(t)\chi^{(i)}=\sum_i tr\left\{\rho\chi^{(i)\dagger}\right\}\chi^{(i)}=\sum_i\left\langle\chi^{(i)\dagger}\right\rangle\chi^{(i)} \qquad [1.3.18a]$$

$$\mathcal{H}=\sum_j h_i\chi^{(j)} \qquad [1.3.18b]$$

which reduces the Liouville equation to a system of coupled first order differential equations among the average values $\rho_i$:

$$\frac{\partial \rho_i(t)}{\partial t} = \sum_j tr\left\{\mathcal{X}^{(i)\dagger}\left[-\tfrac{i}{\hbar}\mathcal{H},\mathcal{X}^{(j)}\right]\right\}\rho_j$$

$$= \sum_j \rho_{ij}(t)\,\rho_j \qquad [1.3.19].$$

Significantly, solution of the system of equations [1.3.19] gives the time evolution of the density matrix in terms of the dynamics of every observable $\rho_{ij}(t)$ from the set of initial conditions $\{\rho_i(0)\}$.

### *Basis States for the Representation of the Spin Density Matrix*

While inferred, no explicit connection has been made to spin angular momentum during this survey of density matrix formalism. Selection of the operator basis set into which the density matrix is expanded, is arbitrary, but should be appropriate to the symmetry of the Hamiltonian. For the consideration of NMR experiments, this amounts to finding a convenient representation for the spin angular momentum. While this formally restricts attention to only the spin variables, relaxation by interaction with the lattice modes can be accounted for perturbatively.

By considering only the spin part of the density matrix, it is possible to find the dimensionality of the Hamiltonian and thus, a finite-dimensional representation of the spin density matrix itself. One representation of the spin density matrix was first proposed by Fano *(29)* for spin $I$=1/2 in terms of the magnetic polarizations $\boldsymbol{P} = \langle\vec{\sigma}\rangle = tr\{\rho\vec{\sigma}\}$

$$\rho(t) = \frac{1}{2}\left(E_{1/2} + \boldsymbol{P}\cdot\vec{\sigma}\right) = \frac{1}{2}\left(E_{1/2} + P_x\sigma_x + P_y\sigma_y + P_z\sigma_z\right)$$

$$= \frac{1}{2}\begin{bmatrix} 1+P_z & P_x - iP_y \\ P_x + iP_y & 1-P_z \end{bmatrix} \qquad [1.3.20].$$

Expectation values $\sigma_i$ of the Pauli spin matrices determine the components of this magnetization $P_i$ and thus, knowledge of the vector $P$ completely desribes the dynamical state of the $I$=1/2 system. Since any 2x2 Hermitian matrix can be written in terms of

$$\sigma_x = \begin{pmatrix} 0 & 1 \\ 1 & 0 \end{pmatrix} \quad \sigma_y = \begin{pmatrix} 0 & -i \\ i & 0 \end{pmatrix} \quad \sigma_z = \begin{pmatrix} 1 & 0 \\ 0 & -1 \end{pmatrix} \qquad [1.3.21]$$

and the unit identity $E_{1/2}$, this set of $(2I+1)^2$ orthogonal operators span the operator space of $I$=1/2. In an equivalent way the Hamiltonian for the interaction of the spin magnetic moment $\bar{\sigma} = \hbar\gamma\bar{\sigma}$ with an external field $H$(t) can be written

$$\mathcal{H}(t) = -\tfrac{1}{2}\hbar\gamma\,\bar{\sigma}\cdot \boldsymbol{H}(t) \qquad [1.3.22]$$

from which can be formed a system of first order differential equations as per [1.3.19]

$$\frac{\partial \boldsymbol{P}(t)}{\partial t} = -\gamma\, \boldsymbol{H}(t) \times \boldsymbol{P}(t) \qquad [1.3.23].$$

For arbitrary spin magnitudes $I \geq 1/2$, vector polarizations are not sufficient to completely span the (2$I$+1)-dimensional spin density matrix. Expressing $\rho$ by [1.3.18] in terms of the set of operators $\{\mathcal{X}^{(i)}, E_I\}$, the transformation of $\rho$ is given by [1.3.16a] and it is left to determine how $\rho(0)$ evolves under the unitary transformation induced by $\mathcal{H}$. Substituting [1.3.18] into [1.3.16a] gives

$$\rho(t) = \sum_i \rho_i(0) \exp\left(-\tfrac{i}{\hbar}\mathcal{H}t\right) \mathcal{X}^{(i)} \exp\left(\tfrac{i}{\hbar}\mathcal{H}t\right) \qquad [1.3.24]$$

which is solved for the $\rho_i(t)$, given the structure of the transformation of $\mathcal{X}^{(i)}$ under $\mathcal{H}$ that is reflected in [1.3.19].

Spin dynamical problems in NMR are frequently dominated by the Zeeman interaction or by the application of RF pulses. Both interactions appear in the spin Hamiltonian by way of propagators of the form $\exp\left(-\tfrac{i}{\hbar}\boldsymbol{\Omega}\cdot \boldsymbol{I}\,t\right)$, recognizable as generators of rotations ( cf. [1.1.34] ). The orthogonal set of multipole operators $\mathcal{Y}^{(k)q}(\boldsymbol{I})$ naturally incorporate this spherical symmetry following [1.2.12]. A generalization of Fano's expression [1.3.20] can be given for arbitrary $I$ by the multipole expansion of the spin density matrix *(19)*

$$\rho(t) = \sum_{k=0}^{2I} \phi^{(k)} \odot^{(k)} \mathscr{T}^{(k)}(I)$$

$$= (2I+1)^{-1} \left[ E_I + \sum_{k=1}^{2I} \sum_{q=-k}^{k} \phi_q^k(t) \mathscr{T}^{(k)q}(I) \right] \qquad [1.3.25]$$

in terms of the multipole polarizations of rank $k$

$$\phi_q^k(t) = \left\langle \mathscr{T}^{(k)q}(I)^\dagger \ \right\rangle = \left\langle \mathscr{T}_q^{(k)}(I) \right\rangle = tr\left\{ \mathscr{T}_q^{(k)}(I)\, \rho(t) \right\} \qquad [1.3.26a]$$

$$\phi_q^k(t) \equiv \phi^{kq}(t)^* = (-1)^{k-q}\, \phi^{k-q}(t) \qquad [1.3.26b].$$

In general $\phi^{(k)} = \left\langle \mathscr{T}^{(k)}(I) \right\rangle$ is the $2^k$-pole moment of the spin angular momentum and labels the associated $q$-quantum coherence dictated by the symmetry in [1.2.15b]. Taking [1.3.25] as the form of the spin density matrtix, the system of differential equations [1.3.19] or the Liouville equation are equivalently expressed by

$$\frac{\partial \phi_q^k(t)}{\partial t} = (2I+1)^{-1} \sum_{k'q'} \left\langle\left\langle \mathscr{T}^{(k)q}(I) \middle\| \left[ -\tfrac{i}{\hbar} \mathscr{H}(t), \mathscr{T}^{(k')q'}(I) \right] \right\rangle\right\rangle \phi_{q'}^{k'}(t) \qquad [1.3.27a]$$

which may also be written in matrix form

$$\frac{\partial \overline{\phi}(t)}{\partial t} = \mathscr{L}_{qq'}^{kk'}(t) \overline{\phi}(t) \qquad \overline{\phi}(t) = \sum_{kq} \phi_q^k(t) \mathscr{T}^{(k)q}(I) \qquad [1.3.27b].$$

The $\phi_q^k(t)$ make up the components of the column vector $\overline{\phi}(t)$ in a Liouville space spanned by the $\mathscr{T}^{(k)q}(I)$.

The concept of irreducible tensor operators is normally introduced for representing NMR Hamiltonians in order to simplify evaluation of matrix elements *via* the Wigner-Eckart theorem. *(30, 31)* Other bases such as the $|IM\rangle\langle IM'|$ are in common use and are paricularly convenient when the Hamiltonian is diagonal in this representation (such as when the Zeeman interaction with an external magnetic field dominates). These become unwieldy for the complete description of a multi-pulse NMR experiment owing to a lack of rotational symmetry. Bases built from simple products of the Cartesian operators have been employed. *(21, 32)* These "product" operators are also not irreducible under rotations and generally require the formulation of often cumbersome commutator tables.

# Chapter 4. THE NUCLEAR SPIN HAMILTONIAN

The fact that most NMR experiments can be discussed within the context of a drastically simplified spin Hamiltonian is one of the most impressive attributes of the NMR experiment, allowing degrees of resolution only theorized about in other forms of spectroscopy. With the representation of the spin density matrix by a finite dimensional Hilbert space, comes the ability to extract closed solutions for even the most sophisticated experiments.

## *The Zeeman Hamiltonian*

The Zeeman interaction is linear in the single spin operators and consists of the interaction of nuclear spin with an applied external field. Generically, in the context of NMR, this consists of interaction with the static magnetic field $B_0$ and the response to a time-dependent radio frequency (r.f.) field

$$\mathcal{H}_Z(t) = -\gamma\hbar \boldsymbol{I}\cdot\boldsymbol{B}(t)$$

$$= -\gamma\hbar\sqrt{\frac{I(I+1)}{3}}\sum_m \mathcal{Y}^{(1)m}(I)B_m(t) \qquad [1.4.1]$$

where $\boldsymbol{I}$ is represented by its spherical components $\mathcal{Y}^{(1)m}(\boldsymbol{I})$. The $z$ component of $\boldsymbol{B}(t)$ is static while the $x$ and $y$ components account for the r.f. pulse of controllable duration $\tau$

$$\boldsymbol{B}(t) = B_0 z + xB_1\cos(\omega\tau-\varphi) - yB_1\sin(\omega\tau-\varphi) \qquad [1.4.2],$$

where $\varphi$ is the phase angle through which the $xy$ oscillating field can be shifted. Before attempting to solve the Liouville equation it is useful to render [1.4.1] time-independent. By transformation into a rotating frame at the radio frequency $\omega = \gamma B_1$

$$\hat{\mathcal{H}} = U^{-1}\mathcal{H}(t)U = e^{i\omega t}\mathcal{H}(t)e^{-i\omega t}$$

$$= -\gamma\hbar(zB_0 + xB_1\cos\varphi + yB_1\sin\varphi) \qquad [1.4.3],$$

an allowable result, since the high field Hamiltonian $\mathscr{H}_0 = \hbar\omega_0$ is invariant under rotations about $z$. Casting the multipole polarizations into the $\omega_0$ rotating frame

$$\hat{\phi}_q^k(t) = e^{-i\omega_0 tq}\phi_q^k(t) \qquad [1.4.4]$$

and using [1.4.1] in spherical tensor form, leads to the general form *(19)* of the Liouville equation in terms of a frequency offset $\Delta\omega = \omega_0 - \omega$

$$\frac{\partial\,\hat{\phi}_q^k(t+\tau)}{\partial t} = \frac{-2\omega}{2I+1}\sqrt{\frac{I(I+1)}{6}}\left\langle\!\left\langle \mathscr{T}^{(k)} \middle\| \mathscr{T}^{(1)} \middle\| \mathscr{T}^{(k)} \right\rangle\!\right\rangle$$

$$\times\left[e^{i\Delta\omega\tau - i\varphi}(-1)^{k-q}\begin{pmatrix} k & 1 & k \\ -q & 1 & q' \end{pmatrix} - e^{-i\Delta\omega\tau + i\varphi}(-1)^{k-q}\begin{pmatrix} k & 1 & k \\ -q & -1 & q' \end{pmatrix}\right]\hat{\phi}_{q'}^k(t)$$

$$= \frac{i\omega}{2}e^{i\Delta\omega\tau - i\varphi}\sqrt{(k+q)(k-q+1)}\;\hat{\phi}_{q-1}^k(t) + \frac{i\omega}{2}e^{-i\Delta\omega\tau + i\varphi}\sqrt{(k-q)(k+q+1)}\;\hat{\phi}_{q+1}^k(t)$$

$$= \mathscr{L}_{qq'}^{(k)}\hat{\phi}_{q'}^k(t) \qquad [1.4.5].$$

Solutions to [1.4.5] have been presented for experimentally relevant conditions in terms of the resonance offset and r.f. pulse frequency *(33, 34)*. The pulse mixes the coherences $q$ in a tensor manifold of rank $k$ and yields a tranformation valid for any spin magnitude $I$

$$\hat{\phi}_q^k(t+\tau) = \sum_{q'}\mathscr{D}_{qq'}^k(\alpha+\varphi, \beta, \alpha-\varphi+\pi)\hat{\phi}_q^k(t) \qquad [1.4.6].$$

Assuming an on-resonance ($\Delta\omega = 0$), "hard" pulse of short duration so that evolution due to internal coupling can be neglected, $\alpha$ and $\beta$ reduce to

$$\alpha = \frac{\pi}{2}; \quad \beta = \omega_0\tau \qquad [1.4.7]$$

which is the case of a resonance rotation through the angle $\beta$, in the rotating frame defined by [1.4.4] and corresponding to quantum absorption of energy. In this case of pure hard pulses, the effects of a pulse or pulse sequence can be mathematically simulated by repeated rotation of the polarizations by [1.4.6]. Relative differences in phase between any two pulses in a pulse sequence are accounted for by an appropriate selection of the angle $\varphi$.

*Broadening by Magnetic Dipole Interactions*

Magnetic dipole coupling between various nuclei in a sample contribute to the width of the Zeeman resonance line. The quantum mechanical interaction between two magnetic moments $\overline{\mu}_i = \gamma_i \hbar I_i$ is reflected in the Hamiltonian giving the dipolar contribution for $N$ spins

$$\mathcal{H}_{dd} = \frac{1}{2} \sum_{m=1}^{N} \sum_{n=1}^{N} \left[ \frac{\overline{\mu}_m \cdot \overline{\mu}_n}{r_{mn}^3} - \frac{3\left(\overline{\mu}_m \cdot r_{mn}\right)\left(\overline{\mu}_{nl} \cdot r_{mn}\right)}{r_{mn}^5} \right] \qquad [1.4.8].$$

Instances of $m = n$ are excluded and the factor of 1/2 ensures that each relevant contribution to the sum is counted only once. Expressing the internuclear vector $r_{mn}$ in terms of the polar angles between the magnetic field $B_0$ and $r_{mn}$ $(\theta_{mn})$ and the azimuthal angle with respect to the $x$-axis $(\varphi_{mn})$, gives [1.4.8] in terms of the irreducible tensor operators

$$\mathcal{H}_{dd} = \hbar \sum_{m \neq n} \sum_{q=-2}^{2} F_{mn}^{(2)q} A_{mn}^{(2)q} \qquad [1.4.9].$$

Spin operators are contained in the functions $A_{mn}^{(2)}$, where the $n$th spin has components $I_{zn}$ and $I_{\pm n}$, while the orientational information is in the $F_{mn}^{(2)}$

$$\begin{aligned}
A_{mn}^{(2)0} &= d_{mn}\left(I_{zm}I_{zn} - \tfrac{1}{4}\left(I_{+m}I_{-n} + I_{-m}I_{+n}\right)\right) \\
F_{mn}^{(2)0} &= 1 - 3\cos^2\theta_{mn} \\
A_{mn}^{(2)\pm 1} &= -\tfrac{3}{2}d_{mn}\left(I_{zm}I_{\pm n} + I_{\pm m}I_{zn}\right) \\
F_{mn}^{(2)\pm 1} &= \sin\theta_{mn}\cos\theta_{mn}e^{\mp i\varphi_{mn}} \qquad [1.4.10a] \\
A_{mn}^{(2)\pm 2} &= -\tfrac{3}{4}d_{mn}I_{\pm m}I_{\pm n} \\
F_{mn}^{(2)\pm 2} &= \sin^2\theta_{mn}e^{\mp 2i\varphi_{mn}}
\end{aligned}$$

where

$$d_{mn} = \frac{\gamma_m \gamma_n \hbar}{2r_{mn}^3} \qquad [1.4.10b]$$

is the dipolar coupling constant in frequency units. *(31, 21)* In the high-field approximation, only the terms that are secular with the representation of the Hamiltonian are maintained, namely those with $q = 0$, resulting in the commonly used truncated form of [1.4.9]

$$\mathcal{H}_{dd} = \frac{\hbar}{2} \sum_{m \neq n} d_{mn}\left(1 - 3\cos^2\theta_{mn}\right)\left[3I_{zm}I_{zn} - \mathbf{I}_m \cdot \mathbf{I}_n\right] \qquad [1.4.11].$$

Further simplification is obtained for heteronuclear spin systems, in which the flip-flop terms $I_+I_-$ appearing in $A^{(2)0}$ of [1.4.10a] are also dropped.

The method of moments proposed by van Vleck *(35)* decomposes the resonant line without actually solving an eigenvalue equation, a method that circumvents the difficulties arising from the non-commutativities present in [1.4.11]. Generalized $n$-spin basis states have also been proposed, in various forms, to arrive at a more detailed account of the dipolar field. *(36)* However, resolution of these individual interactions in the solid state depends upon orientational averaging of $F^{(2)0}$, and is further exacerbated for $I > 1/2$ where contributions from electric quadrupole interactions usually dominate the spin Hamiltonian.

### *Evolution under the Electric Quadrupole Interaction*

Spin-bearing nuclei of $I > 1/2$ do not have spherical charge density and the electrostatic effects of re-orientation of the nucleus must be accounted for. Non-spherical charge densities interact with the electronic potentials $V(\mathbf{r})$ around the nucleus. Following the development by Slichter *(31)*, the classical interaction energy of a charge of density $\sigma$ with $V(\mathbf{r})$ is

$$E = \int \sigma(r) V(r) d\tau \qquad [1.4.12].$$

Expanding $V(r)$ in a series about the origin, chosen as the centre of mass of the nucleus, gives

$$V(r) = V(0) + \sum_{i} x_i \frac{\partial V}{\partial x_i} + \frac{1}{2!} \sum_{i,j} x_i x_j \frac{\partial^2 V}{\partial x_i \partial x_j} + \cdots \qquad [1.4.13a]$$

$$E = V(0) \int \sigma d\tau + \sum_{i} V_i \int x_i \sigma d\tau + \frac{1}{2!} \sum_{i,j} V_{ij} \int x_i x_j \sigma d\tau + \cdots \qquad [1.4.13b]$$

where the indices *i*, *j* run over each of the *x*, *y* and *z* coordinates and

$$V_i = \frac{\partial V}{\partial x_i} \qquad\qquad V_{ij} = \frac{\partial^2 V}{\partial x_i \partial x_j} \qquad [1.4.13c].$$

The first term is the electrostatic energy of the point charge nucleus. Since the centre of mass of the nucleus and the centre of charge coincide, the second term involving the electrical dipole moment of the nucleus, vanishes. The third term is the interaction of the nuclear quadrupole moment $Q$ with electric field gradients about the nucleus. Considering only these tensorial components $V_{ij}$, it is convenient to define an expression for the quadrupole operator $\mathcal{Q}$ in terms of the quantum mechanical operator for the charge density given by $\hat{\sigma}(r) = e \sum_{k} \delta(r - r_k)$

$$\begin{aligned} \mathcal{Q} &= \int \left(3x_i x_j - \delta_{ij} r^2\right) \hat{\sigma}(r) d\tau \\ &= e \sum_{k} \int \left(3x_i x_j - \delta_{ij} r^2\right) \delta(r - r_k) d\tau \\ &= e \sum_{k} \left(3x_{ik} x_{jk} - \delta_{ij} r_k^2\right) \qquad [1.4.14] \end{aligned}$$

where *k* runs over the protons in the nucleus. In what amounts to changing from the position to the momentum representation (being mindful of the commutation relations

[1.1.2] and [1.1.15]), it can be shown that the matix elements of [1.4.14] can be equivalently evaluated as eigenvalues of angluar momentum states

$$\left\langle IM \middle| e\sum_k \left(3x_{ik}x_{jk} - \delta_{ij}{r_k}^2\right) \middle| IM' \right\rangle = K\left\langle IM \middle| \tfrac{3}{2}\left(I_iI_j + I_jI_i\right) - \delta_{ij}I^2 \middle| IM' \right\rangle \qquad [1.4.15].$$

Here $K$ is constant within a fixed nuclear state i.e. is independent of both the spin labels $M$ and the co-ordinate indices. Given this, for the matrix element wherein $M = M' = I$ and $i = j = z$, $K$ can be expressed in terms of the electric quadrupole moment $Q$ of the nucleus

$$eQ = \left\langle II \middle| e\sum_k \left(3z_k^2 - {r_k}^2\right) \middle| II \right\rangle = K\left\langle II \middle| 3I_z^2 - I^2 \middle| II \right\rangle = KI(2I-1) \qquad [1.4.16]$$

yielding the electric quadrupole contribution to the Hamiltonian

$$\mathcal{H}_Q = \tfrac{1}{6}\sum_{i,j} V_{ij}\mathcal{Q} = \frac{eQ}{6I(2I-1)}\sum_{i,j} V_{ij}\left[\tfrac{3}{2}\left(I_iI_j + I_jI_i\right) - \delta_{ij}I^2\right] \qquad [1.4.17a].$$

The factor of 1/6 is a direct consequence of the relationship between [1.4.13b] and [1.4.14]. Choosing a set of suitable axes local to the nucleus leads to the restriction that $V_{ij} = 0$ if $i \neq j$. In this so called "Quadrupolar Principal Axis System" (QPAS) representation, the field gradient tensor is diagonal and the above expression can be rewritten by further defining the quadrupolar asymmetry parameter $\eta = \dfrac{V_{xx} - V_{yy}}{V_{zz}}$ and the maximum component along the local axis of quantization $eq = V_{zz}$

$$\mathcal{H}_Q = \frac{e^2qQ}{4I(2I-1)}\left[3I_z^2 - I^2 + \frac{\eta}{2}\left(I_x^2 - I_y^2\right)\right] \qquad [1.4.17b],$$

thus reducing the problem to the consideration of just two parameters.

Solution to the evolution of a spin system under $\mathcal{H}_Q$ may not be straightforward in the presence of an external magnetic field, owing to the difference in the symmetry between the Zeeman and quadrupole Hamiltonians. Making the assumption that the field to which $Q$ is coupled bears cylindrical symmetry sets $\eta = 0$ and exact solutions to the combined effects of $\mathcal{H}_Q$ and $\mathcal{H}_Z$ can be found. Further, a clear distinction should be drawn between the principal $z$-axis of the QPAS and that defined by the external magnetic field. Applying the positive rotation through the angle $\theta_{LD}$ between the local director and the lab axis

$$I_z = I_{z'} \cos\theta_{LD} + I_{x'} \sin\theta_{LD} \qquad [1.4.18]$$

to [1.4.17b] $(\eta = 0)$, produces a result in terms of the observed first order splitting $\overline{\omega_q}$, in the laboratory $z'$-axis

$$\langle \mathcal{H}_Q \rangle \cong \frac{\overline{\omega_q}}{2}\left[3I_{z'}^2 - I^2\right]$$

$$\overline{\omega_q} = \frac{e^2qQ}{2I(2I-1)}\left(\frac{3\cos^2\theta_{LD} - 1}{2}\right) \qquad [1.4.19].$$

In this regard, $\overline{\omega_q}$ is interpreted as being proportional to the small net projection of the axial component of the field tensor ($V_{zz}$ in the molecular frame) onto the laboratory axis. It would seem most convenient to seek solutions in the $|IM\rangle\langle IM'|$ basis as it is here that [1.4.19] is diagonal. However, specific solutions for $1 \leq I \leq 9/2$ have been presented and discussed in the multipole formalism *(37)* and a general solution for arbitrary spin $I$ has also been presented *(38)*. Explicit solutions relevant to this thesis will be developed in PART 2.

## Chapter 5. DENSITY MATRIX FOR A DISSIPATIVE SYSTEM

For a quantum mechanical system that is closed, or isolated from interactions with its surroundings, there exists a time independent Hamiltonian giving the time evolution of the system defined by the unitary transformation [1.3.24] or equivalently by the Liouville equation [1.3.27]. *(22)* Under such an evolution, pure states are always transferred into other pure states, meaning that mixtures are neither created nor destroyed. The conventional framework of spin dynamics in terms of some set of basis operators is an idealization, however, in that all physical systems are somehow interrelated and it is never possible to completely isolate a system. In this chapter, the interaction of a spin system with its surroundings is formally introduced. The Liouville equation describes a reversible time evolution of the microscopic particles. Since relaxation phenomena are macroscopic and irreversible, it is left to account for the gradual evolution of a spin system (typically polarized) towards thermal equilibrium. In a strict account, both lattice and spin states must be accounted for in a total density matrix as in [1.3.3].

### *Second Order Perturbation Formalism*

For a spin system $I$ interacting with some unobserved lattice $L$, a total Hamiltonian is given by

$$\mathcal{H} = \mathcal{H}_I + \mathcal{H}_L + \mathcal{H}_1 \qquad [1.5.1]$$

where $\mathcal{H}_0 = \mathcal{H}_I + \mathcal{H}_L$ is a static secular term acting on both the spin and lattice variables and $\mathcal{H}_1$ is a small time-dependent perturbation coupling the spin to the lattice. The equation of motion of the density matrix is, as suggested by [1.4.3] and [1.4.4]

$$i\hbar\frac{d\rho(t)}{dt} = \left[\mathcal{H}_0 + \mathcal{H}_1(t), \rho(t)\right] \qquad [1.5.2a]$$

or, in the interaction representation whereby $\hat{\mathcal{H}}(t) = e^{\frac{i}{\hbar}\mathcal{H}_0 t}\mathcal{H}e^{-\frac{i}{\hbar}\mathcal{H}_0 t}$

$$i\hbar\frac{d\hat{\rho}(t)}{dt} = \left[\hat{\mathcal{H}}_1(t), \hat{\rho}(t)\right] \qquad [1.5.2b].$$

Integrating [1.5.2b] from $t$=0 gives

$$\hat{\rho}(t) = \rho(0) - \frac{i}{\hbar}\int_0^t \left[\hat{\mathcal{H}}_1(t'), \hat{\rho}(t')\right]dt' \qquad [1.5.3].$$

Successive approximations are obtained by iteratively substituting $\hat{\rho}(t)$ for $\hat{\rho}(t')$ in [1.5.3]. To second order, this perturbative procedure yields

$$\hat{\rho}(t) = \rho(0) - \frac{i}{\hbar}\int_0^t \left[\hat{\mathcal{H}}_1(t'), \rho(0)\right]dt' + \left(\frac{i}{\hbar}\right)^2 \int_0^t\int_0^{t'} \left[\hat{\mathcal{H}}_1(t'), \left[\hat{\mathcal{H}}_1(t''), \rho(t'')\right]\right]dt''dt' \qquad [1.5.4]$$

and subsequently taking the time derivative gives

$$\frac{d\hat{\rho}(t)}{dt} = -\frac{i}{\hbar}\left[\hat{\mathcal{H}}_1(t), \rho(0)\right] + \left(\frac{i}{\hbar}\right)^2 \int_0^t \left[\hat{\mathcal{H}}_1(t), \left[\hat{\mathcal{H}}_1(t'), \rho(t')\right]\right]dt' \qquad [1.5.5].$$

*Conditions of Reversibility*

At this point, coupling of the two systems may still result in a reversible exchange of polarization, since no explicit allowance for irreversibility has been made. It is therefore assumed that $L$ has so many degrees of freedom the the effects of coupling with $I$ dissipate quickly enough for coherent energy transfer back into $I$ to be neglected. Thus, $L$ remains determined by a distribution of states in thermal equilibrium and any correlations ( beyond establishment of a spin temperature ) between $I$ and $L$ are ignored. In the absence of $\mathcal{H}_1$ (say at $t = 0$) the spins and lattice are uncoupled and the total density operator consists of a product $\rho(0) = \rho_I(0)\,\rho_L(0)$ of its spin and lattice contributions.

Under these conditions, the representation of the lattice is given by a Boltzmann distribution akin to [1.3.7]

$$\rho_L(0) = \frac{e^{-E^{(l)}/kT}}{\sum_l e^{-E^{(l)}/kT}} \qquad [1.5.6]$$

and a reduced spin density matrix $\rho_I(t)$ is formed by taking the trace over all lattice variables, hence

$$\underset{L}{tr}\ \rho(t) = \underset{L}{tr}\left\{\rho_I(t)\,\rho_L(0)\right\} = \rho_I(t) \qquad [1.5.7].$$

This is the basic condition of irreversibility, since the lattice is given by [1.5.6] at any time $t$. Recognizing the commutativity of the lattice and spin operators, expansion of [1.5.7] in the high temperature approximation indicates that, as regards [1.5.5], it is more suitable to consider not just the components of the spin density matrix, but the polarization relative to the thermal average $\langle\ \rangle_T$

$$\rho_I(t) \rightarrow \rho_I(t) - \left\langle \rho_I(0)\right\rangle_T \qquad [1.5.8].$$

*Time Correlation Functions and the Markoff Approximation*

In order to follow the details of the evolution of the density operator, it is now neccessary to consider an explicit form of the interaction Hamiltonian. It is assumed that $\mathcal{H}_1$ can be expanded into tensors of general rank

$$\mathcal{H}_1 = \sum_k F^{(k)} A^{(k)} \qquad [1.5.9]$$

where $F^{(k)}$ are the lattice operators and the $A^{(k)}$ are operators acting on the spin variables only. In the interaction representation

$$\hat{\mathcal{H}}_1(t) = \exp\left(\tfrac{i}{\hbar}\left(\mathcal{H}_I + \mathcal{H}_L\right)t\right)\mathcal{H}_1 \exp\left(-\tfrac{i}{\hbar}\left(\mathcal{H}_I + \mathcal{H}_L\right)t\right) = \sum_k F^{(k)}(t)\, A^{(k)}(t) \qquad [1.5.10a]$$

where

$$F^{(k)}(t)=\exp\left(\tfrac{i}{\hbar}\mathcal{H}_L t\right)F^{(k)}\exp\left(-\tfrac{i}{\hbar}\mathcal{H}_L t\right) \qquad [1.5.10b]$$

and

$$A^{(k)}(t)=\exp\left(\tfrac{i}{\hbar}\mathcal{H}_I t\right)A^{(k)}\exp\left(-\tfrac{i}{\hbar}\mathcal{H}_I t\right) \qquad [1.5.10c].$$

Substituting [1.5.10] and [1.5.7] into [1.5.5] and taking advantage of the fact that the $F^{(k)}$ and the $A^{(k)}$ commute gives

$$\frac{\partial\hat{\rho}_I(t)}{\partial t}=-\frac{i}{\hbar}\sum_k\left(\underset{L}{tr}\left\{F^{(k)}(t)\,\rho_L(0)\right\}\left(A^{(k)}(t)\,\rho_I(0)-\rho_I(0)A^{(k)}(t)\right)\right)$$

$$+\left(\frac{i}{\hbar}\right)^2\sum_{k,l}\int_0^t\left[\underset{L}{tr}\left\{F^{(k)}(t)F^{(l)}(t')\,\rho_L(0)\right\}\left(A^{(k)}(t)A^{(l)}(t')\,\rho_I(t')-A^{(l)}(t')\,\rho_I(t')A^{(k)}(t)\right)\right.$$

$$\left.-\underset{L}{tr}\left\{F^{(l)}(t')F^{(k)}(t)\,\rho_L(0)\right\}\left(A^{(k)}(t)\,\rho_I(t')A^{(l)}(t')-\rho_I(t')A^{(l)}(t')A^{(k)}(t)\right)\right]dt' \qquad [1.5.11].$$

The trace in [1.5.11] is defined in terms of the eigenstates of $\mathcal{H}_L$, defining the expectation value as,

$$\left\langle F^{(k)}(t)\right\rangle=\underset{L}{tr}\left\{F^{(k)}(t)\,\rho_L(0)\right\}=0 \qquad [1.5.12].$$

This vanishing time average causes $\hat{\mathcal{H}}_1(t)$ to have a vanishing ensemble average as well, equivalent to the assumption that $\hat{\mathcal{H}}_1(t)$ does not produce an average frequency shift. Such a restriction is somewhat misleading, however, as any stationary shift can be incorporated into a reconstituted $\mathcal{H}_0$ ( as will be illustrated in PART 2 ).

Of great physical importance are the time correlation functions

$$\left\langle F^{(k)}(t)F^{(l)}(t')\right\rangle=\underset{L}{tr}\left\{F^{(k)}(t)F^{(l)}(t')\,\rho_L(0)\right\} \qquad [1.5.13]$$

which describe the average correlation existing between physical interactions occurring at different times $t$ and $t'$. Variations of the perturbating Hamiltonian can be thought of as being due to some physical movement of the system. In [1.5.13] it is assumed that the ensemble average depends on $t$ and $t'$ only through the difference $\tau=t-t'$, indicative of a perturbation that is effectively stationary. *(39)* It has already been decided that the lattice quickly dissipates any effects of interaction with the spin system, that is to say, the lattice quickly "forgets" any such interactions and remains in equilibrium. Over some short time interval where molecular motions are not negligible, $\left\langle F^{(k)}(t)F^{(l)}(t-\tau)\right\rangle$ will be non-zero. However, as $\tau$ increases this correlation becomes progressivley diminished until, beyond some correlation time $\tau_c$, the lattice quickly loses all memory of its former self. Thus [1.5.13] has a maximum at $\tau = 0$ and vanishes for $\tau >> \tau_c$, in which case

$$\left\langle F^{(k)}(t)F^{(l)}(t-\tau)\right\rangle \approx \left\langle F^{(k)}(t)\right\rangle\left\langle F^{(l)}(t-\tau)\right\rangle = 0 \qquad [1.5.14].$$

The correlation time is a function of the lattice and intimately depends upon the nature of the system under observation. It might, for example, be interpreted as the mean time that a pair of nuclei are in close enough proximity to allow for interaction of their respective nuclei, before diffusing away. Any stress that would influence the efficacy of this mechanism would manifest itself as a change in the correlation time ( unless accounted for otherwise ).

It is, however, the macroscopic behaviour of the system on the time scale of spin dynamics that is of interest, rather than the detailed correlations of the fluctuating field. If $\tau_c$ is much smaller than some characteristic time for relaxation, required for $\hat{\rho}_I(t)$ to change appreciably, then

$$\hat{\rho}_I(t') = \hat{\rho}_I(t) \qquad [1.5.15]$$

which is a satisfactory result, since it is expected that $\hat{\mathscr{H}}_1(t)$ is small causing $\hat{\rho}_I(t)$ to vary slowly. Substitution of [1.5.15] into [1.5.11] is the Markoff approximation, implying that no attempt can be made to seek resolution of the dynamics of the system over short time intervals comparable to $\tau_c$. Taking into account the arguments introducing [1.5.14], the upper limit of integration of [1.5.11] may be extended to $t = \infty$ with negligible error under the Markoff approximation. Dropping the stationary terms [1.5.12] and recognizing that $d\tau = -dt'$, modifies [1.5.11] to give

$$\frac{\partial \rho_I(t)}{\partial t} = \frac{1}{\hbar^2}\sum_{k,l}\int_0^\infty \Big[\Big\langle F^{(k)}(t)F^{(l)}(t-\tau)\Big\rangle\Big(A^{(k)}(t)A^{(l)}(t-\tau)\,\rho_I(t) - A^{(l)}(t-\tau)\,\rho_I(t)A^{(k)}(t)\Big)$$

$$-\Big\langle F^{(l)}(t-\tau)F^{(k)}(t)\Big\rangle\Big(A^{(k)}(t)\,\rho_I(t)A^{(l)}(t-\tau) - \rho_I(t)A^{(l)}(t-\tau)A^{(k)}(t)\Big)\Big]d\tau \qquad [1.5.16].$$

Applying [1.5.10c] to the matrix elements between the eigenstates $|\alpha\rangle$ of $\mathcal{H}_I$ gives

$$\langle\alpha|A^{(k)}(t)|\alpha'\rangle = e^{i\omega_{\alpha\alpha'}t}\langle\alpha|A^{(k)}|\alpha'\rangle \qquad [1.5.17a]$$

for which

$$\hbar\omega_{\alpha\alpha'} = E_\alpha - E_{\alpha'} \qquad [1.5.17b].$$

Using this notation, the components of the correlation function are resolved

$$G_{\alpha\alpha'\beta\beta'}(\tau) = \sum_{k,l}\Big\langle\alpha\Big|A^{(k)}\Big|\alpha'\Big\rangle\Big\langle\beta'\Big|A^{(l)}\Big|\beta\Big\rangle\Big\langle F^{(k)}(t)F^{(l)}(t+\tau)\Big\rangle$$

$$= \sum_{k,l}\Big\langle\alpha\Big|A^{(k)}\Big|\alpha'\Big\rangle\Big\langle\beta'\Big|A^{(l)}\Big|\beta\Big\rangle g_{kl}(\tau) \qquad [1.5.18a],$$

the Fourier transform of which yielding the spectral density at frequency $\omega$

$$J_{\alpha\alpha'\beta\beta'}(\omega) = \int_{-\infty}^{\infty} G_{\alpha\alpha'\beta\beta'}(\tau)\,e^{i\omega\tau}\,d\tau \qquad [1.5.18b]$$

where even symmetry about the origin has been assumed for the correlation function. Combining [1.5.18], [1.5.17], [1.5.16] and [1.5.8] gives the final result

$$i\frac{\partial \rho_{I,\alpha\alpha'}(t)}{\partial t} = \omega_{\alpha\alpha'}\,\rho_{I,\alpha\alpha'}(t) + i\sum_{\beta,\beta'} R_{\alpha\alpha'\beta\beta'}\Big(\rho_{I,\beta\beta'}(t) - \Big\langle\rho_{I,\beta\beta'}(0)\Big\rangle\Big) \qquad [1.5.19]$$

where the Redfield relaxation matrix elements *(40)* are given as

$$R_{\alpha\alpha'\beta\beta'} = \frac{1}{\hbar^2}\Big[J_{\alpha\beta\alpha'\beta'}\Big(\omega_{\alpha'\beta'}\Big) + J_{\alpha\beta\alpha'\beta'}\Big(\omega_{\alpha\beta}\Big)$$

$$-\delta_{\alpha'\beta'}\sum_\gamma J_{\gamma\beta\gamma\alpha}\Big(\omega_{\gamma\beta}\Big) - \delta_{\alpha\beta}\sum_\gamma J_{\gamma\alpha'\gamma\beta'}\Big(\omega_{\gamma\beta'}\Big)\Big] \qquad [1.5.20].$$

( Note that high frequency oscillations have been neglected as only terms satisfying $\alpha - \alpha' = \beta - \beta'$ are expected to contribute to [1.5.16].

The elements $J_{\alpha\beta\alpha'\beta'}$ can be evluated by use of the Wigner-Eckart theorem [1.2.13]

$$J_{\alpha\beta\alpha'\beta'}\left(\omega_{\alpha\beta}\right) = \sum_n \left[ \int_{-\infty}^{\infty} e^{i\omega_{\alpha\beta}t} g_{\alpha\beta\alpha'\beta'}(t)dt \left\langle \alpha \middle| \mathcal{T}^{(k)-n} \middle| \beta \right\rangle \left\langle \beta' \middle| \mathcal{T}^{(k)n} \middle| \alpha' \right\rangle \right] \qquad [1.5.21a]$$

where

$$\left\langle I\alpha \middle| \mathcal{T}^{(k)n} \middle| I\beta \right\rangle = (-1)^{I-\alpha} \begin{pmatrix} I & k & I \\ -\alpha & n & \beta \end{pmatrix} \left\langle I \middle\| \mathcal{T}^{(k)} \middle\| I \right\rangle \qquad [1.5.21b]$$

and the reduced matrix element is as given in [1.2.14].

*Quadrupole Relaxation due to Molecular Reorientation*

Taking [1.5.9] to represent the tensor coupling between the nuclear spin and the electric field gradient at the nucleus

$$\mathcal{H}_Q = \sum_q F^{(2)q}(\Omega) A^{(2)q}(I) \qquad [1.5.22]$$

$$= \frac{e^2 qQ}{4I(2I-1)} \left[ A^{(2)0} + \frac{\eta}{\sqrt{6}} \left( A^{(2)2} + A^{(2)-2} \right) \right]$$

where the lattice and spin operators are both of rank $k = 2$ and $\Omega$ specifies the set of Euler angles defining the orientation of the molecule with respect to the laboratory frame. The spin operators are defined as

$$A^{(2)0} = 3I_z^2 - I(I+1)$$

$$A^{(2)\pm 2} = \frac{\sqrt{6}}{2} I_\pm^2 \qquad [1.5.23].$$

The lattice operators reflect the magnitude and symmetry of the electric field gradients. Taking the correlation function of the field gradients surrounding the nucleus as a simple exponential, identical for all tensor ranks

$$g_{\alpha\alpha'\beta\beta'}(\tau)=\sum_{k,l}\left\langle F^{(k)}(t)F^{(l)}(t+\tau)\right\rangle=\exp\left(\frac{-|t|}{\tau_c}\right) \qquad [1.5.24]$$

is a crude but reasonable approximation. The isotropic spectral densities at the Larmor frequency are then

$$J(n\omega_0)=\frac{1}{160}\left(\frac{eq^2Q}{I(2I-1)\hbar}\right)^2\left(1+\frac{\eta^2}{3}\right)\left(\frac{2\tau_c}{1+(n\omega_0\tau_c)^2}+i\frac{n\omega_0\tau_c^2}{1+(n\omega_0\tau_c)^2}\right)$$

$$=C\left(\frac{2\tau_c}{1+(n\omega_0\tau_c)^2}+i\frac{n\omega_0\tau_c^2}{1+(n\omega_0\tau_c)^2}\right) \qquad [1.5.25].$$

Here $C$ is the second order quadrupolar interaction constant. The real part of [1.5.25] contributes to the relaxation while the imaginary part is a small second order dynamic frequency shift.

# PART 2

# MULTIPLE QUANTUM FILTERED NMR STUDIES OF $I = 3/2$ NUCLEI IN BIOLOGICAL SYSTEMS: EXPERIMENTAL EVIDENCE AND THEORETICAL LINE SHAPE ANALYSES DESCRIBING ORIENTATIONAL ANISOTROPY

## Chapter 1. INTRODUCTION

The application of NMR methods to problems in cellular biology has significantly contributed to the evolution of the modern concept of the cell. One area of interest that has enjoyed a renaissance of late concerns itself with the environments and dynamics of the ions found in the proximity of the cell membrane; most notably $^{23}Na^+$ and $^{39}K^+$ (both $I = 3/2$ ). Nuclear magnetic relaxation of quadrupolar ions provides a sensitive method for studying the ion binding properties on a molecular level, in colloidal and other macromolecular systems. For example, the composition of the fluid within the cell differs markedly from that of its natural medium. The intracellular cytosol contains a host of proteins and other macromolecules that endow it with a much more viscous consistency and suggest differential, possibly identifiable, binding sites within the cell. The cell membrane itself is also the object of many investigations as its role in the regulatory processes of the cell continues to emerge. Transmembrane ionic gradients can be measured using methods that can distinguish between intracellular and extracellular ion pools. Thus, differences in NMR visibility of the ions in question would presumably become manifest in the NMR signal. *(42)* Since the earliest experiments *(43–45)* the challenge has been to identify and characterize the ion binding sites, with the aim of developing a non-invasive methodology for studying cellular ionic processes and to produce a physical model of ion binding sites. ( Without committing to a definition of "binding", the term will be used to describe some association resulting in restricted molecular motion. )

The common assumption in these experiments is that the ions are in large excess relative to the available binding sites and a substantial fraction of these ions are in an aqueous isotropic environment. It is reasonable to assume that these "free" ions undergo chemical exchange with the ions associated with a macromolecule or the cell membrane. Overall relaxation characteristics of the ions under consideration are thus strongly affected by the occurrence of said bound states, exchange dynamics, local fields and molecular motion, providing a link between the spin dynamics and the molecular properties of the system.

Redfield theory is often sufficient to describe the spin relaxation of quadrupolar nuclei. In isotropic phase, where the residual quadrupolar interaction is averaged to zero ($\overline{\omega_q} = 0$), Redfield theory applies to all but those systems characterized by very long rotational correlation times, $\tau_c$. *(46, 47)* Provided $\tau_c$ is not in the extreme narrowing limit, it is possible to induce the formation of multiple quantum (MQ) coherences in an NMR experiment owing to the presence of multiexponential relaxation. *(46)* Coupled relaxation transfers magnetization in higher rank multipoles which can subsequently transformed into MQ coherences by r.f pulses. Multiple quantum filtered (MQF) experiments, consisting of appropriate pulse sequences and phase cycling, may thus be used to directly distinguish pools in which the nuclei are bound or otherwise associated with slowly rotating macromolecules, since single exponentials describe the uncoupled relaxation of the free spin concentration . In many cases the static quadrupolar interaction term of the Hamiltonian contains a contribution from a non-zero quadrupole splitting resulting from an anisotropic distribution of the electric field gradients (EFG) in the sample. In a macroscopically oriented sample with local anisotropy, a static quadrupole splitting results if the diffusion of the spin-bearing particle is slow, i.e., the residence time within each "domain" is much longer than the inverse of the quadrupole splitting. In this context, "domain" may be a microcrystallite as in some liquid crystal samples *(48)* or may be a nomer for the long orientational correlation length of some biomolecular associations. The splitting within one domain is then determined by the orientation with respect to the external magnetic field and the spectrum is the average over many domains.

Observations from some MQF experiments of biological tissue are best interpreted in the context of this latter example. *(42, 49-51)* Rooney and Springer have produced an exhaustive review of tissue resonances of $I = 3/2$ nuclei *(52, 53)* where the influence of a residual quadrupole is discussed from an experimental perspective. Subsequent efforts describe specific studies of $^{23}Na^+$ in biological systems. *(54)* More general considerations include chemical exchange between the bound sites and the isotropic surroundings; some theoretical studies examine the modulation of both $\overline{\omega_q}$ and $\tau_c$ by chemical exchange by means of a discrete exchange model (DEM). *(55-58)* This allows discussion of the intermediate and slow exchange regimes since in the fast exchange limit, macroscopic parameters are found to be weighted averages of the exchanging sites *(56, 58)* and may therefore be discussed in the context of Redfield theory. Eliav and Navon have defined the limits of Redfield theory *(58)* in terms of the MQF experiment by extending their general treatment of the quantum Liouville equation to describe the contributions of the higher quantum coherences to the line shapes of a single spin pool over a range of $\tau_c$ values for an isotropically oriented system.

This section will summarize the experimental methods used and observations made in the more recent NMR studies of $^{23}Na^+$ ion environments. Despite the large number of NMR experiments conducted and the diverse biological systems observed, a rather limited amount of information can be extracted from such a study without a detailed understanding of the dynamics of the spin system. The major theoretical models currently exploited to help explain the experimental findings will also be discussed as well as the method developed by the author to simulate these $^{23}$Na line shapes.

Nuclei with electric quadrupole moments ( $I > 1/2$ ) are usually strongly affected by interactions with electric field gradients to the extent that this mechanism dominates the evolution of the quadrupolar nucleus. These interactions harbour much information regarding the dynamics of the spin system under investigation that cannot be tapped by the typical single quantum experiment. The isolated $I = 3/2$ nucleus can, in principle, undergo single, double and triple quantum NMR transitions ( see Figure 2.3 ). The states involved in these transitions may be brought into coherent superposition by suitable manipulation of the system, which is the realm of multiple quantum NMR. *(21)* In isotropic phase where the extreme narrowing condition is met i.e. the correlation time of the fluctuating field that induces relaxation is much shorter than the inverse of the Larmor frequency, $\omega_0\tau_c << 1$, the expressions for the longitudinal and transverse relaxation rates may only be described by single exponential decays. *(30, 59, 60)* However, if the nuclei are associated with macromolecules or are subject to the conditions of similarly motionally constrained environs in which the correlation time becomes more appreciable, the coupled relaxation is multi-exponential and MQ coherence transfer processes become possible even in the absence of splittings.

In an ordered environment where the principal axes of the EFG tensor are frozen in a narrow distribution of orientations with respect to the magnetic field, the typical single quantum NMR spectrum consists of a sharp central component (representing the transition between the $|1/2\rangle$ and $|-1/2\rangle$ states) accounting for 40% of the total signal intensity flanked by two broader components (the $|\pm3/2\rangle \leftrightarrow |\pm1/2\rangle$ transitions) with 30% intensity each. The result is a single crystal type spectrum of three lines split by a residual quadrupolar coupling constant $\overline{\omega_q}$. If $\tau_c$ is still much shorter than the inverse frequency of this interaction, the EFG may become partially averaged, however the time averaged value of $\overline{\omega_q}$ will still be non-zero. This is the situation observed in oriented liquid crystals and oriented biopolymers. *(61)*

It is much more common in biological samples to observe unoriented, macroscopically isotropic sodium environments. Here, the effective EFG axes have random orientations relative to the magnetic field and the contributions to the line shape and the mechanism inducing MQ coherences must be carefully distinguished. In one extreme $\tau_c >> \overline{\omega_q}^{-1}$ and the single quantum spectrum is a superposition of the centre line and a number of satellites resulting from a distribution of randomly oriented nuclei; a so called powder pattern. In the other extreme $\tau_c << \overline{\omega_q}^{-1}$. Again, provided that the correlation time does not follow the extreme narrowing limit, both longitudinal and transverse processes exhibit multiexponential behaviour. The resulting single quantum spectrum consists of a superposition of narrow (40%) and broad (60%) lines at or near the same resonant frequency. MQ coherences can be induced in this case owing to the multiexponential relaxation even though the residual quadrupole coupling approaches zero. *(62, 63, 46)*

The MQ NMR results from the biological samples reported here display behaviour consistent with this last class of conditions. There exists a residual quadrupolar coupling that is typically less than a line width and a correlation time that is not in the extreme narrowing limit. Dependence of these results on such seemingly benign considerations such as sample preparation reflect the inherent sensitivity of the experiment on the quadrupolar interactions. It is the origins of these interactions on a cellular level that the theoretical models hope to identify.

The state multipole formalism *(37, 64, 66)* describes the evolution of a spin system in a multi-pulse NMR experiment. Relaxation under the Redfield operator of an isotropic system has been described in the multipole basis *(66)* and the evolution of the tensors corresponding to higher quantum coherences for $I \leq 9/2$, in the absence of relaxation, has been explored. *(65)* More recently, Furó and Halle have investigated the spin relaxation of nuclei in anisotropic systems in two dimensional quadrupolar echo *(67)* and inversion recovery *(68)* experiments using the multipole formalism. They have also developed a theoretical framework for the use of MQF for the detection of the evolution of various MQ coherences, *(60)* again in the multipole basis. While the Redfield superoperator was used to describe spin relaxation, Furó *et al.* ignored contributions from the off-diagonal elements of the resulting relaxation matrices, assuming that the various components of the observable magnetization were uncoupled. The resulting rate equations for the components of the spin density matrix then relax independently and can be solved separately. However, for cases in which $\overline{\omega_q}$ is less than the line width of the central line, this approximation will not adequately describe the spin dynamics, since the magnitudes of both $\tau_c$ and $\overline{\omega_q}$ contribute to the resonant lineshape. For example, we have found that the second rank tensor generated in an MQF experiment, the presence of which is the direct result of an orientationally anisotropic environment, displays strikingly rich behavior at small $\overline{\omega_q}$ values that can be accounted for only if the contributions from these off diagonal matrix elements of the Redfield equation are considered.

## Chapter 2. MULTIEXPONENTIAL RELAXATION IN I=3/2 SYSTEMS

In order to motivate discussion of relaxation processes, the results from a standard Redfield relaxation treatment are applied to a simple one pulse experiment. As mentioned previously, for $I = 3/2$ systems for which $\overline{\omega_q} = 0$, there are three degenerate single quantum transitions. Using the formalism of Jaccard *et al. (46)* the spin density matrix $\hat{\rho}(t)$ may be expanded in terms of the single element product operators.

$$\hat{\rho}(t) = \sum \hat{\rho}_{rs}(t)|r\rangle\langle s| \qquad [2.2.1].$$

The coefficients $\hat{\rho}_{rs}(t)$ of the product operators represent the elements of the density matrix in the interaction representation of the free precession Hamiltonian as in [1.4.3]. The four eigenstates can be re labeled; $|1\rangle = |3/2\rangle$, $|2\rangle = |1/2\rangle$, $|3\rangle = |-1/2\rangle$, $|4\rangle = |-3/2\rangle$ giving a set of coupled differential equations for the evolution of the single quantum elements.

$$\begin{pmatrix} \frac{d\hat{\rho}_{12}(t)}{dt} \\ \frac{d\hat{\rho}_{23}(t)}{dt} \\ \frac{d\hat{\rho}_{34}(t)}{dt} \end{pmatrix} = R^{(1)} \begin{pmatrix} \hat{\rho}_{12}(t) \\ \hat{\rho}_{23}(t) \\ \hat{\rho}_{34}(t) \end{pmatrix} \qquad [2.2.2]$$

for which the Redfield relaxation matrix in the single quantum manifold is calculated from [1.5.20]

$$R^{(1)} = C \begin{pmatrix} -(J_0 + J_1 + J_2) & 0 & J_2 \\ 0 & -(J_1 + J_2) & 0 \\ J_2 & 0 & -(J_0 + J_1 + J_2) \end{pmatrix} \qquad [2.2.3].$$

As per [1.5.24], $C$ is the second order qudrupolar interaction constant and real parts of the spectral densities that contribute to relaxation are defined as

$$J_n = \frac{2\tau_c}{1+\left(n\omega_0\tau_c\right)^2} \qquad [2.2.4].$$

Diagonalization of [2.2.2] leads to a decoupled set of differential equations and the time dependence of the single quantum (SQ) elements.

$$\begin{pmatrix} \frac{d\hat{\rho}_1^{(1)}(t)}{dt} \\ \frac{d\hat{\rho}_2^{(1)}(t)}{dt} \\ \frac{d\hat{\rho}_3^{(1)}(t)}{dt} \end{pmatrix} = R_{diag}^{(1)} \begin{pmatrix} \hat{\rho}_1^{(1)}(t) \\ \hat{\rho}_2^{(1)}(t) \\ \hat{\rho}_3^{(1)}(t) \end{pmatrix} \qquad [2.2.5]$$

with

$$R_{diag}^{(1)} = \begin{pmatrix} R_1^{(1)} & 0 & 0 \\ 0 & R_2^{(1)} & 0 \\ 0 & 0 & R_3^{(1)} \end{pmatrix} \qquad [2.2.6].$$

Each combination of coupled SQ coefficients follows an exponential decay

$$\hat{\rho}_n^{(1)}(t) = \hat{\rho}_n^{(1)}(0)\exp[R_n^{(1)}t] \qquad [2.2.7]$$

with the following rate constants.

$$\begin{aligned} R_1^{(1)} &= -C(J_0+J_1), \quad \hat{\rho}_1^{(1)} = \frac{1}{\sqrt{2}}(\hat{\rho}_{12}+\hat{\rho}_{34}) \\ R_2^{(1)} &= -C(J_1+J_2), \quad \hat{\rho}_2^{(1)} = \hat{\rho}_{23} \qquad [2.2.8] \\ R_3^{(1)} &= -C(J_0+J_1+2J_2), \quad \hat{\rho}_3^{(1)} = \frac{1}{\sqrt{2}}(\hat{\rho}_{12}-\hat{\rho}_{34}) \end{aligned}$$

This is the simplest derivation of an evolution matrix that may be applied with some success to the problem at hand. It is limited in that it cannot account for the residual quadrupolar coupling and the dynamic effects that ensue. However, it does serve to illustrate the features of the dynamics of the $I = 3/2$ nucleus. The sum of the 12 and 34 satellite transitions in an isotropic medium decays by $\exp\left(R_1^{(1)}t\right)$ while the centre 23 transition follows $\exp\left(R_2^{(1)}t\right)$. From this example it can be seen directly that in the extreme narrowing limit, from [2.2.4] $J_0 = J_1 = J_2 = 2\tau_c$ and the elements $\hat{\rho}_1^{(1)}$ and $\hat{\rho}_3^{(1)}$ decay with the same rate. However, inducing the formation of MQ coherences in the absence of a residual quadrupolar splitting is incumbent upon the existence of multi-exponential relaxation, as will be presently illustrated. Evolution in the other $q$-quantum manifolds can be derived in an exactly analogous manner to give expressions for $T_1$ ( spin-lattice relaxation of the populations in the zero quantum manifold ) and analytical expressions for relaxation in an arbitrary pulse sequence.

The density matrix may also be expressed in terms of normalized irreducible tensor operators, *(8, 9, 70)* which provide a more physically intuitive model of the spin dynamics. After an initial $(\pi/2)_y$ hard pulse applied to a system in thermal equilibrium (corresponding to a right-handed rotation of the component of magnetization parallel to the external field about the positive $y$ axis ), the state of an $I = 3/2$ system is ( [1.2.11] )

$$\hat{\rho}(0^+) \propto I_x = \sqrt{5/2}\left(\mathcal{T}^{(1)-1} - \mathcal{T}^{(1)+1}\right) \qquad [2.2.9]$$

where the factor recognizing the normalization of $N$ spins has been omitted. Without loss of generality, the contribution of the $q = +1$ transition need only be considered

$$\sqrt{\frac{5}{2}}\mathcal{T}^{(1)1} = -\frac{1}{2}\left(\sqrt{3}|1\rangle\langle 2| + 2|2\rangle\langle 3| + \sqrt{3}|3\rangle\langle 4|\right) \qquad [2.2.10a]$$

clearly showing that the single element operators appear with relative intensities 3:4:3. While only the $k = 1$ operator is present immediately following the pulse, coupling mechanisms can induce the formation of the higher rank tensors.

$$\mathcal{T}^{(2)1} = \frac{1}{\sqrt{2}}\left(|2\rangle\langle 3| - |3\rangle\langle 4|\right) \qquad [2.2.10b]$$

$$\mathcal{T}^{(3)1} = \frac{2}{\sqrt{5}}\left(|1\rangle\langle 2| - \sqrt{3}|2\rangle\langle 3| + |3\rangle\langle 4|\right) \qquad [2.2.10c]$$

Yet, given the symmetry of [2.2.3], the coefficient of $\mathcal{T}^{(2)1}$ will be non-vanishing only if the coherences associated with the outer transitions decay unequally. The time evolution of [2.2.9] is found by incorporating [2.2.8]

$$\hat{\rho}^{(+1)}(t) = \frac{\sqrt{3}}{2}\left(|1\rangle\langle 2| + |3\rangle\langle 4|\right)\exp[R_1^{(1)}t] + |2\rangle\langle 3|\exp[R_2^{(1)}t] \qquad [2.2.11]$$

or, in the tensor operator basis

$$\hat{\rho}^{(+1)}(t) = -\frac{1}{\sqrt{10}}\left[\mathcal{T}^{(1)1}\left(3\exp[R_1^{(1)}t] + 2\exp[R_2^{(1)}t]\right) + \frac{\mathcal{T}^{(3)1}}{\sqrt{6}}\left(\exp[R_1^{(1)}t] - \exp[R_2^{(1)}t]\right)\right]$$

[2.2.12].

Both transverse and longitudinal relaxation are characterized by two relaxation rate constants. From [2.2.8] the relevant terms corresponding to the "fast" and "slow" relaxing components for $T_2$ processes are

$$R_1^{(1)} = \frac{1}{T_{2f}} = -C\left(J_0 + J_1\right) \qquad R_2^{(1)} = \frac{1}{T_{2s}} = -C\left(J_1 + J_2\right) \qquad [2.2.13].$$

From the evolution of the polarizations in the zero quantum manifold *(46)* can be derived the $T_1$ rate constants

$$R_1^{(0)} = \frac{1}{T_{1f}} = -2CJ_1 \qquad R_2^{(0)} = \frac{1}{T_{1s}} = -2CJ_2 \qquad [2.2.14].$$

Equation [2.2.12] describes the transfer of coherence from the $k = 1$ to the $k = 3$ tensors in the single quantum manifold due to the effects of biexponential relaxation. The dipole operator ( rank one ) is responsible for the directly observable transverse magnetization while the presence of the third rank tensor, or octupole spin operator, implies that MQ coherences are accessible *via* the application of subsequent r.f. pulses. The degree to which the signal is represented by the third rank tensor is proportional to the difference between the two single quantum rates. Ions which are subject to strong relaxation ( and hence, may exhibit lower NMR "visibility" ) will contribute more strongly to the DQ signal than those ions which are weakly relaxed ( and more visible ). In the fast motion regime, when the three relaxation eigenvectors are equal, the third rank tensor is not produced. The absence of a second rank tensor is a direct result of an isotropically averaged quadrupole coupling, a primary assumption in the above development. Clearly, the effects of orientational anisotropy must be considered in a full development of the dynamics of this spin system.

# Chapter 3. RESULTS FROM THE MQF EXPERIMENT

The MQF sequence consists of four pulses

$$D\left(0,\tfrac{\pi}{2},0\right)-\tfrac{\tau}{2}-D(0,\pi,0)-\tfrac{\tau}{2}-D(\beta,\varphi_1)-\dot{\sigma}-D(\beta,\varphi_2)-AQ(t) \qquad [2.3.1].$$

Details of the evolution of the components of the spin operators will be discussed in the next section. For now, suffice it to say that multiple quantum coherences are developed subsequent to the third pulse and that the contributions to any $q$-quantum manifold may be isolated by apropriate phase cycling of angles $\varphi_n$.

With the production of higher rank tensors it is possible to filter biexponentially relaxing nuclei through a state of multiple quantum coherence. *(63, 46)* MQF methods may thus be used to directly distinguish between intracellular and extracellular sodium environments as the latter are almost invariably in the extreme narrowing region. More precisely, only those sites on which the ion is somewhat motionally hindered will contribute to a multiquantum signal. In the original papers describing these experiments both the double and triple quantum filter ( TQF ) techniques have been described in detail. *(63, 46)* It has been shown that the triple quantum experiment generally enjoys an increase in S/N, compared to DQF experiments. *(70)* However, the DQ analogue has been used almost exclusively, presumably in anticipation of the production of a second rank tensor contribution to the line shape, but also because of single quantum leakage arising from experimental "non-idealities".

Sodium and potassium are distributed inhomogeneously in tissue; the sodium concentration is lower inside cells than outside while the reverse is true for potassium. These ionic gradients are supported by metabolic processes and are sensitive to cell injury. As alluded to previously, differences in the NMR visibility of these ion pools could possibly provide a non-invasive means to monitor intracellular and extracellular ions. One non-invasive approach would be to utilize the strong dependency of the quadrupolar signals on relaxation rates. While there is no direct evidence to date that the ion pools can be so distinguished, transient decreases in the $^{23}$Na signal from cat brain undergoing seizures have been reported, *(71)* but the technique has not met with universal success and may not be a reliable method for the study of *in vivo* ion gradients. Another study on *in situ* rat brain notes changes upon death in the DQ NMR signal that are consistent with differential relaxation. *(42)* After death the line shape is typical for a biexponentially relaxing nucleus, going through a maximum for some optimal preparation time. Before death, however, the line shape can no longer be fully described by a biexponential relaxation model as it adopts what appears to be a dispersive component. The change is presumably due to the breakdown of the metabolically sustained ionic gradients, with more pronounced differences noted in the DQ experiments. In these results reported by Lyon *et al. (42)*, in contrast to the small decreases observed in single pulse spectrum following death, large increases are observed in the DQF sodium spectra. This is consistent with an influx of sodium into the cell following death. If quadrupolar relaxation is more effective for intracellular sodium than for the extracellular pools, the intracellular sodium would have a reduced visibility in the single pulse spectrum and an enhanced DQ signal owing to greater production of the third rank tensor.

One proven, but invasive, method involves the use of shift reagents: chelating agents that change the chemical shift of the ion of interest. Their effect on the physiological processes of the cell are poorly understood but they do serve to effectively distinguish intracellular and extracellular ion pools. Experimental results produced in collaboration with Dr. Joe Tauskela ( then of the Montréal Neurological Institute ) are now introduced. *(72)* Figure 2.1a shows the effect of addition of the shift reagent $Dy(PPP)_2^{7-}$ on the single quantum spectrum of $^{23}$Na in human red blood cells. The shift reagent does not permeate the cell membrane and thus isolates the intracellular signal from extracellular signal. Nystatin is a substance known as an ionophore which breaks down the physiologically maintained ionic gradients, thus simulating the death of the cell and reproducing the requisite influx of $Na^+$, as discussed above. Both signals contain the membrane bound contribution and that from the isotropic medium. Figure 2.1b shows a DQF experiment ( which excludes the free sodium ) with the evolution time $\tau = 0.014s$, performed on the same sample. Prior to the general acknowledgement of the influence of orientational anisotropy on such lineshapes, the experimental protocol for the determination of transmembrane ionic gradients consisted mainly of relating the net change in the DQ signal, upon the addition of Nystatin, to changes in the concentrations of bound sodium in the cell. This technique of relating the signal amplitude to chemical concentration, works reasonably well for narrow lines consisting of contributions with the same relaxation characteristics. However, as Figure 2.1c shows, for shorter values of the evolution time there exists an additional contribution to the signal that is out of phase with the previously well-explained DQ signal. Here the signal amplitude is a meaningless parameter, without a proper account of the origins of all contributions to the resonant line. Figure 2.2 shows the results of a similar experiment, with the addition of a relaxation reagent that effectively removes the contribution from the sodium bound to the external cell wall. At short evolution times, the frequency domain spectra consistently display two independently relaxing contributions. It is interesting to note that in order for these results to be reproduced, the red blood cell sample must be centrifuged, thus packing these disc shaped bodies and imparting some degree of orientational order.

The production of even rank tensors in these experiments is thus experimental evidence for the existence of order in biological tissues. In the study by Lyon *et al. (42)* these anomalous line shapes were tentatively ascribed to dispersive contributions. Almost identical line shapes have been observed in the inversion-recovery experiments performed

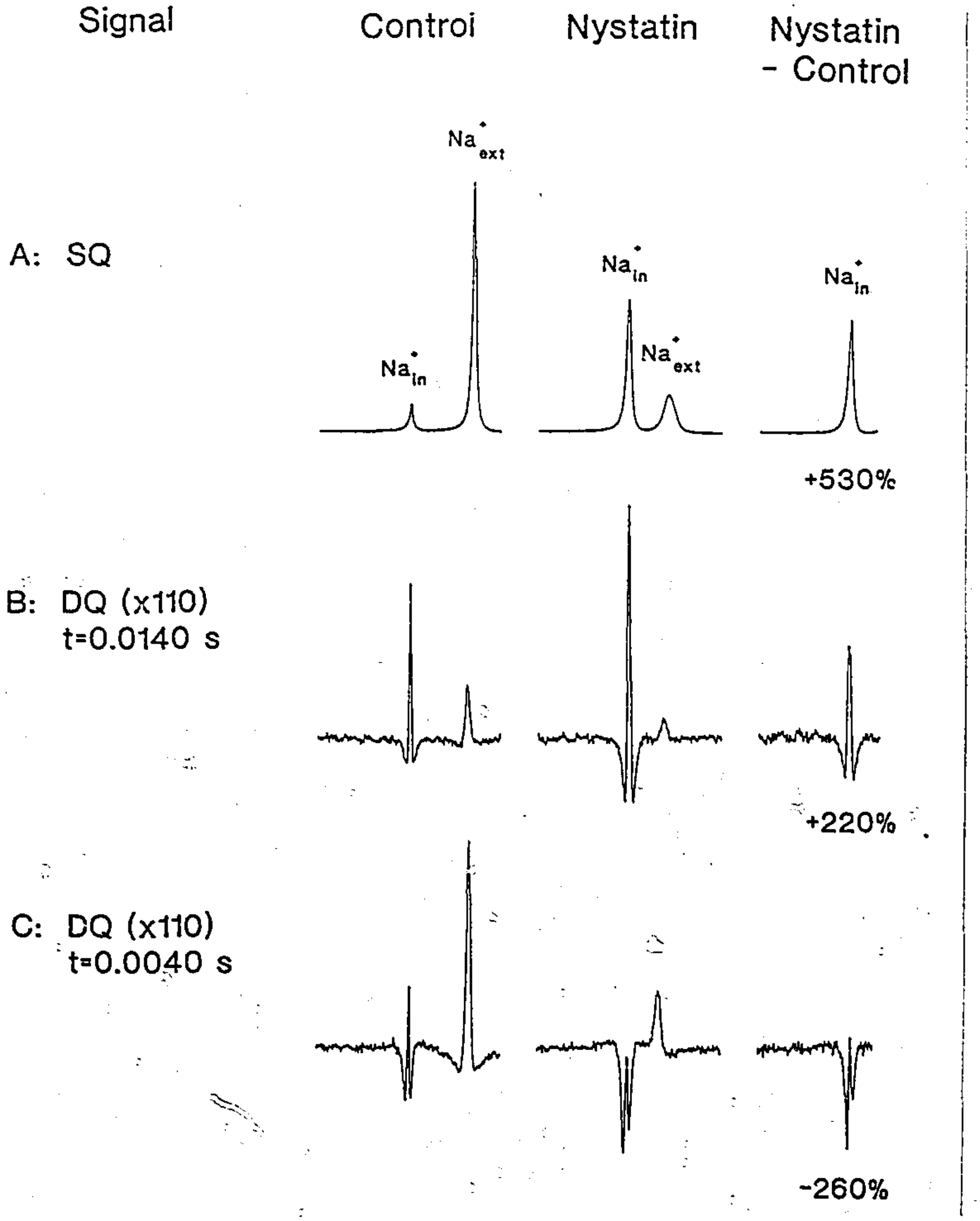

Figure 2.1. Single quantum ( SQ ) and double quantum ( DQ ) spectra of Na in human red blood cells *(72)*. Addition of a shift reagent to the sample isolates the contributions from the intracellular and extracellular spin pools, while Nystatin breaks down the metabolically sustained transmembrane ion gradients, simulating the death of the cell. At short MQ preparation times, the DQ signal adopts what appears to be a dispersive component.

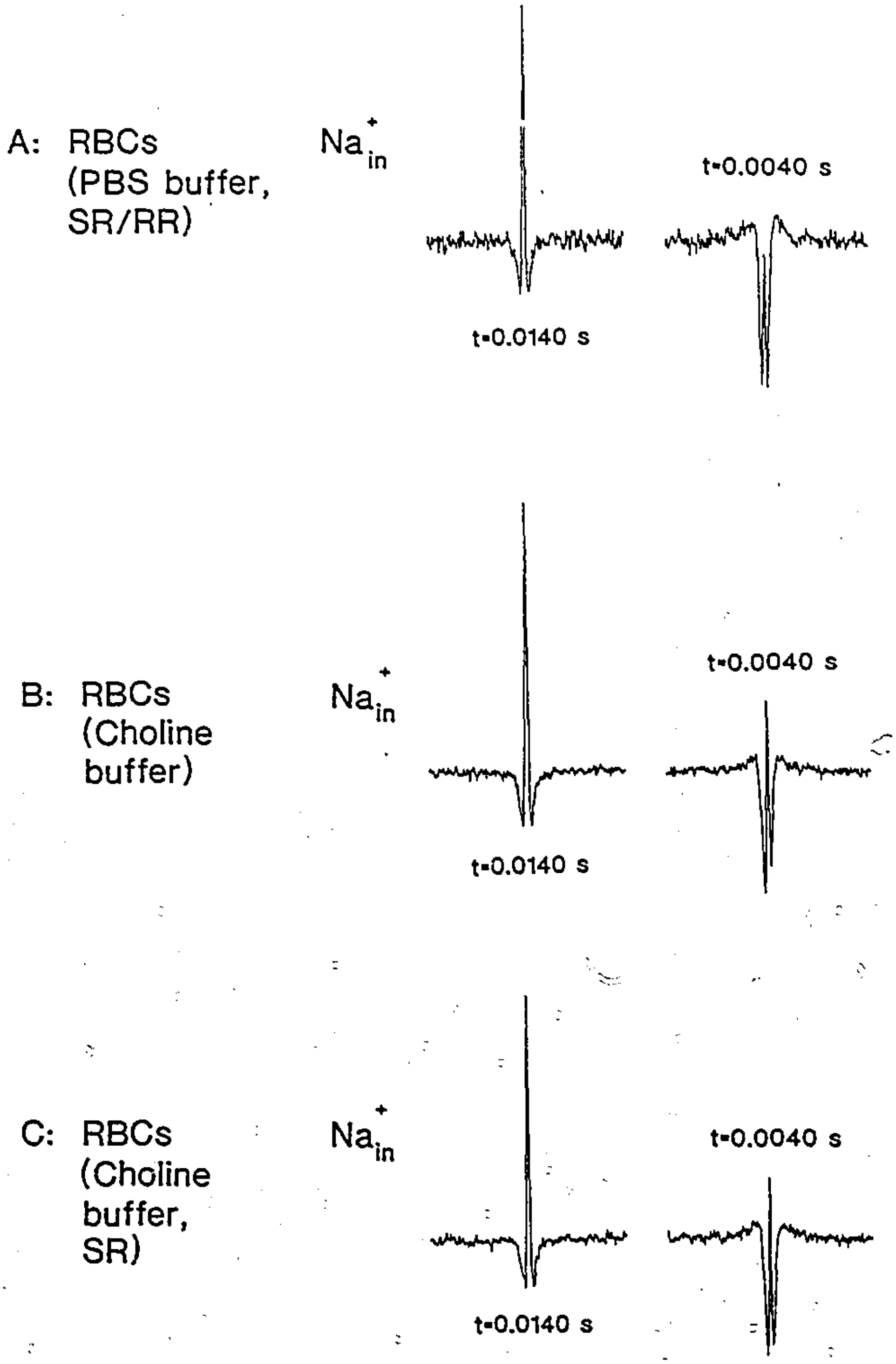

Figure 2.2. DQF spectra of human RBC's in the presence of a relaxation reagent that removes the contribution from the ions bound to the external cell wall. At short MQ preparation times the spectra consistently display two distinct contributions to the signal. *(72)*

by Price *(73, 74)* on LiCl owing to a combination of dynamic frequency shifts and dispersive components near the null point. In the case of the biological samples discussed here, the dependence of the ratio of the broad and narrow components of the line on $\tau$ can only be explained by the production of a second rank tensor and thus indicate the presence of orientational anisotropy.

# Chapter 3. SIMULATION OF THE MQF EXPERIMENT

Here, solutions for the time evolution and relaxation of the eigenvectors of the spin density matrix for $I = 3/2$ subject to a residual quadrupole coupling, are given. Cast into the multipole basis, the resulting rate equations may be conveniently used to generate an analytical response function to a general h[illegible]ulse sequence. The response to a typical MQF experiment is dicussed in the contex[illegible]e tensorial contributions to the line shape.

## *Equations of Motion*

Applying the high field approximation, the Liouville superoperator [1.3.27] is diagonal in the direct product basis. The static quadrupole coupling is introduced as a first order perturbation of these stationary states. Assuming the relaxation may be sufficiently described by Redfield theory, the evolution of the spin density operator in the absence of an oscillating r.f. field is governed by

$$i\frac{\partial \rho}{\partial t} = \mathcal{L}\rho - iR\rho \qquad [2.3.1]$$

where $\mathcal{L}$ is generated by the static Zeeman interaction and the secular contributions from the quadrupolar Hamiltonian [1.4.19]

$$\mathcal{L} = \frac{1}{\hbar}\left[\mathcal{H}_0 + \left\langle \mathcal{H}_Q \right\rangle, \ \right] \qquad [2.3.2].$$

The effect of this splitting on the stationary states of $I = 3/2$, along with the convention used for labelling these states, is shown in Figure 2.3. Relaxation is treated as a second order perturbation, as discussed in § 1.5, and The Redfield relaxation superoperator, $\boldsymbol{R}$, factors into distinct blocks for each of the four possible $n$-quantum manifolds of the $I$=3/2

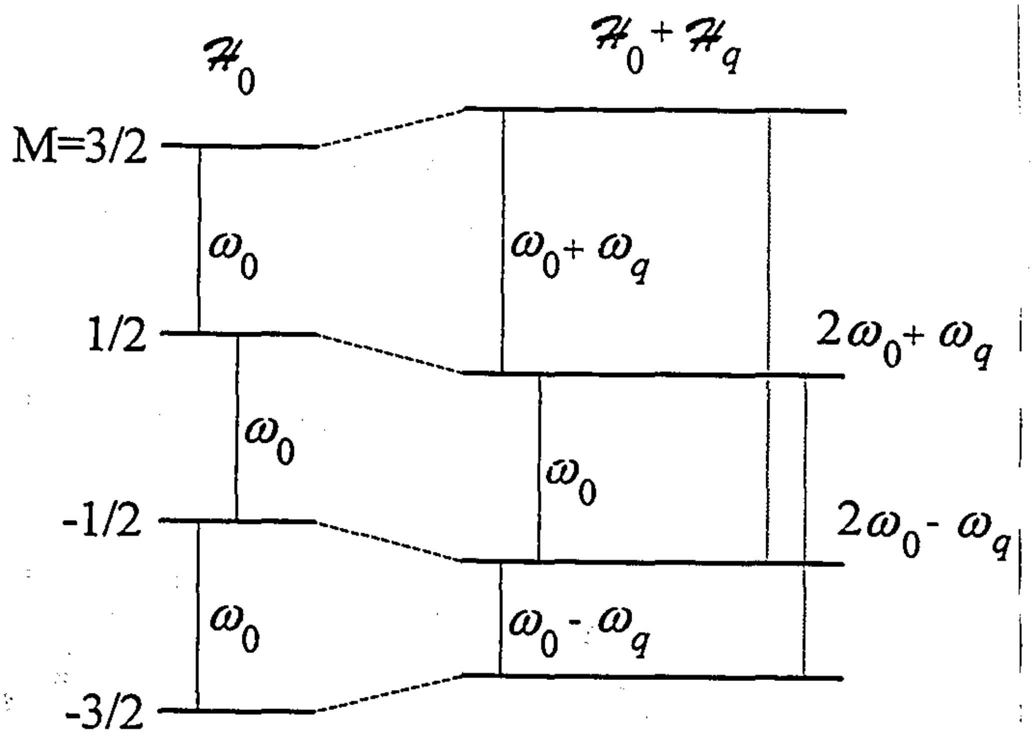

Figure 2.3. Schematic representation of the $I$ = 3/2 energy eigenvectors subject to a residual quadrupolar splitting showing the various multi-quantum frequencies.

spin, with matrix elements given by [1.5.20]. (These have been given elsewhere for the $I$ = 3/2 case *(60)*, however, a MAPLE routine has been developed for determining [1.5.20] for general $I$ and is given as an appendix to this thesis. ) The spin density operator is expanded in terms of the product operators as in [2.2.1] ( but not in the rotating frame),

$$\rho(t) = \sum \rho_{rs}(t)|r\rangle\langle s| \qquad [2.3.3]$$

with the time dependence being contained exclusively in the coefficients $\rho_{rs}(t)$. Unlike the Liouville superoperator, the relaxation matrix has off-diagonal terms involving the non-secular spectral densities $J_1$ and $J_2$ which couple the operators governing the relaxation of the satellite lines. *(75)* If the $\overline{\omega_q}$ is large relative to the width of the central line then the elements of the equation of motion [2.3.1] decouple and may be treated independently. *(67)* For the quadrupolar spin in an orientationally ordered environment, the spectral degeneracy of the $2I$+1-$n$ $n$-quantum coherences is lifted for any $\overline{\omega_q} \neq 0$ ( see Figure 2.3 ). Incorporating the effects of this residual $\overline{\omega_q}$ gives for the evolution of the single quantum coefficients

$$-(i\mathcal{L}+R) = C\begin{pmatrix} -i\left(\omega_0' + \omega_q'\right) - \left(J_0 + J_1 + J_2\right) & 0 & J_2 \\ 0 & -i\omega_0' - \left(J_1 + J_2\right) & 0 \\ J_2 & 0 & -i\left(\omega_0' - \omega_q'\right) - \left(J_0 + J_1 + J_2\right) \end{pmatrix} \qquad [2.3.4].$$

For convenience the resonant frequencies have been reduced by $C$, i.e.,

$$\omega_q' = \frac{\overline{\omega_q}}{C} \qquad \omega_0' = \frac{\omega_0}{C} \qquad [2.3.5].$$

In the treatment of the isotropic case $\mathcal{L} = \omega_0 E$ where $E$ is the unit matrix, $i\mathcal{L}$ and $R$ may then be treated and solved separately as shown in § 2.2. To reiterate, the off-diagonal relaxation terms are relevant whenever the detected quadrupolar splitting is comparable to, or less than, the width of the central line. In systems where all spins are homogeneously oriented relative to some external reference axis, as in crystals and oriented liquid crystals, there exists a single valued $\omega_q$. In samples exhibiting local anisotropy *(47)*, the splitting observed in the laboratory frame is an average over all possible alignments of the local director of the EFG. However, if the splitting shown by the "powder" peaks is large the relative weight of regions exhibiting a small $\omega_q$ is minor. Orientations in a heterogeneous environment can be assumed to follow a distribution about the mean value $\overline{\omega_q}$ with a width $\Delta\omega_q$. Taking chemical exchange into consideration, if exchange of a single spin between anisotropic sites with different $\omega_q$ values is assumed to be slow, then the observed value of $\overline{\omega_q}$ is one that is moderated by exchange with unbound fraction.

The spectral densities that determine the evolution of the diagonal terms in [2.3.4] are not strictly real valued and contain a second order dynamic frequency shift term as per [1.5.24]. However, since the evolution of the central line is decoupled from the evolution of the satellites, the small dynamic shift effects can be accounted for by adding a relative frequency shift to the central line only and will be neglected in this treatment. The real part of the spectral density is defined as [2.2.4]. In the product operator basis, off-diagonal relaxation terms are strictly real valued. *(22)*

Solutions to [2.3.1] are found by diagonalizing [2.3.3] and solving the resulting set of uncoupled differential equations.

$$T[-(i\mathcal{L}+R)]T^{-1} = R^{(1)}_{diag} = \begin{pmatrix} R_1^{(1)} & 0 & 0 \\ 0 & R_2^{(1)} & 0 \\ 0 & 0 & R_3^{(1)} \end{pmatrix} \qquad [2.3.6].$$

Because [2.3.4] is not Hermitian, the transformation is not unitary and

$$T = \frac{1}{\sqrt{2}\,J_2}\begin{pmatrix} -\left(\sqrt{J_2^2 - \omega_q'^2} + i\omega_q'\right) & 0 & J_2 \\ 0 & \sqrt{2}J_2 & 0 \\ J_2 & 0 & \sqrt{J_2^2 - \omega_q'^2} + i\omega_q' \end{pmatrix} \qquad [2.3.7].$$

Then, for the relaxation eigenvalues and corresponding product basis eigenfunctions, the following evolution is found:

$$R_1^{(1)} = -C\left(J_0 + J_1 + J_2 + \sqrt{J_2^2 - \omega_q'^2}\right)$$

$$\rho_1^{(1)} = \frac{1}{\sqrt{2}\,J_2}\left(-\left(\sqrt{J_2^2 - \omega_q'^2} + i\omega_q'\right)\rho_{12} + J_2\,\rho_{34}\right)$$

$$R_2^{(1)} = -C(J_1 + J_2)$$

$$\rho_2^{(1)} = \rho_{23}$$

$$R_3^{(1)} = -C\left(J_0 + J_1 + J_2 - \sqrt{J_2^2 - \omega_q'^2}\right)$$

$$\rho_3^{(1)} = \frac{1}{\sqrt{2}\,J_2}\left(J_2\,\rho_{12} + \left(\sqrt{J_2^2 - \omega_q'^2} + i\omega_q'\right)\rho_{34}\right) \qquad [2.3.8].$$

As solutions to [2.3.1], each coefficient decays exponentially:

$$\rho_n^{(1)}(t) = \rho_n^{(1)}(0)\exp[R_n^{(1)}t] \qquad [2.3.9].$$

Suitable manipulation of [2.3.8] gives the time dependence of the coefficients of the single quantum operators

$$\begin{pmatrix} \rho_{12}(t) \\ \rho_{23}(t) \\ \rho_{34}(t) \end{pmatrix} = \boldsymbol{R}^{(1)} \begin{pmatrix} \rho_{12}(0) \\ \rho_{23}(0) \\ \rho_{34}(0) \end{pmatrix} \qquad [2.3.10]$$

where

$$R^{(1)} = K^{(1)}(t)\begin{pmatrix} \sqrt{J_2^2-\omega_q'^2}\cosh\left(C\sqrt{J_2^2-\omega_q'^2}\,t\right) - i\omega_q'\sinh\left(C\sqrt{J_2^2-\omega_q'^2}\,t\right) & 0 & J_2\sinh\left(C\sqrt{J_2^2-\omega_q'^2}\,t\right) \\ 0 & \sqrt{J_2^2-\omega_q'^2}\exp[CJ_0t] & 0 \\ J_2\sinh\left(C\sqrt{J_2^2-\omega_q'^2}\,t\right) & 0 & \sqrt{J_2^2-\omega_q'^2}\cosh\left(C\sqrt{J_2^2-\omega_q'^2}\,t\right) + i\omega_q'\sinh\left(C\sqrt{J_2^2-\omega_q'^2}\,t\right) \end{pmatrix}$$

[2.3.11]

and

$$K^{(1)}(t) = \frac{\exp\left[-C\left(J_0+J_1+J_2\right)t\right]\exp\left[-i\omega_0t\right]}{\sqrt{J_2^2-\omega_q'^2}} \equiv \frac{\exp\left[-C\left(J+i\omega_0'\right)t\right]}{\sqrt{J_2^2-\omega_q'^2}} \qquad [2.3.12].$$

Even with the added influence of orientational anisotropy and relaxation coupling via $J_2$, the satellite and central lines remain uncoupled and relax independently. *(63)*

Additional physical insight may be gained by transforming the spin dynamics to a spherical tensor basis through [1.2.15]. In this basis, the spin density of the nucleus is materially described, in contrast to describing the eigenvectors of the product operator basis that are derived from the lab frame energy levels. Also, taking advantage of the rotational symmetry propertites of the spherical tensors [1.2.1] facilitates the simulation of multi-pulse experiments. $\mathcal{T}^{(k)q}(I)$ are the operators that span the Liouville space for spin *I*. In the operator basis of $\mathcal{T}^{(k)q}(I)$ the tensor rank, *k*, and MQ coherence order, *q*, are the Liouville space quantum numbers equivalent to the *IM* quantum numbers in state space. The spin density operator for a single spin can be expanded into the multipole polarizations [1.3.26]

$$\rho(t) = \sum_{k=0}^{2I} \phi^{(k)} \odot^{(k)} \mathcal{T}^{(k)}(I)$$

$$= (2I+1)^{-1}\left[ E_I + \sum_{k=0}^{2I} \sum_{q=-k}^{k} \phi_q^k(t) \mathcal{T}^{(k)q}(I) \right] \qquad [1.3.25]$$

$$\phi_q^k(t) = \left\langle \mathcal{T}^{(k)q}(I)^{\dagger} \right\rangle = \left\langle \mathcal{T}_q^{(k)}(I) \right\rangle = tr\left\{ \mathcal{T}_q^{(k)}(I)\, \rho(t) \right\} \qquad [1.3.26a]$$

$$\phi_q^k(t) \equiv \phi^{kq}(t)^* = (-1)^{k-q} \phi^{k-q}(t) \qquad [1.3.26b].$$

Since the product and multipole operator bases span the same space, they are related by a unitary transformation defined by [1.2.15].

$$\mathcal{T}^{(k)q}(I) = (i)^k \sqrt{(2I+1)(2k+1)} \sum_{MM'} (-1)^{I-M} \begin{pmatrix} I & k & I \\ -M & q & M' \end{pmatrix} |IM\rangle\langle IM'| \qquad [1.2.15a].$$

Applying the appropriate transformation *(37)* to [2.3.11] gives the evolution supermatrix in the multipole basis

$$UR^{(1)}U^{-1} = -\frac{i}{2}\sqrt{\frac{2}{5}} \begin{pmatrix} \sqrt{3} & 2 & \sqrt{3} \\ i\sqrt{5} & 0 & -i\sqrt{5} \\ -\sqrt{2} & \sqrt{6} & -\sqrt{2} \end{pmatrix} R^{(1)} \sqrt{\frac{2}{5}} \frac{i}{2} \begin{pmatrix} \sqrt{3} & -i\sqrt{5} & -\sqrt{2} \\ 2 & 0 & \sqrt{6} \\ \sqrt{3} & i\sqrt{5} & -\sqrt{2} \end{pmatrix}$$

$$= R_{MP}^{(1)} = \frac{\exp[-CJt]\exp[-i\omega_0 t]}{5} \begin{pmatrix} r_{11}^{\pm 1} & r_{12}^{\pm 1} & r_{13}^{\pm 1} \\ r_{21}^{\pm 1} & r_{22}^{\pm 1} & r_{23}^{\pm 1} \\ r_{31}^{\pm 1} & r_{32}^{\pm 1} & r_{33}^{\pm 1} \end{pmatrix} \qquad [2.3.13].$$

The matrix elements for [2.3.13] are given in Table 2.1.

### TABLE 2.1

$R^{(1)}_{MP}$ Evolution Matrix Elements

| $r^{q}_{kk'}$ | |
|---|---|
| $r^{\pm 1}_{11}$ | $3\left[\cos\left(C\sqrt{\omega'^2_q - J_2^2}\; t\right) + \frac{J_2}{\sqrt{\omega'^2_q - J_2^2}}\sin\left(C\sqrt{\omega'^2_q - J_2^2}\; t\right)\right] + 2\exp\left[CJ_0 t\right]$ |
| $r^{\pm 1}_{12}$ | $\mp\sqrt{15}\,\frac{\omega'_q}{\sqrt{\omega'^2_q - J_2^2}}\sin\left(C\sqrt{\omega'^2_q - J_2^2}\; t\right) = -r^{\pm 1}_{21}$ |
| $r^{\pm 1}_{13}$ | $\sqrt{6}\left[\exp\left[CJ_0 t\right] - \cos\left(C\sqrt{\omega'^2_q - J_2^2}\; t\right) - \frac{J_2}{\sqrt{\omega'^2_q - J_2^2}}\sin\left(C\sqrt{\omega'^2_q - J_2^2}\; t\right)\right] = r^{\pm 1}_{31}$ |
| $r^{\pm 1}_{22}$ | $5\left[\cos\left(C\sqrt{\omega'^2_q - J_2^2}\; t\right) - \frac{J_2}{\sqrt{\omega'^2_q - J_2^2}}\sin\left(C\sqrt{\omega'^2_q - J_2^2}\; t\right)\right]$ |
| $r^{\pm 1}_{23}$ | $\mp\sqrt{10}\,\frac{\omega'_q}{\sqrt{\omega'^2_q - J_2^2}}\sin\left(C\sqrt{\omega'^2_q - J_2^2}\; t\right) = -r^{\pm 1}_{32}$ |
| $r^{\pm 1}_{33}$ | $2\left[\cos\left(C\sqrt{\omega'^2_q - J_2^2}\; t\right) + \frac{J_2}{\sqrt{\omega'^2_q - J_2^2}}\sin\left(C\sqrt{\omega'^2_q - J_2^2}\; t\right)\right] + 3\exp\left[CJ_0 t\right]$ |

Evolution of the $q = 1$ multipole coefficients is then given by

$$\begin{pmatrix} \phi_{\pm 1}^{1}(t) \\ \phi_{\pm 1}^{2}(t) \\ \phi_{\pm 1}^{3}(t) \end{pmatrix} = R_{MP}^{(1)} \begin{pmatrix} \phi_{\pm 1}^{1}(0) \\ \phi_{\pm 1}^{2}(0) \\ \phi_{\pm 1}^{3}(0) \end{pmatrix} \qquad [2.3.14].$$

From the multipole expansion in [2.3.13] and [2.3.14] and the explicit form of the relaxation matrix elements in Table 2.1, it is readily apparent that in anisotropic media, it is possible for a second rank tensor component, i.e, $\phi_{\pm 1}^{2}$, to couple to the transverse magnetization, $\phi_{\pm 1}^{1}$, produced in an NMR experiment. Moreover, as $\omega_q'$ approaches zero the contribution from this vanishes as seen from $r_{12}^{1}$ in Table 2.1.

The double quantum coherences can be treated in a manner analogous to the SQ coherences above. With the Redfield matrix applicable to the DQ transitions *(46)* the DQ eigenvectors evolve according to

$$-(i\mathcal{L} + R) = C\begin{pmatrix} -i\left(2\omega_0' + \omega_q'\right) - \left(J_0 + J_1 + J_2\right) & J_1 \\ J_1 & -i\left(2\omega_0' - \omega_q'\right) - \left(J_0 + J_1 + J_2\right) \end{pmatrix} [2.3.14].$$

As in the single quantum case, the Liouville and Redfield supermatrices cannot be separated and simultaneously diagonalized. Again, diagonalization of [2.3.14] and subsequent solution of [2.3.1] gives the exponential time dependence of the DQ product basis eigenvectors, from which can be calculated the time dependence of the $\rho_n$ coefficients:

$$\begin{pmatrix}\rho_{13}(t)\\ \rho_{24}(t)\end{pmatrix}=K^{(2)}(t)\begin{pmatrix}\sqrt{J_1^2-\omega_q'^2}\cosh\left(C\sqrt{J_1^2-\omega_q'^2}\;t\right) & \\ -i\omega_q'\sinh\left(C\sqrt{J_1^2-\omega_q'^2}\;t\right) & J_1\sinh\left(C\sqrt{J_1^2-\omega_q'^2}\;t\right)\\ & \\ J_1\sinh\left(C\sqrt{J_1^2-\omega_q'^2}\;t\right) & \sqrt{J_1^2-\omega_q'^2}\cosh\left(C\sqrt{J_1^2-\omega_q'^2}\;t\right)\\ & +i\omega_q'\sinh\left(C\sqrt{J_1^2-\omega_q'^2}\;t\right)\end{pmatrix}\begin{pmatrix}\rho_{13}(0)\\ \rho_{24}(0)\end{pmatrix}$$

[2.3.15]

for which

$$K^{(2)}(t)=\frac{\exp\left[-C\left(J+i2\omega_0'\right)t\right]}{\sqrt{J_1^2-\omega_q'^2}} \qquad [2.3.16].$$

Applying [1.2.15] to [2.3.15] gives the DQ coherences in the multipole expansion

$$\begin{pmatrix}\phi_{\pm2}^2(t)\\ \phi_{\pm2}^3(t)\end{pmatrix}=\exp[-C(J+i2\omega_0)t]\begin{pmatrix}r_{22}^{\pm2} & r_{23}^{\pm2}\\ r_{32}^{\pm2} & r_{33}^{\pm2}\end{pmatrix}\begin{pmatrix}\phi_{\pm2}^2(0)\\ \phi_{\pm2}^3(0)\end{pmatrix} \qquad [2.3.17]$$

from the unitary transformation

$$\boldsymbol{U}=-\frac{1}{\sqrt{2}}\begin{pmatrix}1 & 1\\ i & -i\end{pmatrix} \qquad [2.3.18].$$

The matrix elements for the double quantum evolution matrix in the multipole basis, $\boldsymbol{R}_{MP}^{(2)}$, are given in Table 2.2. Again, in isotropic media where $\omega_q'=0$, there is no coupling between the even and odd rank tensors.

TABLE 2.2

$R^{(2)}_{MP}$ Evolution Matrix Elements

| $r^{q}_{kk'}$ | |
|---|---|
| $r^{\pm2}_{22}$ | $\cos\left(C\sqrt{\omega_q'^2 - J_1^2}\ t\right) + \frac{J_1}{\sqrt{\omega_q'^2 - J_1^2}}\sin\left(C\sqrt{\omega_q'^2 - J_1^2}\ t\right) = r^{\pm2}_{33}$ |
| $r^{\pm2}_{23}$ | $\mp\frac{\omega_q'}{\sqrt{\omega_q'^2 - J_1^2}}\sin\left(C\sqrt{\omega_q'^2 - J_1^2}\ t\right) = -r^{\pm2}_{32}$ |

Jaccard *et al.* *(46)* have treated the longitudinal relaxation processes of the zero quantum polarizations $\phi^k_0$ so they are not discussed here, except to say that in the zero quantum manifold the $\phi^k_0$ alignments are associated with the $T_{k,0}$ spherical tensors and the off-diagonal elements of $R^{(0)}$ reduce to zero in the extreme narrowing limit. The only triple quantum transition is fully given by

$$\rho_{14}(t) = \phi^3_{\pm3}(t) = \phi^3_{\pm3}(0)\exp\left[-C\left(J_1 + J_2 + i3\omega_0\right)t\right] \qquad [2.3.19].$$

*Simulation of the MQF Experiment*

For $I = 3/2$ nuclei, MQF spectra are typically recorded using the pulse sequence *(46, 76, 77)*

$$d^{(k)}_{qq'}\left(\tfrac{\pi}{2}\right) - \tau/2 - d^{(k)}_{qq'}(\pi) - \tau/2 - \left[d^{(k)}_{qq'}(\beta)\right]_{\varphi_1} - \delta - \left[d^{(k)}_{qq'}(\beta)\right]_{\varphi_2} - AQ(t) \qquad [2.3.20].$$

MQ coherence pathways are selected by appropriate phase cycling through the $\varphi_n$. *(77)* Hereafter, discussion will be restricted to the DQ experiment only. For $\beta = \frac{\pi}{2}$ both the contributions from the quadrupolar (second rank) and octupolar (third rank) tensors are maintained. In the context of systems with a finite $\omega_q'$, the effect of this pulse sequence may be summarized as follows. The first $\pi/2$ pulse converts the equilibrium magnetization ( see [1.2.11] )

$$\phi_0^1(0) = -i\sqrt{\frac{3}{I(I+1)}}\langle I_z \rangle_T \qquad [2.3.21]$$

to the transverse plane, where it is described by $\phi_{\pm 1}^1(t)$. During the MQ preparation time $\tau$, the relaxation processes governed by the modulation of the quadrupolar interaction, transfer polarization to the quadrupole and octupolar modes, $\phi_{\pm 1}^3(t)$ and $\phi_{\pm 1}^2(t)$ as per [2.3.17]. The $\pi$ pulse in the middle of the preparation period serves to refocus any field inhomogeneities. Since this is a purely experimental consideration that has no effect on the relaxation, it will not be taken into account. The second pulse would normally mix all $q$-quantum coherences amongst tensor contributions of the same rank, as described in [1.2.1]. However, phase cycling enables the discrete selection of particular tensor components. Thus, the second pulse has the presumed effect of transferring $\phi_{\pm 1}^3(t)$ and $\phi_{\pm 1}^2(t)$ into the DQ manifold to produce $\phi_{\pm 2}^3(t)$ and $\phi_{\pm 2}^2(t)$. These evolve according to [2.3.17] during the short MQ evolution time $\delta$. This evolution time is of long enough duration to allow the spectrometer to recover from the effects of the previous pulse. These DQ coherences are subsequently converted back to the SQ manifold by the read pulse to contribute to the directly observable $\phi_{-1}^1(t)$, which is monitored during the acquisition period $AQ$.

In isotropic media, coupling can exist only between tensors differing in rank by an even integer value, a fact borne out by [2.3.14] and [2.3.17]. Thus, only odd rank tensors are produced in an NMR experiment on an isotropic system evolving from thermal equilibrium. Conversely, anisotropic orientational ordering permits coupling to $\phi_{\pm 1}^2$ for $I =$

3/2 nuclei in the preparation period. The DQF phase cycling selects both $\phi^3_{\pm 2}$ and $\phi^2_{\pm 2}$ while only the contribution from $\phi^3_{\pm 3}$ is retained in the triple quantum filtered experiment.

In the DQF experiment it is necessary to follow only those tensors that contribute to and evolve from the $q = 2$ coherences. By using the conventional notation for the reduced Wigner rotation matrix elements, $d^{(k)}_{qq'}(\beta)$, and the evolution matrix elements, $r^{(q)}_{kk'}(t)$, identified from Table 2.1 and Table 2.2

$$\phi^k_q(t) = \sum_{q'=-k}^{k} d^{(k)}_{qq'}(\beta)\ \phi^k_{q'}(0) \qquad \phi^k_q(t) = \sum_{k'} r^{(q)}_{kk'}(t)\ \phi^{k'}_q(0) \qquad [2.3.22]$$

and extracting the relevant terms, one finds for the detectable vector magnetization

$$\phi^1_{-1}(FID) = \frac{\exp\left[-i\omega_0\left(AQ+\tau+2\delta\right)\right]\exp\left[-CJ\left(AQ+\tau+\delta\right)\right]}{25} \qquad [2.3.23]$$

$$\begin{aligned}
&\times\Big[r^1_{13}(AQ)\Big[r^2_{32}(\delta)r^1_{21}(\tau)\Big(d^3_{-12}(\beta)\big(d^2_{21}(\beta)-d^2_{2-1}(\beta)\big)-d^3_{-1-2}(\beta)\big(d^2_{-21}(\beta)-d^2_{-2-1}(\beta)\big)\Big)\\
&\qquad +r^2_{33}(\delta)r^1_{31}(\tau)\Big(d^3_{-12}(\beta)\big(d^3_{21}(\beta)+d^3_{2-1}(\beta)\big)+d^3_{-1-2}(\beta)\big(d^3_{-21}(\beta)+d^3_{-2-1}(\beta)\big)\Big)\Big]\\
&+r^1_{21}(AQ)\Big[r^2_{22}(\delta)r^1_{21}(\tau)\Big(d^2_{-12}(\beta)\big(d^2_{21}(\beta)-d^2_{2-1}(\beta)\big)+d^2_{-1-2}(\beta)\big(d^2_{-21}(\beta)-d^2_{-2-1}(\beta)\big)\Big)\\
&\qquad +r^2_{23}(\delta)r^1_{31}(\tau)\Big(d^2_{-1-2}(\beta)\big(d^3_{-21}(\beta)+d^3_{-2-1}(\beta)\big)-d^2_{-12}(\beta)\big(d^3_{21}(\beta)+d^3_{2-1}(\beta)\big)\Big)\Big]\Big]d^1_{10}\phi^1_0(0)
\end{aligned}$$

Assuming hard, delta function pulses, evolution and relaxation are ignored during the pulse interval. As written, all relaxation matrix elements are positive, since relevant signs for the elements coupling the even and odd rank tensors have been extracted and appear in the pulse terms.

The FID given by [2.3.23] is exact, within the limits of the theory, and incorporates the effects of evolution of the DQ, $q = 2$, coherences in the short $\delta$ period. Simulation of the DQF experiment setting $\omega'_q = 0$ gives results identical to those described in § 2.2 and shown in Figure 2.2b, after Fourier transforming a suitably partitioned FID, as expected for an isotropic system. Figure 2.4a shows the frequency domain spectrum that derives from a pure octapolar signal. With the onset of orientational anisotropy, increased values of the quadrupole splitting generate a contribution from the second rank tensor. For splittings less than the resonant line width, the more complex shape of the signal is due to the overlap of the quadrupolar and octapolar contributions, shown in Figures 2.4c and 2.4d. The difference between these two spectra with the relatively small change in $\omega_q'$ is somewhat startling, but is in keeping with the observation that the line shape is sensitive to experimental conditions. As $\omega_q'$ increases beyond the magnitude of the composite resonant line width, the satellite lines become resolved ( Figure 2.4e ). Here, the correlation time of molecular motion is set such that $\omega_0\tau_c = 1$, in the region of the "$T_1$ minimum" where spin-lattice relaxation is most efficient. In general, it was found that the value $\omega_0\tau_c$, as it appears in the spectral densities, has a relatively small effect on the width of the line. Over at least two orders of magnitude, $0.1 < \omega_0\tau_c < 10$, the line shape is dictated primarily by $\omega_q'$. Below this lower limit, the extreme narrowing limit is approached and the MQ signal disappears. Beyond the upper limit, the theory is limited in that extremely long correlation times are precluded by the Markoff approximation taken in the development of the Redfield matrices.

By setting $\beta$ = 54.73° in the DQF pulse sequence it is possible to isolate the contribution of the second rank tensor, owing to the presence of terms proportional to $3\cos^2\beta - 1$ in the $d^{(3)}$ of [2.2.23]. That is, the explicit form of the Wigner rotation matrix selectively filters out any third rank tensor components. *(46, 49)* Simulation of this modified pulse sequence produces results nearly identical to those shown in Figure 2.4b, showing that this line is indeed dominated by the presence of a second rank tensor. Notice is made here of the line shape of the isolated contribution from the second rank tensor, which may be thought of as a powder distribution of antiphase doublets. It is antiphase in the sense that this signal is 90° out of phase with respect to the third rank tensor contribution to the observable. Consequently, the $\phi_{-1}^{2}$ contribution to the signal appears to be in dispersive mode when plotted so that the contribution from $\phi_{-1}^{3}$ is in absorptive

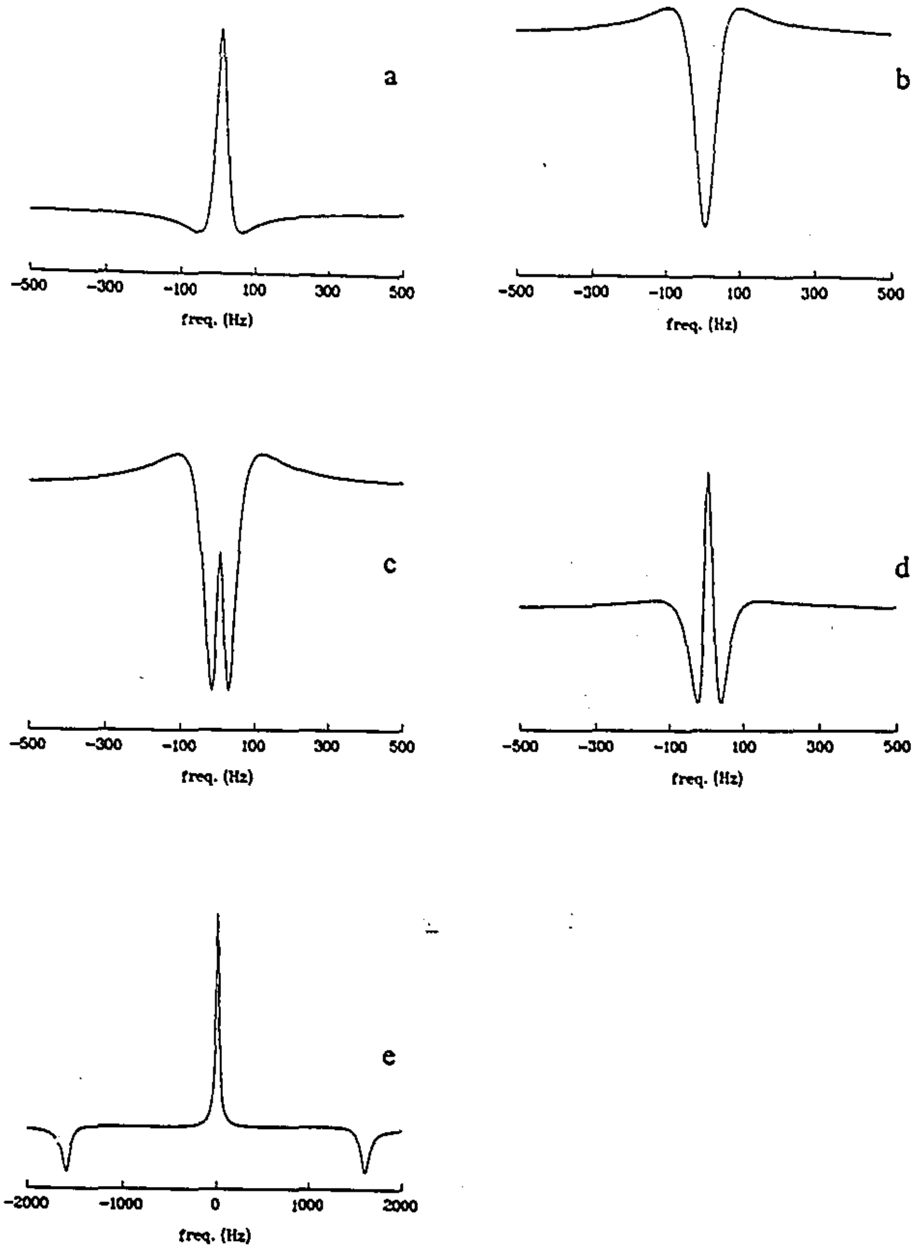

Figure 2.4. Fourier transforms of [2.3.22] with $\tau$= 4 ms, $\delta$= 60 $\mu$s, $\tau_c\omega_0$ = 1, $C$ = 6.14x10$^9$ s$^2$ and $\overline{\omega_q}$ values a) $\overline{\omega_q}$ = 0 Hz: pure octapole contribution, b) $\overline{\omega_q}$ = 40 Hz (= $CJ_2$), c) $\overline{\omega_q}$ = 45 Hz, d) $\overline{\omega_q}$ = 50 Hz, e) $\overline{\omega_q}$ = 10 000/2π Hz. The isolated contribution from $\phi_{-1}^2$ (β = 54.73°) is identical to b). For $\omega_q = J_1$, $\phi_{-1}^2$ is negligible and the line is as shown in a).

mode, as is the custom. When properly shown in absorptive mode, the poorly resolved antiphase doublet appears with an apparent dispersive line shape, from which the experimentally observed $\omega_q'$ can be measured. For clarity, in Figure 2.4b the isolated $\phi_{-1}^{2}$ portion of the signal is presented as it would appear in dispersive mode so that its contribution to the reported experimental results is more obvious. Figure 2.5 shows the results of one such experiment, performed on centrifuged human red blood cells. *(72)* From this spectrum, the peak-to-peak separation is about 50Hz, giving $2\overline{\omega_q} \cong 2\pi(50)$ rad/s. Figure 2.6 shows how this doublet would appear, if the spectrum is displayed such that $\phi_{-1}^{3}$ appears in absorptive mode. It is by this quirk of nature that the poorly resolved antiphase doublet, displayed in dispersive mode, looks like a Lorentzian line, causing some degree of grief amongst experimentalists, some of whom thought this indicated the presence of two distinct ion pools.

In order to directly judge the efficacy of this theoretical model in describing the experimental results, Figure 2.7 shows the DQ spectra from experiments performed with different evolution times. Here again, the signal due to the ions bound to the external cell wall has been excluded by the addition of a relaxation reagent. At short evolution times, both the FID and the frequency spectrum show contributions from both second and third rank tensors. The simulated resonant lines are found for $\omega_0\tau_c = 1.2$ ( and hence, should appear broader than those shown in Figure 2.4 where $\omega_0\tau_c = 1.0$, however, the spectral width of the two figures is different ) and $\overline{\omega_q} = 48$Hz. Without any direct connection to the signal amplitude and the number of visible spins in the sample, an arbitrary amplitude normalization is assumed for the puposes of simulation ( [2.3.21] ). The simulation not only repoduces the general shapes of the lines, but is also able to predict the dependence of the line shape on the preparation time $\tau$. Therefore, this formulation requires only two independent parameters, namely $\overline{\omega_q}$ and $\omega_0\tau_c$, both of direct physical significance. All other variables appearing in [2.3.23] are experimentally controlled.

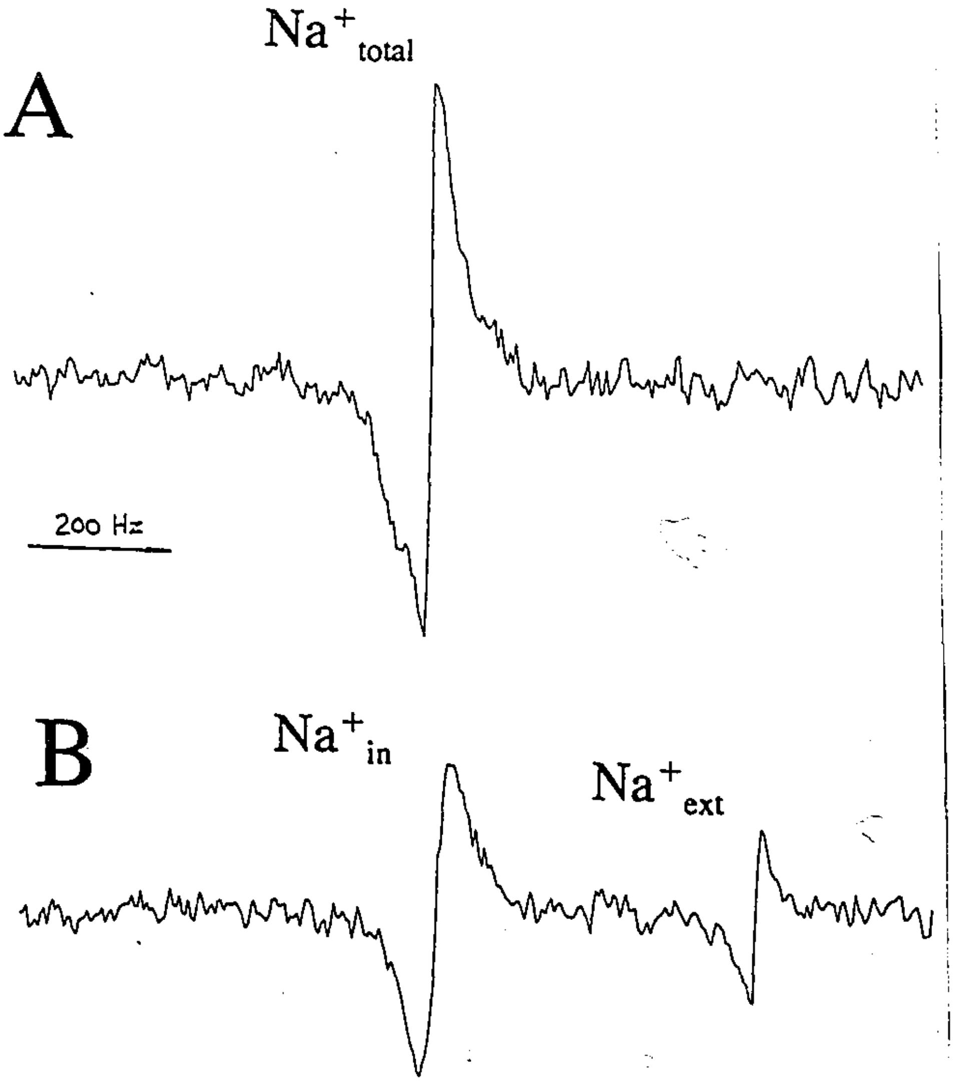

Figure 2.5. DQF spectra taken from Na in red blood cells showing the isolated contribution from $\phi^{2}_{-1}$ obtained from an experiment with β = 54.73°. *(72)* Again, a shift reagent discerns between the intra and extracellular signals. The poorly resolved antiphase doublet appears as it would if plotted in absorptive mode. Peak-to-peak separation gives $\overline{\omega_q}$ = 50Hz.

$$90 - \tau/2 - 180 - \tau/2 - \theta - t_1 - \theta - \text{ACQ}$$

$$\theta = 54.7^\circ \text{ (for 2nd-rank tensor)}$$

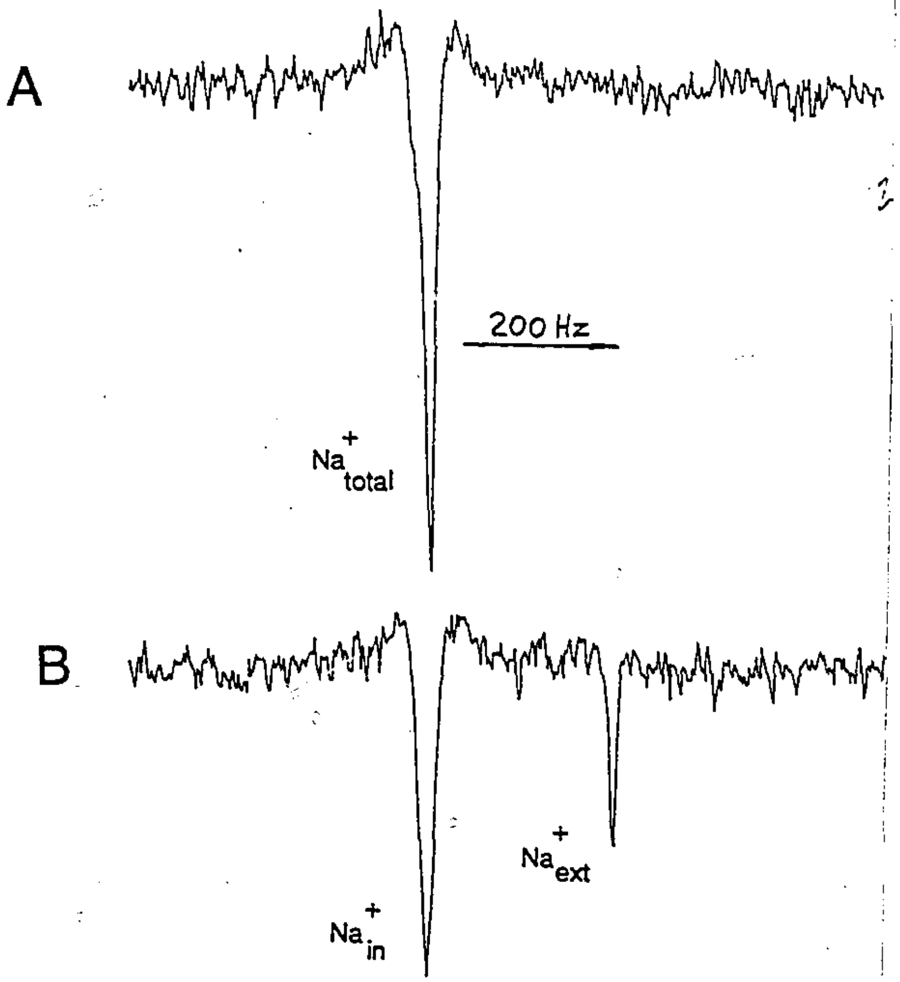

Figure 2.6 Same spectra as in Figure 2.5 plotted in dispersive mode as it normally appears in the context of a DQF experiment. *(72)*

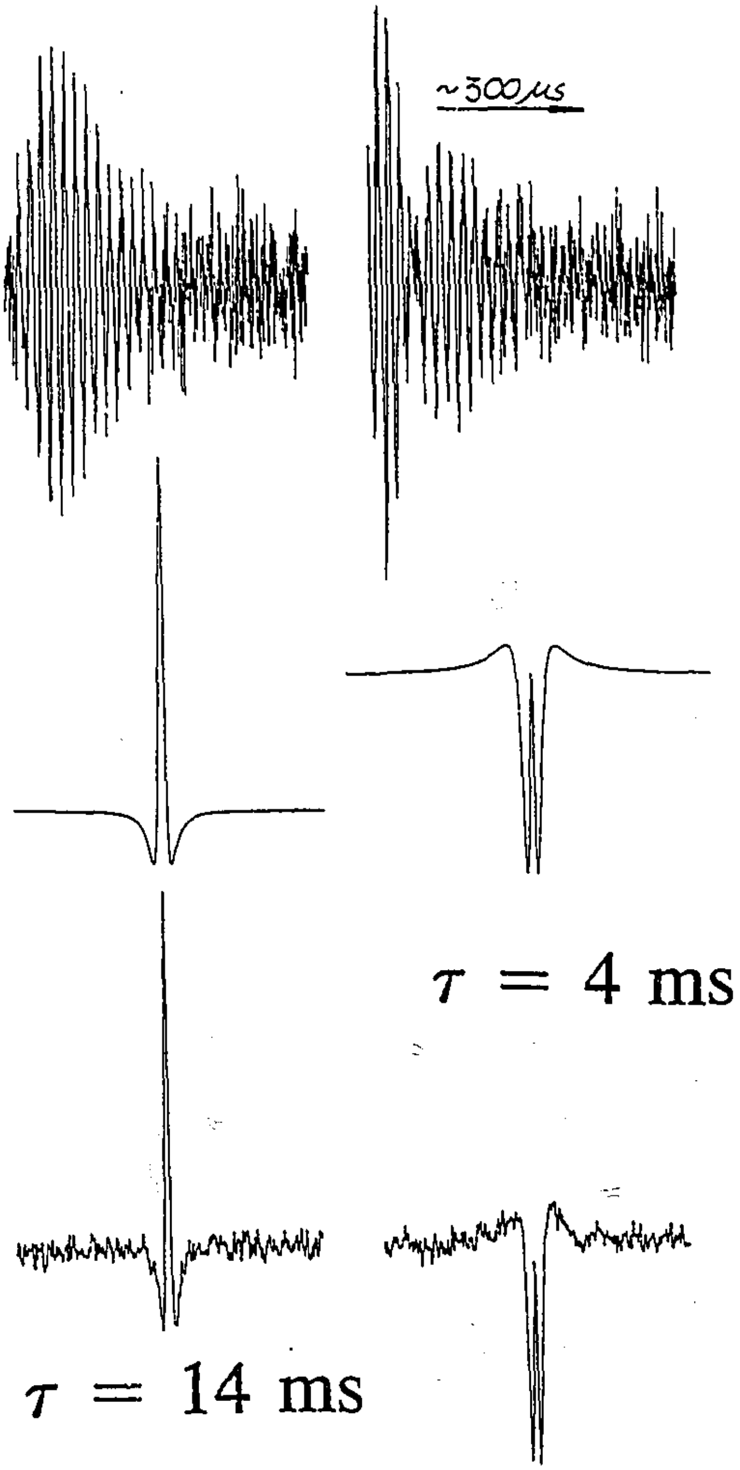

Figure 2.7. DQF spectra from red blood cells taken at different preparation times. Both the FID's and the frequency domain spectra show contributions from the second and third rank tensors. *(72)* The simulated lines are found for $\omega_0\tau_c = 1.2$ and $\overline{\omega_q} = 48$ Hz.

It remains to be shown why $\overline{\omega_q}$ has such a dramatic effect on the line shape. Figure 2.8 shows the relative amplitudes of the real parts of the second and third rank tensors at the end of the read pulse ( at the beginning of the acquisition period i.e., $\phi^{k}_{-1}\left(\pi/_2 - \tau - \pi/_2 - \delta - \pi/_2\right)$ ) with varying $\overline{\omega_q}$. As expected, the third rank tensor oscillates through a range of positive values maintaining the DQF signal through all conditions. In contrast, $\phi^{2}_{-1}$ is zero for $\overline{\omega_q}$ = 0 and subsequently oscillates through positive and negative values as $\overline{\omega_q}$ increases. Moreover, $\phi^{2}_{-1}$ goes through two cusps at small $\overline{\omega_q}$ values: the first is at $\omega_q' = J_2$ ( $\overline{\omega_q} = CJ_2$ ) where the second rank tensor completely dominates the spectrum as shown in Figures 2.4b and 2.8b. The contribution of $\phi^{2}_{-1}$ to the FID may be further elucidated by the form of the analytical expressions of the relaxation elements in [2.3.13] governing the development of $\phi^{2}_{-1}$ and the value of the expression $r^{2}_{22}(\delta)r^{1}_{21}(\tau)D1 + r^{2}_{23}(\delta)r^{1}_{31}(\tau)D2$ ($D$'s represent pulse terms) from [2.3.23]. As $\omega_q'$ approaches $J_2$ the $\dfrac{\sin x}{x}$ term in $r^{1}_{21}$ rapidly approaches its finite value

$$\lim_{\omega_q' \to J_2} r^{1}_{21}(\tau) = \lim_{\omega_q' \to J_2}\left(\sqrt{15}\,C\tau\, J_2 \frac{\sin\left(C\sqrt{\omega_q'^{2} - J_2^{2}}\,\tau\right)}{C\sqrt{\omega_q'^{2} - J_2^{2}}\,\tau}\right) = \sqrt{15}\,C\tau\, J_2 \qquad [2.3.24].$$

The contribution from the sine term in $r^{1}_{31}(\tau)$ is also maintained, although it is much less significant for small values of $\delta$. Simulation of the line shape with this splitting value accordingly gives a line out-of-phase ( Figure 2.4b ) with respect to that produced by the third rank tensor. In addition, as $\omega_q'$ approaches $J_1$ the amplitude of the contribution from $\phi^{2}_{-1}$ follows

$$\phi^{2}_{-1}\left(\omega_q' = J_1\right) \propto \left(1 + J_1 C\delta\right)\frac{\sqrt{15}\,\omega_q'}{\sqrt{\omega_q'^{2} - J_2^{2}}}\sin\left(C\sqrt{\omega_q'^{2} - J_2^{2}}\,\tau\right)D1 \qquad [2.3.25]$$

$$-\sqrt{6}J_1 C\delta\left(\exp\left[CJ_0\tau\right]-\cos\left(C\sqrt{\omega_q'^2-J_2^2\tau}\right)-\frac{J_2}{\sqrt{\omega_q'^2-J_2^2}}\sin\left(C\sqrt{\omega_q'^2-J_2^2\tau}\right)\right)D2$$

in which $\phi_{-1}^{2}$ is rapidly minimized for finite values of $\delta$. It should be noted that while the intensities of each of these tensorial components is modulated by $\tau$ and $\delta$, the positions of these cusps are determined by the non-secular spectral densities, $J_1$ and $J_2$. While such asymptotic terms exist in the evolution of $\phi_{-1}^{3}$ they are mitigated by the preponderance of other exponential terms that dominate the evolution of the odd rank tensor components. Thus, over a narrow range in which $\overline{\omega_q}$ is less than the line width, the line shape is highly sensitive to the residual quadrupole splitting. In this regime, the magnitude of $\overline{\omega_q}$, which is observed in the laboratory frame and tends to resolve the satellite lines, matches the off-diagonal relaxation elements that couple the same satellite lines. These are, in turn, determined by the correlation time of molecular reorientation. It would be formally incorrect to describe this phenomenon as a resonance condition, as the lattice is modelled by random functions that should not have coherent phases to which the spin system can couple. However, in a self-consistent sense, it is acceptable for the combined effects of the static quadrupolar coupling and the second order quadrupolar relaxation to become manifest in $\phi_{-1}^{2}$, a feature of the spectrum that is particularly sensitive to the conditions previously discussed. Similar behaviour has been observed in the microwave inversion spectrum of ammonia, in cases where pressure broadening is comparable to the resonant line width. *(78)* In practice, it should be expected that $\overline{\omega_q}$ would be better represented by a distribution of values about the average and consequently, such severe asymptotic behaviour might not be observed. At least not to the extent in which it is portrayed here.

Using this multipole approach it is not difficult to show the dependence of the line shape on the preparation time as observed in many biological tissues. *(49, 51, 72, 75)* In Figure 2.9 the relative amplitudes of the real parts of $\phi_{-1}^{3}$ and $\phi_{-1}^{2}$ at the end of the read pulse are plotted as a function of $\tau$: Figure 2.9a $\overline{\omega_q} = 45$ Hz and $\omega_0\tau_c = 1.0$, Figure 2.9b $\overline{\omega_q} = 45$ Hz and $\omega_0\tau_c = 0.6$, Figure 2.9c $\overline{\omega_q} = 50$ Hz and $\omega_0\tau_c = 1.0$, Figure 2.9d $\overline{\omega_q} = 50$ Hz and $\omega_0\tau_c = 1.5$. Under the conditions used to generate the line reported in Figure 2.4c, Figure 2.9a shows that $\phi_{-1}^{2}$ has a significant contribution only up to about 20 ms after which it quickly decays. $\phi_{-1}^{3}$ maintains a significant contribution to approximately 40 ms. This underscores the fact that each of the tensorial components of the observed signal, including the higher quantum coherences, are governed by distinct relaxation behavior. The fact that the lines in a resonant signal may be the result of several tensorial contributions may complicate the interpretation of relaxation data inferred from analysis using a product operator basis.

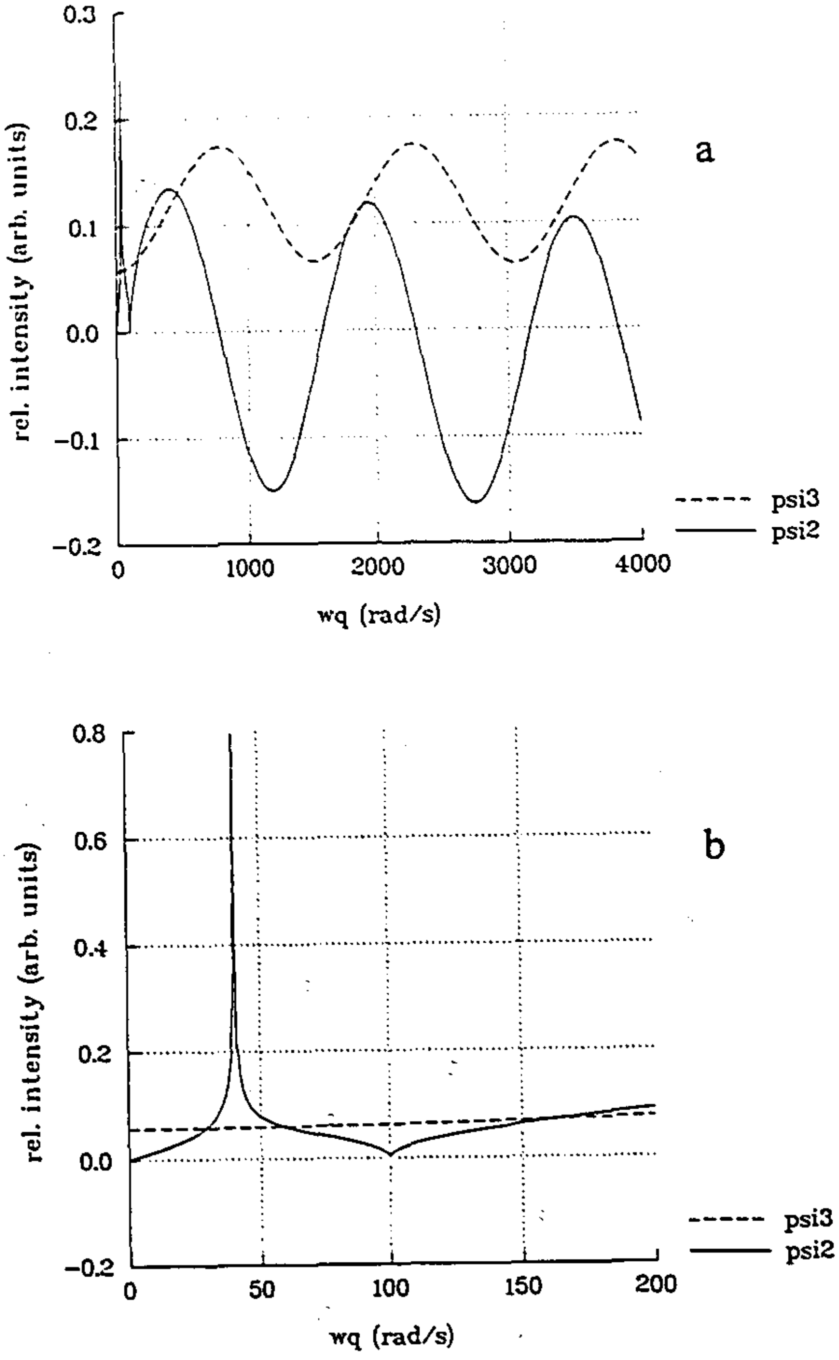

Figure 2.8. Dependence on the quadrupolar splitting of the relative amplitudes of $\phi^{2}_{-1}$(solid line) and $\phi^{3}_{-1}$(dashed line) at the end of the read pulse in the DQF experiment: a) large splittings showing the oscillation in both tensors b) small splittings showing the dominance of $\phi^{2}_{-1}$ near $\overline{\omega_q} = 40$ Hz (= $CJ_2$). Parameters as in Figure 2.4.

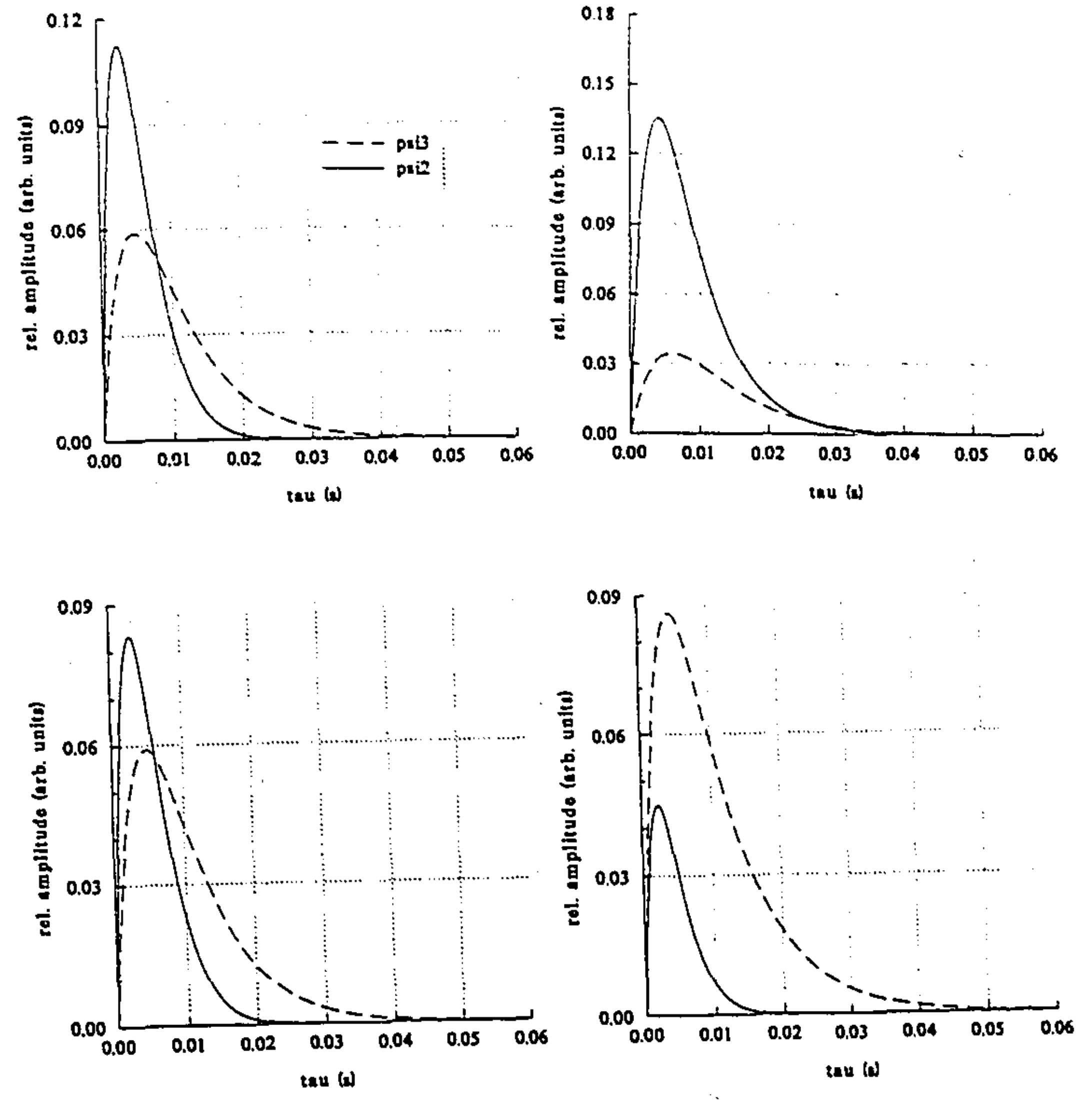

Figure 2.9. Dependence of the relative amplitudes of $\phi^{2}_{-1}$(solid line) and $\phi^{3}_{-1}$(dashed line) at the end of the read pulse in the DQF experiment on the preparation time. The relative amplitudes depend upon the values of both $\overline{\omega_q}$ and $\omega_0\tau_c$. Figure 2.9a $\overline{\omega_q}$ = 45 Hz and $\omega_0\tau_c$ = 1.0, Figure 2.9b $\overline{\omega_q}$ = 45 Hz and $\omega_0\tau_c$ = 0.6, Figure 2.9c $\overline{\omega_q}$ = 50 Hz and $\omega_0\tau_c$ = 1.0, Figure 2.9d $\overline{\omega_q}$ = 50 Hz and $\omega_0\tau_c$ = 1.5.Other parameters as in Figure 2.4.

# Chapter 5. CONCLUSION

The I = 3/2 nucleus is a potentially sensitive probe for analysing a host of nuclear interactions. As described here a detailed study of the dynamics of the nucleus via NMR line shape analysis can provide information about the forces influencing these dynamics allowing us to intuit something about the physical surrounds of the spin. In the context of biological systems there is no shortage of mechanisms that have the potential to manifest themselves in NMR experiments. NMR exclusively has shown evidence for orientational anisotropy and has supported the previously assumed notions of fast ion exchange and motional hinderance. In contrast, there is a relatively small number characteristics of the quadrupolar nucleus that avail themselves to interpretation by relaxation studies. The problem, then, is to try to directly relate this nuclear dynamic behaviour to well established attributes of the biological system in question. While several, seemingly disparate, theories may be used to successfully model spin dynamics, no information is gained if these models cannot be directly related to some physical quality of the system.

This review is a good example of the synergistic relationship between the development of theory and experimental methods. With the first observation of anisotropy in the DQF experiments described, many experimentalists were at a loss to correctly account for the origins of the "anomalous" line shape. With the establishment of working theoretical models, the challenge is to discover new evidence, prompting the development of new theories.

The formation of even-rank tensors in a MQF experiment on a half-integer spin system initially at thermal equilibrium is a direct result of the existence of a finite residual quadrupole splitting. When $\overline{\omega_q}$ is less than the resonant line width of the $|-1/2\rangle \rightarrow |1/2\rangle$ transition, it is necessary to account for the off-diagonal terms in the Redfield perturbation treatment of the relaxation. Even though relaxation does not couple the central line to the innermost satellites for half-integer spins, inclusion of these non-secular terms is required to generate the asymptotic behavior of the even rank tensor and, thus, the full contribution to the line shape in a MQF experiment.

The use of Redfield theory to describe the evolution of the tensorial components of the spin density matrix has been shown to provide a convenient method for the analysis of the dynamics of a spin system in a MQF pulse sequence; with the multipole evolution matrices presented here it is easy to recognize the response to a general hard pulse sequence and the origins of each of the tensor components. The analytical solutions offered here not only describe the relaxation behaviour of each of the tensor components, but have reproduced some of the general features observed in experiment and in more fundamental analyses.

# PART 3

# THEORY OF PULSED NMR STUDIES ON SOLID $D_2$ IN THE SHORT-RANGE ORDERED hcp PHASE

## Chapter 1. INTRODUCTION

Solid *ortho* and *para* mixtures of the molecular hydrogens, $H_2$ and $D_2$, have been investigated over the past four decades. Much of the reason for this persistent interest is due to the cooperative orientational ordering in these crystals that is brought about by well understood anisotropic intermolecular electrostatic forces. The interaction responsible for this ordering originates from the coupling between the electric quadrupoles of non-spherical molecules, namely those with an orbital angular momentum $J$ different from zero. References *(79-82)* describe experiments and theoretical progress towards the understanding of the orientational ordering in the hydrogens, both in the regime of long-range order and in that of the gradual freezing into a "quadrupolar glass" state.

When cooled through their respective triple points at 14.7 and 18.6K both $H_2$ and $D_2$ form crystals with a hcp structure. In their solid state, only the ground rotational energy levels are populated, where both $o$-$H_2$ and $p$-$D_2$ have an angular momentum $J$=1 with an electric quadrupole moment $Q_e$, while $p$-$H_2$ and $o$-$D_2$ have $J = 0$ and $Q_e = 0$. Mixtures characterized by the molar fraction $X(J = 1)$ of the $J = 1$ component can be prepared in any proportion.

The anisotropic electric quadrupole-quadrupole ( EQQ ) interaction between two isolated neighbouring $J = 1$ molecules tends to align these into a perpendicular "T" formation. The alignment in three dimensions is frustrated by the presence of both several $J = 0$ and $J = 1$ neighbours in the solid state. This frustration, minimized in the long-range ordered state, is most pronounced in the glassy phase. The orientational ordering that occurs as the temperature is decreased is a function of the mixture composition. *(79)* At temperatures below a transition line $T_\lambda(X)$, where $X_C < X < 1.0$, the ordering is long-range and there is a crystalline phase change into a fcc structure ($Pa_3$ with interpenetrating sub lattices). For the critical concentration $X_C = 0.53$, the transition is at $T_\lambda = 0$, while for the pure $J = 1$ solids $T_\lambda = 3.0K$ and $4.0K$ for $H_2$ and $D_2$. For mixtures with $X < X_C$, the rotational motion freezes gradually into the quadrupolar glass state, the crystalline structure remaining hcp.

There have been numerous nuclear magnetic resonance ( NMR ) studies of these mixtures giving abundant information on the static and dynamic properties of the spin systems. In both $H_2$ and $D_2$ the orientational ordering process is found to be similar and an approximate scaling of the characteristic temperatures of ordering in terms of the quadrupolar interaction energy parameter $\Gamma$ is obtained. *(79, 82)* In $H_2$, the molecules with $J = 1$ have a total nuclear spin $I = 1$, while those with $J = 0$ bear $I = 0$. Even though the spin lattice relaxation is modulated by the relative motions of all molecules in the crystal, only the former species are capable of producing an NMR signal. In contrast, for $D_2$ both modifications have nuclear spins, namely the $J = 1$ molecules have $I = 1$ and of the $J = 0$ species, 5/6 have $I = 2$ while the remaining 1/6 are $I = 0$. Therefore, both $D_2$ species produce an NMR signal.

As the temperature is decreased in the solid phase, the NMR line, initially only broadened by intermolecular dipolar interactions, becomes substantially wider below $T \approx$ 2K through the intramolecular nuclear interactions as orientational order in both $H_2$ and $D_2$ increases. *(83, 84)* This is particularly so for the $J = 1$ molecules that are directly coupled by the EQQ interaction. In contrast, orientational ordering for $J = 0$ molecules is possible only through admixture of the $J = 2$ state into the $J = 0$ ground state via perturbation by the $J = 1$ molecules, *(85)* and this ordering is observable for $o$-$D_2$. Therefore, the line broadening in the frequency domain is appreciably smaller than that for the $J = 1$ molecules and as a result the signals from both species in $D_2$ can be resolved.

There are nuclear dipolar interactions between *ortho* and *para* neighbours in solid $D_2$. Thus, the NMR spectrum of $D_2$ is complicated because of the presence of two distinct spin-bearing components and of their dynamic interaction. As a result the spin dynamics in $D_2$ are less well understood than those in the simpler $H_2$ system. In a strict account of the dipolar interactions, intermolecular coupling to all other spin bearing deuterons must be considered. However, since the distance between two molecules is much greater than that between two atoms in the same molecule, atomic spin states need not be accounted for *per se*, and intermolecular dipolar interactions are formally restricted to atoms with $I \neq 0$.

Two-pulse and three-pulse NMR experiments have been carried out on $H_2$ and were analysed. *(86, 87)* In particular, the response signal "solid echo" from the two-pulse and three-pulse sequences was studied experimentally and theoretically in some detail and could be well understood. *(86)* In $D_2$, a similar experimental program was carried out, *(88, 89)* but at that time the theoretical formalism for the $I = 2$ spins had not yet been developed. Furthermore, for the solid echo data, the analysis of the results consisted of a simple extension of the $I = 1$ theory used for $H_2$, without proper consideration of the complete intermolecular dipolar interaction.

In these solid echo experiments on $D_2$, a search for the satellite echoes, predicted to occur for $I = 2$ systems and previously observed for $D_2$ embedded in an amorphous silicon matrix *(90)* ( in which exist large crystal fields ), was unsuccessful. A formal theory was needed to estimate the amplitude expected for these satellites in $D_2$ given the known local magnetic fields acting on the nuclei.

In this section, a theory for the spin signal amplitude for both *ortho* and *para* solid $D_2$ for two-pulse experiments is presented and comparison of the predictions with the experimental results is made. In Chapter 2, the formal theory using a "closed form" method, analogous to that previously developed for $I = 1$ in $H_2$ is presented. In Chapter 3, the calculated solid echo profiles are compared with experimental data and the positions and amplitudes of the principal and satellite echoes are discussed. Chapter 4 brings a summary.

## Chapter 2. THEORETICAL DEVELOPMENT OF THE $D_2$ SOLID ECHO

### *Symmetry Designations of the Hydrogens*

TABLE 3.1 Symmetry Designations of the Hydrogens

| *designation* | $H_2$ ( $i = 1/2$ ) | $D_2$ ( $i = 1$ ) |
|---|---|---|
| *ortho*<br>$\Psi_s$ symmetrical | $I = 1$<br>$J = 1$ | $1/6\ I = 0$, $5/6\ I = 2$<br>$J = 0^*$ |
| *para*<br>$\Psi_s$ antisymmetrical | $I = 0$<br>$J = 0$ | $I = 1$<br>$J = 1$ |

* small admixture with J=2 state in the solid state

Here the symmetry designations of the solid hydrogens are briefly recapitulated. These are based on the fundamental premise of quantum theory to deny the existence of a transition on exchange of two identical particles. For the case of diatomics, if the nuclear spins have integral spin quantum number $i$, as in the case of $D_2$, then the total wave function must be symmetrical with respect to exchange of homonuclear bosons; if the spins are half-integral, as for $H_2$, the total wave function must be antisymmetrical to exchange of the fermions. Since both the ground state electronic and vibrational modes are always symmetrical in a diatomic molecule, the symmetry of the total wave function is determined by the product of the rotational and nuclear contributions, if coupling between these four modes can be ignored. Systems with even (symmetrical) spin wave functions are designated *ortho* while those with odd (antisymmetrical) spin wave functions are designated *para*. These considerations are summarized in Table 3.1.

### *The Single Spin Hamiltonian*

As mentioned in Chapter 1, only the ground rotational states are populated at temperatures where the hydrogens are crystalline. This implies that the single molecule rotational wavefunctions are functions of the spherical harmonics $Y_{Jm}(\theta,\varphi)$. The $J = 0$ state corresponds to the scalar $Y_{00}$, a spherically symmetrical state for which no orientational dependence is expected. This is not the case for $Y_{1m}(\theta,\varphi)$, upon which the effects of anisotropic potentials are anticipated. In the presence of intermolecular nuclear dipolar interactions, $J = 1 \rightarrow J = 0$ conversion takes place. *(79)* In $D_2$, where the nuclear dipole moment is much smaller than that for $H_2$, the $J = 1 \rightarrow J = 0$ conversion rate is only of the order *(84)* of $\Delta X$=0.5%/24h for $X$=0.3 and therefore the concentration remains essentially constant during the course of a day's experiments, certainly constant on the time scale of the pulse sequence.

To consider the intramolecular interactions involving the nuclear spins, the spin Hamiltonian, $\mathcal{H}_S$, for non-interacting $H_2$ or $D_2$ molecules is introduced. *(91)*

$$\frac{\mathcal{H}_S}{\hbar} = -\alpha I_z - b_J J_z - c_{IJ} \boldsymbol{I}\cdot\boldsymbol{J} + \hbar\frac{\gamma_1\gamma_2}{i^2}\left[\frac{\boldsymbol{i}^{(1)}\cdot\boldsymbol{i}^{(2)}}{r_{12}^3} - \frac{3\left(\boldsymbol{i}^{(1)}\cdot\hat{\boldsymbol{n}}\right)\left(\boldsymbol{i}^{(2)}\cdot\hat{\boldsymbol{n}}\right)}{r_{12}^3}\right]$$

$$+\frac{eQ_n}{4i(2i-1)\hbar}\frac{\partial^2 V_e}{\partial z^2}\left[3\left(\boldsymbol{i}^{(1)}\cdot\hat{\boldsymbol{n}}\right)^2 + 3\left(\boldsymbol{i}^{(2)}\cdot\hat{\boldsymbol{n}}\right)^2 - i^{(1)}\left(i^{(1)}+1\right) - i^{(2)}\left(i^{(2)}+1\right)\right] \qquad [3.2.1]$$

Again, $I_z$ and $J_z$ are the projections of the total spin $\boldsymbol{I} = \boldsymbol{i}^{(1)} + \boldsymbol{i}^{(2)}$ and rotational angular momentum $\boldsymbol{J}$ of the molecule onto the axis of the external magnetic field. The two spin operators for the nuclei in a molecule are denoted $\boldsymbol{i}^{(1)}$ and $\boldsymbol{i}^{(2)}$ and $\hat{\boldsymbol{n}}$ is the unit vector determining the orientation of the molecular axis. The first two terms represent the Zeeman interaction and the energy of the magnetic moment associated with molecular rotation. Spin-rotation coupling is represented by the third term. The fourth term accounts for dipole-dipole coupling of the magnetic moments $\mu = \hbar\gamma\, \boldsymbol{i}$ of the atoms separated by the distance $r_{12}$ ( [1.4.8] ) while the last term, relevant only for deuterium, is the coupling of the deuteron nuclear quadrupole moment $Q_n$ to the electric field gradient along the bond axis of the molecule ( [1.4.19] ) in the QPAS system. A careful distinction should be made between the *nuclear* quadrupole moment and the *electric* quadrupole moment $Q_e$ of the molecule, which mediates the orientational ordering.

*Intermolecular Interactions*

Molecular hydrogens are the only examples of orientational quantum solids, in which the lattice molecules have a large zero point motion or a broad spatial distribution about the lattice sites and in which the angular distribution is non localized, even at $T = 0$. On condensation, the molecular hydrogens maintain their properties as free rotors ( as suggested by low heats of melting ) owing to the large energy differences between rotational states and the relatively weak anisotropic potentials in the solid, which are dominated by the permanent electric quadrupole-quadrupole (EQQ) interactions between $J = 1$ molecules. *(79)* These anisotropic electronic energies are, in turn, much larger than the nuclear spin energies appearing in [3.2.1], so the rotational states in $\mathcal{H}_S$ can be replaced by their thermodynamic averages. At temperatures above a few mK, the magnetic energies are also negligible in comparison with $k_B T$, in which case all components of the rotational angular momentum $J_\alpha$ $(\alpha = x,y,z)$ have zero thermodynamic averages, $\langle J_\alpha \rangle_T = 0$. *(82, 85, 30)* In other words, the rotational correlation times are much shorter than those corresponding to the nuclear spin part of $\mathcal{H}_S$ so the effect of the operators $-b_J J_z$ and $-c_{IJ}\, I \cdot J$ is effectively zero due to quenching of the orbital angular momentum.

Restricting discussion to $D_2$ in the crystalline state, the relevant nuclear spin Hamiltonian, including the intermolecular magnetic dipolar interaction, can be written as a sum over all molecules *i* in the sample.

$$\frac{\mathcal{H}_{TOT}}{\hbar}=\sum_j \left(\begin{array}{l} -\overline{\alpha_j} I_{zj}+a_j\left(3i_{zj}^{(1)2}+3i_{zj}^{(2)2}-i_j^{(1)}\left(i_j^{(1)}+1\right)-i_j^{(2)}\left(i_j^{(2)}+1\right)\right) \\ +b_j\left(i_{zj}^{(1)}i_{zj}^{(2)}-\frac{1}{4}i_{+j}^{(1)}i_{-j}^{(2)}-\frac{1}{4}i_{-j}^{(1)}i_{+j}^{(2)}\right)+I_{zj}\sum_{k\neq j}\overline{\delta_{jk}}I_{zk} \end{array}\right) \qquad [3.2.2]$$

Here the first three terms are the nuclear Zeeman term and the intramolecular terms resulting from the nuclear quadrupolar and nuclear dipolar interactions with coefficients $a_j$ and $b_j$. Due to the fact that the atoms in $D_2$ are homonuclear, the flip-flop terms in the intramolecular dipolar contribution are not quenched, resulting in a mixing of the *ortho* ( $I$ = 2 and $I$ = 0 ) states and consequently $I$ is not a good quantum number for *o*-$D_2$. The final term is the contribution from the intermolecular nuclear dipole-dipole interaction. Taking into consideration local field inhomogeneities, the frequency representing the average local magnetic field change is defined

$$\overline{\alpha_j}=2\mu_D\left(B_j-B_0\right)/\hbar \qquad [3.2.3]$$

where $B_0$ and $B_j$ represent the external and local magnetic fields. By homogeneous broadening, it is meant that each spin is equally associated with all energies of the resonant line, as would be achieved in an ideal cubic crystal. Since the dipolar interaction varies as $r_{jk}^{-3}$, small deviations in position can produce huge shifts of the Larmor frequency, due to the large local field experienced by the coupled spin pair, relative to the effects of all other spins. The resonance of such an inhomogeneously broadened spin pair is so far removed from the rest of the sample, that it can be considered isolated and is associated with its own energy. Inhomogeneously broadened lines consists of many such contributions.

Only the contribution of the expanded intramolecular dipole term that is secular with the Zeeman term is considered. Furthermore, both the intramolecular quadrupole and dipole coupling terms, $a_j$ and $b_j$, are moderated by the degree of orientational ordering of the neighbouring $J = 1$ molecules in the sample. As the direct EQQ interaction between molecules with $Q_e \neq 0$ tends to induce orientational alignment in the $p$-$D_2$ fraction, this molecular field also produces a perturbative alignment of the $o$-$D_2$ molecules resulting in the admixture of the $J = 2$ state into the ground state, *(85)* owing to the existence of off-diagonal matrix elements in an otherwise vanishing $Q_e$. The EQQ interaction dominates the orientationally dependent part of the intermolecular potential *(92)* and can be written in terms of the irreducible tensor operators.

$$\mathcal{H}_{EQQ} = \tfrac{16}{45}\pi\Gamma_0\sqrt{70\pi}\sum_{mn}\langle J_1 m J_2 n | J_1 J_2 J\, m+n\rangle \mathcal{Y}^{(2)m}(J_1)\mathcal{Y}^{(2)n}(J_2)Y_{4\,m+n}(\Omega_{jk}) \quad [3.2.4]$$

The EQQ coupling constant is defined by the electric quadrupole moment of the $J = 1$ molecule and the equilibrium intermolecular distance

$$\Gamma_0 = \frac{6e^2Q_e^2}{25R_0^2} \qquad [3.2.5].$$

Taking the quantization axis to lie parallel to the intermolecular vector requires only one component of the spherical harmonic $Y_{4\,m+n}(\Omega_{jk})$, simplifying [3.2.4]

$$\mathcal{H}_{EQQ} = \tfrac{8}{15}\pi\Gamma_0\sqrt{70}\sum_{m}\langle 2m2-m|2240\rangle \mathcal{Y}^{(2)m}(J_1)\mathcal{Y}^{(2)-m}(J_2) \qquad [3.2.6].$$

The factor $C_j(X)$ expressing this admixture has been derived by Harris *(85)* for the regime of long-range orientational order where $X > X_C = 0.53$ and is given by $C_j(X) = \tfrac{38}{9}\frac{\Gamma}{B}X$ to lowest order in $\Gamma/B$, where $\Gamma/k_B$=1.04K and the rotational energy constant $B/k_B$= 43K for $D_2$. For lower concentrations, where the orientational order is short-range, an adequate approximation for $C_j(X)$ is obtained *(92)* by scaling the expression above by the local order parameter of the $J = 1$ fraction in the hcp phase, $\sigma = \left\langle 1 - \tfrac{3}{2}J_{zj}^2 \right\rangle_T$, divided by the order parameter in the long-range ordered phase, $\sigma \approx 1$ in which case $\sigma$ is the same for each domain $j$. Here $J_{zj}^2$ is the small net projection of the angular momentum on the local symmetry axis. For these expressions of the order parameter, a cylindrical symmetry is assumed, as is reasonable for nuclei in states of well-defined angular momentum, signifying that the transverse components $J_{xj}^2$ and $J_{yj}^2$ remain quenched. *(93)* Hence, the admixture coefficient in [3.2.8] is replaced by a temperature dependent coefficient applicable to the short-range ordered regime "sr".

$$C_{sr}(X,T) = \tfrac{38}{9}\frac{\Gamma}{B}X\left\langle 1-\tfrac{3}{2}J_{zj}^2\right\rangle_T \qquad [3.2.7].$$

Expressions for the intramolecular interaction coefficients are then obtained

$$a_j = \tfrac{5}{8}C_{sr}(X,T)\left(1-3\cos^2\theta_{B,zj}\right)d_Q \qquad [3.2.8a]$$

$$b_j = -\tfrac{5}{4}C_{sr}(X,T)\left(1-3\cos^2\theta_{B,zj}\right)d_M \qquad [3.2.8b]$$

where $\theta_{B,zj}$ is the angle between the magnetic field and the local symmetry axis and where *(85)*

$$d_Q = \frac{2e^2Q_n}{5\hbar}\frac{\partial^2 V_e}{\partial z_0^2} = 22.50 \text{ kHz}$$

and

$$d_m = \frac{2\gamma_D^2\hbar}{5}\left\langle\frac{1}{r^3}\right\rangle = 2.74 \text{ kHz}$$

with the quantum mechanical expectation value of the interatomic distance given by $\left\langle\frac{1}{r^3}\right\rangle$.

For the typical concentration $X$ = 0.3, $C_{sr}$ = 0.02 at $T$ = 0.2K and represents the admixture of the $J = 2$ rotational state into the ground state forming a symmetrical total spin state $I = 2$. Of course, to consider the admixture of states in the rotational manifold of the $p$-$D_2$ fraction is irrelevant, so $C_{sr}$ is replaced by $\sigma$ for the $J = 1$ molecules as regards [3.2.8] above.

For the last term of [3.2.2], that describes the intermolecular nuclear dipolar interaction for both $I = 2$ and $I = 1$ spins, it should be noted that a typical intermolecular distance is much greater than that between two nuclei of the same molecule. Therefore, the expression for the intermolecular nuclear dipole-dipole interaction is well approximated by that representing single spins of magnitude $I$ localized at the centres of gravity of molecules separated by a distance $R_{jk}$, with the orientation of the intermolecular axis given by an angle $\theta_{R_{jk}B}$ relative to the external field. Therefore, the average dipolar field experienced by a spin $j$ due to the surrounding spins $k$ is approximated by

$$\sum_{k \neq j} \frac{\gamma_D^2 \hbar}{2R_{jk}^3}\left(1 - 3\cos^2\theta_{R_{jk}B}\right) I_{zj} = \sum_{k \neq j} \overline{\delta_{jk}}\, I_{zk} \qquad [3.2.9]$$

and is treated as a first order perturbation of the single molecule states. Here $\gamma_D$ is the gyromagnetic ratio of the deuteron. This formulation does not take into account the individual spin states of the deuterons in adjacent molecules, hence the dipolar interaction is restricted to atoms in $I \neq 0$ molecules. Given the relatively large intermolecular distances, this imposed limitation of theoretical resolution is acceptable as it merely reduces the number of intermolecular dipole coupling constants inherent to the theory.

This local field description of the dipolar interactions suggests that the dipolar field at a lattice site $j$ is the sum of the fields arising from all other moments in the sample. Two distinct contributions to this dipolar field might then be expected, namely those due to the presence of neighbouring $I = 1$ and $I = 2$ molecules, with respective frequencies $\overline{\delta_{j1}}$ and $\overline{\delta_{j2}}$. Of the four possible forms of $\overline{\delta_{jk}}$, the constant $\overline{\delta_{21}}$, for example, is the average intermolecular dipolar frequency experienced by an $I = 2$ molecule due to the presence of neighbouring $I = 1$ spins in the lattice. In the absence of the non-trivial calculation of the lattice sum in [3.2.9] over the range in which the dipole-dipole interaction is effective, *(94)* it might be argued that the relative magnitudes of these fields will increase with the concentration of the spin species generating the field, i.e. $\overline{\delta_{j1}}$ should increase with $X$ while $\overline{\delta_{j2}}$ should decrease. Since the magnitudes of these field contributions should be independent of $I_{zj}$, it might be considered superfluous to retain the subscript $j$ in the $\overline{\delta_{jk}}$'s. However, this convention is maintained throughout this development in order to provide both a clearer description of the theoretical results and a means by which to gauge the validity of the suppositions regarding the intermolecular nuclear dipolar interactions, once the numerical results are presented. Based on the discussion above, the following relations are expected

$$\delta_{11} \approx \delta_{21} \qquad \text{and} \qquad \delta_{12} \approx \delta_{22} \qquad [3.2.10].$$

The accuracy of these relations can be independently ascertained as the $\overline{\delta_{jk}}$'s are treated as *four independent parameters* to fit the theoretical expressions to the experimental data. Analysis of the results from both the four-parameter and the two-parameter regimen will be discussed in Chapter 3.

### *Development of the Closed-Form Expression for the Solid Echo Experiment*

A density matrix calculation of the two-pulse solid echo has been performed for the $p$-$H_2$ system. *(80)* Here again the intermolecular interaction is treated as a perturbation of the non-interacting Hamiltonian operating on the total product spin states $|M\rangle = \prod_j |M_j\rangle$ formed from the single molecule spin states $|M_j\rangle$. Formally, the product applies to all like spins in the sample; in practice only the aforementioned spin-pair interactions need be considered in the short-range ordered regime, reducing the problem's computational complexity. Other total spin operators may also be defined

$$I_x = \sum_j I_{xj} \qquad I_x^2 = \sum_{j,k.} I_{xj} I_{xk} \qquad [3.2.11a]$$

$$I_+ = \sum_j I_{+j} \qquad [3.2.11b].$$

Before application of the first r.f. pulse, the density matrix in the rotating frame of a system of spins $I$ in thermal equilibrium with the lattice at temperature $T$ is introduced.

$$\rho(0) = \frac{\exp(-H_{TOT} / k_B T)}{tr\exp(-H_{TOT} / k_B T)} \qquad [3.2.12]$$

Expanding [3.2.12] and applying the high field and high temperature approximations gives

$$\rho(0) \approx \frac{\hbar}{kT(2I+1)} \sum_j I_{zj} = gI_z \qquad [3.2.13]$$

where $g$ is a constant of the system. Time evolution of the density matrix, again in the absence of a r.f. pulse, is determined by ( [1.3.16] )

$$\rho(t) = \exp(-\tfrac{i}{\hbar}\mathcal{H}_{TOT}t)\,\rho(0)\exp(\tfrac{i}{\hbar}\mathcal{H}_{TOT}t) \qquad [3.2.14].$$

The effect of hard pulses is determined by the Wigner rotation matrix ( [1.1.37] )

$$\mathcal{D}^I_{M'M}(\alpha, \beta, \gamma) = d^I_{M'M}(\beta)\exp(i(M - M')\varphi) \qquad [3.2.15]$$

expressed in terms of the pulse angle $\beta$ and phase $\varphi$. By convention, a pulse with $\varphi = 0$ is denoted $x$ and one with $\varphi = \pi/2$ is denoted $y$. In this investigation, it is always the case that the first pulse has $\beta = \pi/2$ and $\varphi = 0$ and therefore this is a $(\pi/2)_x$ pulse. Subsequent to such a pulse, transformation of [3.2.13] gives

$$\rho(0^+) = \mathcal{D}^\dagger \rho(0)\mathcal{D} = gI_X \qquad [3.2.16].$$

The remainder of the pulse sequence involves a period of evolution as per [3.2.14] of duration $\tau$, followed by a second hard pulse $\mathcal{D}_2(\beta, \varphi)$ of arbitrary angle and phase with a final evolution period $t$, in which the solid echo is collected. The evolution of the density matrix in this time interval is given by

$$\rho(t) = \exp(-\tfrac{i}{\hbar}\mathcal{H}_{TOT}t)\mathcal{D}_2{}^\dagger\exp(-\tfrac{i}{\hbar}\mathcal{H}_{TOT}\tau)(gI_X)\exp(\tfrac{i}{\hbar}\mathcal{H}_{TOT}\tau)\mathcal{D}_2\exp(\tfrac{i}{\hbar}\mathcal{H}_{TOT}t)$$

$$[3.2.17].$$

Since the expectation value of an operator is determined by the quantum mechanical trace and by the time evolution of the density matrix [1.3.9], the detectable transverse signal at time $t$ after the second pulse is

$$S_+(t) = \frac{tr(\rho(t)I_+)}{tr(\rho(0^+)I_X)} = \frac{tr(\rho(t)I_+)}{tr(gI_X^2)} \qquad [3.2.18].$$

In order to calculate the trace in the denominator of [3.2.18], consider an $N$ spin system with angular momentum components given by a form similar to [3.2.11]. Taking as the set of basis functions the product of $N$ single spin states, it is neccessary to evaluate the sum

$$\sum_{M_1M_2\ldots M_N} \left\langle M_1M_2\ldots M_N \left| I_X^2 \right| M_1M_2\ldots M_N \right\rangle \qquad [3.2.19].$$

If the $M$'s are considered eigenvalues of $I_z$, then all diagonal elements of $I_x$ and $I_y$ are identically zero. However, since the assignment of the observable component of magnetization is arbitrary, the $2I+1$ values of $M$'s can be equivalently taken as the eigenvalues of $I_x$. From the definition of the square of the total angular momentum [1.1.17] and [1.1.18], for the $N$ identical terms for which $j = k$ in [3.2.11a]

$$tr\left(gI_x^2\right) = g\frac{I(I+1)}{3}N(2I+1)^N \qquad [3.2.20]$$

which amounts to a normalization over the sample containing $N$ *ortho* or *para* deuterium molecules. It should be noted at this time that, in practice, this normalization is treated as an arbitrary amplitude correction, for reasons to be discussed shortly.

In evaluating the trace in the numerator of [3.2.18], a closed form method is used to explicitly calculate the independent contributions to the echo by evaluating the non-zero matrix elements subject to the selection rules to be discussed. While any equivalent representation of the spin space will lead to the same result, this method is chosen over that used in PART 2 ( where the line is decomposed into its tensorial contributions ) for several reasons: a) the experiment consists of a two pulse sequence so it is not as imperative to appeal to the rotationally invariant properties of the spherical tensors, b) the form of $\mathcal{H}_{TOT}$ is diagonal in the $|IM\rangle\langle IM'|$ basis, c) a tensor operator approach is based upon the average values of the interactions appearing in $\mathcal{H}_{TOT}$ and does not resolve their individual contributions and d) it would be neccessary to construct a coupled tensor basis of the type [1.2.20] and its transformation properties under $\mathcal{H}_{TOT}$. Direct evaluation in the $|IM\rangle\langle IM'|$ basis circumvents these difficulties. To begin, [3.2.17] is expanded making use of the completeness relation [1.1.19b] so that

$$S_+(t) = \frac{1}{tr\left(gI_x^2\right)} \sum_j \Big( \langle M|\exp(-\tfrac{i}{\hbar}\mathcal{H}_{TOT}t)\mathcal{D}_2{}^{\dagger}|M'\rangle\langle M'|\exp(-\tfrac{i}{\hbar}\mathcal{H}_{TOT}\tau)gI_X|M''\rangle$$

$$\langle M''|\exp(\tfrac{i}{\hbar}\mathcal{H}_{TOT}\tau)\mathcal{D}_2|M'''\rangle\langle M'''|\exp(\tfrac{i}{\hbar}\mathcal{H}_{TOT}t)I_+|M\rangle\Big) \qquad [3.2.21].$$

Again, it is anticipated that the intermolecular dipolar interaction may be effectively treated as a sum of pairwise interactions in the short-range ordered hcp phase of $D_2$. As mentioned previously, the pair eigenstates and the rotation matrices are defined as

$$\left|M_jM_k\right\rangle = \left|M_j\right\rangle\left|M_k\right\rangle \qquad [3.2.22]$$

$$\mathcal{D}_{jk} = \mathcal{D}_j\mathcal{D}_k \qquad [3.2.23]$$

resulting in

$$S_+(t) = \frac{1}{tr\left(gI_x^2\right)} \sum_{M_jM'_jM''_jM'''_j} \; \sum_{M_kM'_kM''_kM'''_k} \left\langle M_jM_k\left|\mathcal{D}_{2jk}{}^{\dagger}\right|M'_jM'_k\right\rangle$$

$$\times\left\langle M'_jM'_k\left|I_{xj}E_k\right|M''_j\,M''_k\right\rangle\left\langle M''_j\,M''_k\left|\mathcal{D}_{2jk}\right|M'''_j\,M'''_k\right\rangle\left\langle M'''_j\,M'''_k\left|I_{+k}E_k\right|M_jM_k\right\rangle$$

$$\times\exp\left[i\left(\left[-\overline{\alpha_j}\left(M'''_j - M_j\right) + \left(E'''_{b_j} - E_{b_j}\right) + \left(E'''_{a_j} - E_{a_j}\right) + \overline{\delta_{jk}}\left(M'''_j\,M'''_k - M_jM_k\right)\right]t\right)\right]$$

$$\times\exp\left[i\left(\left[-\overline{\alpha_j}\left(M''_j - M'_j\right) + \left(E''_{b_j} - E'_{b_j}\right) + \left(E''_{a_j} - E'_{a_j}\right) + \overline{\delta_{jk}}\left(M''_j\,M''_k - M'_jM'_k\right)\right]\tau\right)\right]$$

[3.2.24].

$\sum_{M_j M'_j M''_j M'''_j}$ and $\sum_{M_k M'_k M''_k M'''_k}$ are sums over the molecular spin states of molecules $j$ and $k$. $E_k$ is the unit matrix operating on spins $k$ and $E_{b_j}$ and $E_{a_j}$ are the intramolecular dipole and quadrupole eigenvalues.

For $I = 2$, the non-zero matrix elements of $I_x$ generate the selection rules:

$$M'_j = \pm 2,\ M''_j = \pm 1 \quad M'_j = \pm 1,\ M''_j = \pm 2{,}0 \quad M'_j = \pm 0,\ M''_j = \pm 1 \qquad [3.2.25a].$$

From the form of $I_+$ the following selection rules are found:

$$M'''_j = 2, M_j = 1 \quad M'''_j = 1, M_j = 0 \quad M'''_j = 0, M_j = -1 \quad M'''_j = -1, M_j = -2 \qquad [3.2.25b]$$

for a total of 24 combinations. The conditions for echo maximum amplitude are determined by the intramolecular interactions which cause the relative spin phases to become refocussed at time $t = \tau$ after the second pulse,. resulting in the formation of the principal echo. This condition imposes a further restriction on [3.2.25], namely $M'''^2_j - M^2_j = -\left(M''^2_j - M'^2_j\right)$, thus reducing the number of selection rules to the following eight combinations:

$$\begin{aligned} M_j &= 1,\ M'_j = \pm 2,\ M''_j = \pm 1,\ M'''_j = 2 \\ M_j &= 0,\ M'_j = \pm 1,\ M''_j = 0,\ M'''_j = 1 \\ M_j &= -1,\ M'_j = 0,\ M''_j = \pm 1,\ M'''_j = 0 \\ M_j &= -2,\ M'_j = \pm 1,\ M''_j = \pm 2,\ M'''_j = -1 \end{aligned} \qquad [3.2.26a]$$

for each of which

$$M_k = M'''_k,\ M'_k = M''_k \qquad [3.2.26b].$$

Considering the relevant matrix elements, for $I = 1$ the same result obtained by Yu *et al.* *(86)* is found

$$\begin{aligned} M_j &= 0,\ M'_j = \pm 1,\ M''_j = 0,\ M'''_j = 1 \\ M_j &= -1,\ M'_j = 0,\ M''_j = \pm 1,\ M'''_j = 0 \end{aligned} \qquad [3.2.27].$$

Computation of [3.2.24] yields expressions for the principal echo amplitude of the form

$$S(I=1)=\tfrac{5}{6}(1-X)\left[a+b\cos\left(\overline{\delta_{12}\tau}\right)+c\cos\left(2\overline{\delta_{12}\tau}\right)+d\cos\left(3\overline{\delta_{12}\tau}\right)+e\cos\left(4\overline{\delta_{12}\tau}\right)\right]$$
$$+X\left[l+m\cos\left(\overline{\delta_{11}\tau}\right)+n\cos\left(2\overline{\delta_{11}\tau}\right)\right]$$

[3.2.28a]

$$S(I=2)=\tfrac{5}{6}(1-X)\left[A+B\cos\left(\overline{\delta_{22}\tau}\right)+C\cos\left(2\overline{\delta_{22}\tau}\right)+D\cos\left(3\overline{\delta_{22}\tau}\right)+E\cos\left(4\overline{\delta_{22}\tau}\right)\right]$$
$$+X\left[L+M\cos\left(\overline{\delta_{21}\tau}\right)+N\cos\left(2\overline{\delta_{21}\tau}\right)\right]$$

[3.2.28b].

The coefficients $A$, $B$, ..., $N$, $a$, $b$, ..., $n$ are functions of the pulse parameters, $\beta$ and $\varphi$ and the inhomogeneous field represented by $\cos\left(2\overline{\alpha_j\tau}\right)$ and are presented explicitly in Appendix 1. Note that for $X = 1$ ( no $I = 2$ spins ), [3.2.28a] reduces to Eq. (12a) reported by Yu *et al.* *(86)* which applies to $H_2$, except for a $\pi/2$ phase shift reflecting the difference in conventions used for the definition of the pulse terms. Assuming that the inhomogeneous field is independent of the intermolecular dipole interactions, for $\beta = \pi/2$, [3.2.28] reduces to a form in which the influence of the inhomogeneous field is more obvious,

$$S_{xx}=-P\left(1-\cos\left(2\alpha_j\tau\right)\right)$$
$$S_{xy}=P\left(1+\cos\left(2\alpha_j\tau\right)\right) \qquad [3.2.29a]$$

in which case $P$ is a function independent of the pulse parameters

$$P(I=1)=\tfrac{5}{6}(1-X)\left(\tfrac{7}{8}+\cos\left(\overline{\delta_{12}\tau}\right)+2\cos\left(2\overline{\delta_{12}\tau}\right)+\cos\left(3\overline{\delta_{12}\tau}\right)+\tfrac{1}{8}\cos\left(4\overline{\delta_{12}\tau}\right)\right)$$
$$+X\left(\tfrac{1}{2}+2\cos\left(\overline{\delta_{11}\tau}\right)+\tfrac{1}{2}\cos\left(2\overline{\delta_{11}\tau}\right)\right) \qquad [3.2.29a]$$

$$P(I=2)=\tfrac{5}{6}(1-X)\left(\tfrac{7}{8}+\cos\left(\overline{\delta_{22}\tau}\right)+2\cos\left(2\overline{\delta_{22}\tau}\right)+\cos\left(3\overline{\delta_{22}\tau}\right)+\tfrac{1}{8}\cos\left(4\overline{\delta_{22}\tau}\right)\right)$$
$$+X\left(\tfrac{1}{2}+2\cos\left(\overline{\delta_{21}\tau}\right)+\tfrac{1}{2}\cos\left(2\overline{\delta_{21}\tau}\right)\right)$$

[3.2.29b].

This interpretation represents a significant departure from the development used for the analysis of $p$-$H_2$ *(86)* where, in the absence of unlike $I$=0 spins, the dipolar field is entirely described by the two terms $\cos(\overline{\delta_{11}}\tau)$ and $\cos(2\overline{\delta_{11}}\tau)$. Moreover, both these terms and the one arising from the inhomogeneous field were taken as averages over the sample ( $\overline{\cos(2\alpha\tau)} = \frac{1}{N}\sum_j \cos(2\overline{\alpha_j}\tau)$ for example ) and used as arbitrary parameters to fit the data obtained for each set of experimental conditions. Assumed to be relevant for the $p$-$D_2$ fraction in solid deuterium, the previous development *(88)* also neglected the dipolar interactions between unlike spins i.e. the tacit assumption that $\overline{\delta_{12}} = 0$ was made. Despite these shortcomings, two useful relations were discovered that remain valid. From [3.2.29] a measure of the inhomogeneous field is obtained by forming the ratio

$$\mathcal{R} = \frac{|S_{xx} + S_{xy}|}{|S_{xx}| + |S_{xy}|} = \cos\left(2\overline{\alpha_j}\tau\right) \qquad [3.2.30].$$

Also, information of the spin-spin relaxation due to the dipolar field can be extracted by combining the results for an $xx$ and $xy$ sequence for a given set of experimental parameters

$$|S_{xx}| + |S_{xy}| = P \qquad [3.2.31].$$

Confirmation of the validity of [3.2.30] and [3.2.31] by comparison to the experimental results will at once verify both the independence of the inhomogeneous field on the dipolar interactions and the detailed form of the echo amplitude decay from dipolar relaxation arrived at in [3.2.24].

# Chapter 3. RESULTS AND DISCUSSION

## *Echo Amplitudes and Decay: the Anomalous p-$D_2$ Behaviour*

One of the most intriguing and as yet unexplained phenomena found in solid $D_2$ is the striking departure from Curie's law for the $I = 1$ magnetization with decreasing temperature. *(84, 88)* This deviation is particularly strong for $X = 0.5$ and in the temperature range where the orientational fluctuation rate $\tau_Q^{-1}$ is of the same order as the Larmor frequency $\omega_0$ of the precessing spins. *(95)* This departure from Curie's law means an apparent "loss" of spins in the sample and various scenarios have been proposed in an unsuccessful attempt to explain this phenomenon. No such "loss" is observed for the $I = 2$ spins in the same sample, nor for the $I = 1$ spins in solid $H_2$ at comparable mole fractions $X$ and at temperatures where $\omega_0 \tau_Q \approx 1$. *(95)* Therefore, in solid $D_2$, the amplitude ratio $S_{xy}(I = 1)/S_{xy}(I = 2)$ in the limit $\tau \rightarrow 0$ is smaller than the calculated ratio of the nuclear susceptibilities and is a function of $T$ and $X$.

For the observable $p$-$D_2$ $I = 1$ spins, the solid echo decay is affected by the orientational fluctuations in the temperature region where $\omega_0 \tau_Q \approx 1$ and the theory of the enhanced echo damping caused by these fluctuations has been presented by Harris *et al.* *(95)* In this analysis of the echo relaxation data, only samples studied under conditions where this fluctuational damping is small are considered. For instance, no attempt is made to account for the behaviour of samples with $X = 0.49$ at temperatures below $T = 0.4$K where orientational fluctuations are considerable. The magnitude of this damping and the damping characteristic temperature decrease with $X$. Hence, samples with $X = 0.28$ at $T = 0.2$K will show only small fluctuation damping *(95)* and will be analyzed as described below.

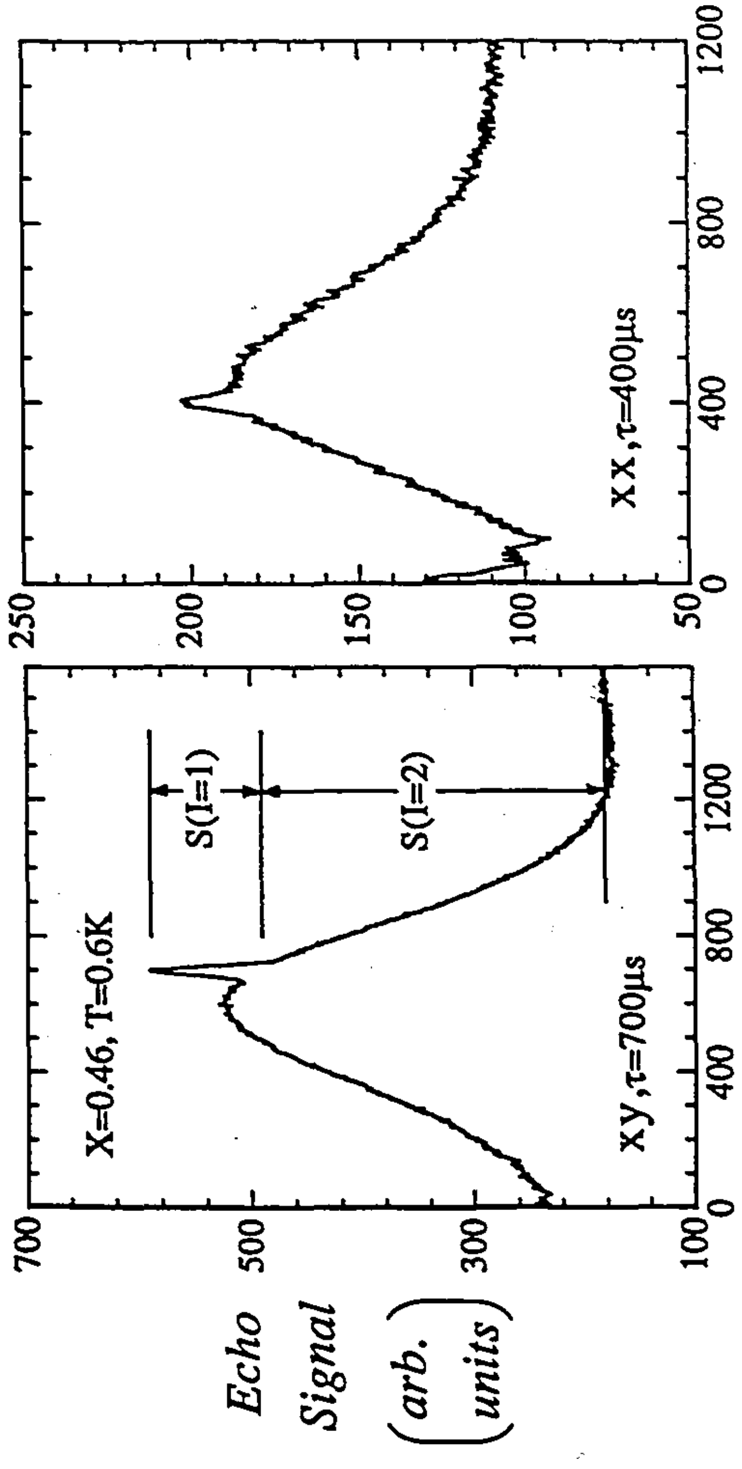

Figure 3.1. Representative echo profiles for the *xy* and *xx* pulse sequences and the absolute amplitudes *S*(*I*=1) and *S*(*I*=2) of the principal echo, in arbitrary units, as taken from *(88)*.

No correlation exists between the observed solid echo magnitudes of the different samples shown in the various figures, since the settings of the electronics are not necessarily kept the same for different experiments, as they were chosen to optimize the recording conditions.

### *Echo Amplitude Relaxation*

The computations are compared with tabulated experimental data of *(88)*. Representative echo profiles for the *xy* and *xx* pulse sequences are shown in Figure 3.1. The absolute value of each in the same arbitrary units is reproduced here, but the amplitude is positive relative to the FID for the *xy* and negative for the *xx* echoes. The signal amplitudes, $S(I=1)$ and $S(I=2)$, for *para* and *ortho*-$D_2$ respectively, are also defined. For $I = 1$, the signal maximum of the principal echo is located at a time $t = \tau$ after the second pulse, as expected. The asymmetry of the broader $I = 2$ echo envelope and the apparent shift of the echo maximum amplitude are due to intermolecular dipole relaxation and have been interpreted in terms of a Gaussian line shape centred at a time $t = \tau$ after the second pulse and damped by an exponential decay. *(88, 96)* From measurements of the inhomogeneous and intermolecular second moments, the typical values found are $\overline{\alpha_j} = 150\text{Hz}$ and $\overline{\delta_{jk}} = 220\text{Hz}$ for the mean dipolar field *(88)* for both *para* and *ortho*-$D_2$. (There is a small relative frequency shift $\delta\overline{\alpha_j}$ *(96)* between *para* and *ortho*-$D_2$ but it does not affect the individual analyses of $S(I=1)$ and $S(I=2)$.)

Figure 3.2 shows the representative echo amplitude decay of a sample with $X=0.49$ at 0.6 K and $X = 0.45$ at 0.4K as a function of the evolution time $\tau$ for both the *xx* and *xy* sequences with $\beta = \pi / 2$. With increasing values of $\tau$ the echo amplitudes are damped through both the intermolecular dipole and inhomogeneous fields. The relevant parameters are determined by simultaneous fit of the theory to the data from the *xx* and *xy* sequences, with the lines representing the best fits of [3.2.29]. Table 3.2 gives a summary of the parameters used to produce relaxation curves similar to those in Figure 3.2 for various samples over a range of conditions, from which a few trends are immediately apparent. (These parameters can be varied individually to within about 5% without deterioration of the fit and are comparable with the experimentally observed values reported in *(88)* from a simpler analysis.) They are consistent in the sense that it is expected that both the *ortho* and *para* fractions are subject to the same inhomogeneous broadening and hold for both the respective $xx$ and $xy$ sequences. There is no well established trend in the magnitude of this inhomogeneous field with $X$. At $\beta = \pi/2$, the amplitude of the $S_{xx}$ signal is small relative to $S_{xy}$ resulting in unfavourable S/N and large experimental scatter. While this problem is not as significant for the $I$=2 signal, the error is amplified when the data are processed via [3.2.30] and [3.2.31]. A survey of Table 3.2 also suggests that the interpretation of the dipolar relaxation is adequate in that $\delta_{11} \approx \delta_{21}$ and $\delta_{12} \approx \delta_{22}$.

In Figure 3.3 the fit of the combined [3.2.29] and [3.2.31] is given for the same set of experimental data used in Figure 3.2. Here the theoretical curves are independent of the inhomogeneous field and show the dependence of the signal amplitude on the intermolecular dipole relaxation alone. The theoretical results for the four-parameter (solid line) and two-parameter (broken line) representations of the dipolar field are compared using the values reported in Table 3.2. Making the assumption that [3.2.10] holds and using average values of the relevant coupling constants yields the broken curve for the two-parameter model. This last fit to the experimental data deviates from them somewhat more than the less restrictive four-parameter fit. However, these theoretical results do support the notion that the dipolar field experienced by all spins in the sample can be effectively represented by two distinct contributions given by $\overline{\delta_{j1}}$ and $\overline{\delta_{j2}}$. It is also significant that these dipolar coupling terms reveal a more sensitive dependence of the signal amplitudes on the presence of the *ortho* spins than on the *para* fraction, which is not

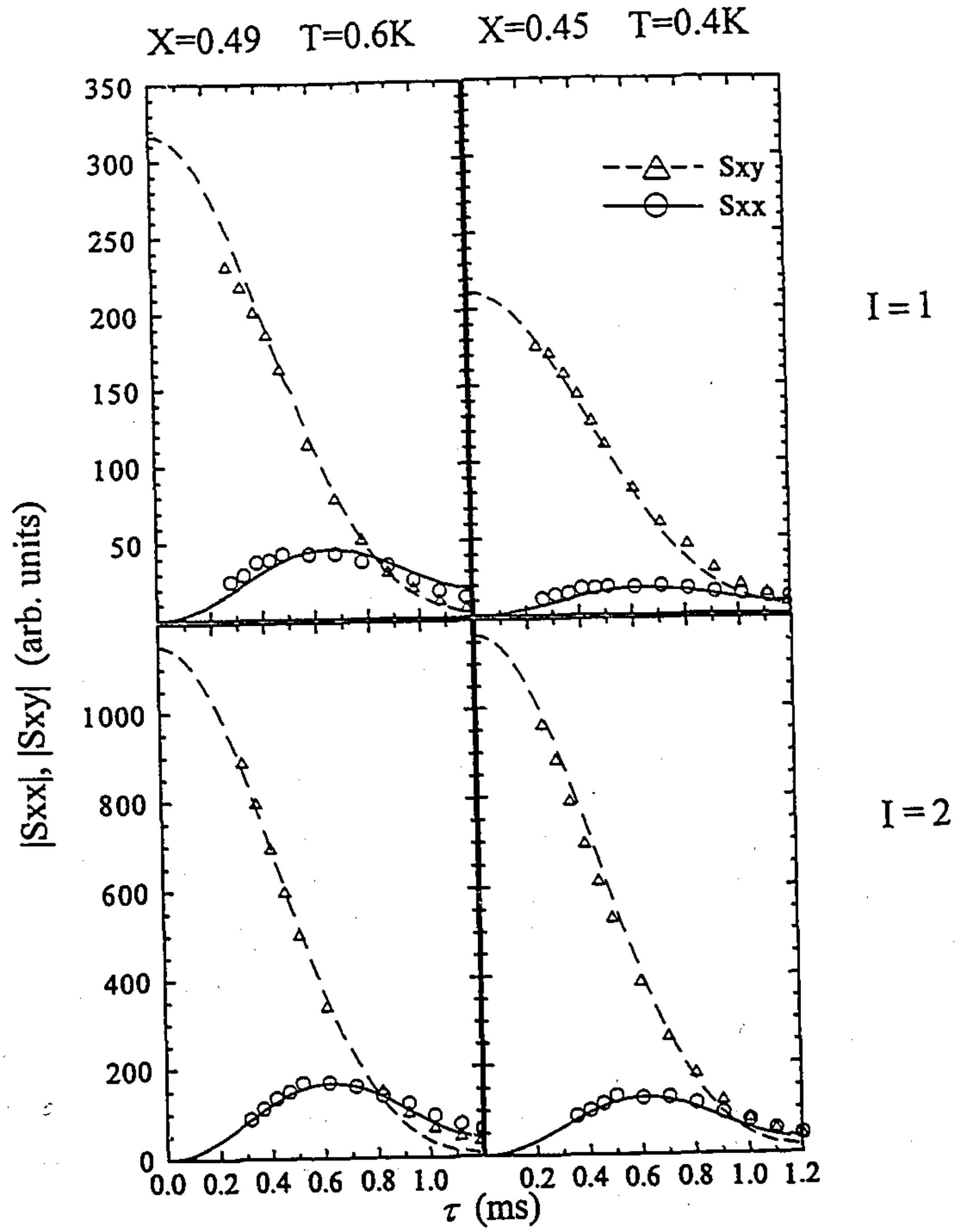

Figure 3.2. Echo amplitude decay of the absolute amplitudes $S(I=1)$ and $S(I=2)$ for a sample with $X=0.49$ at 0.6K and $X=0.45$ at 0.4K as a function of the evolution time $\tau$ for both the *xy* (triangles) and *xx* (circles) pulse sequences with $\beta=90°$. For each sample, the arbitrary units are the same. The symbols represent the experimental data while the broken and solid curves are the computed decays using the coupling constants reported in Table 3.1 and described in the text.

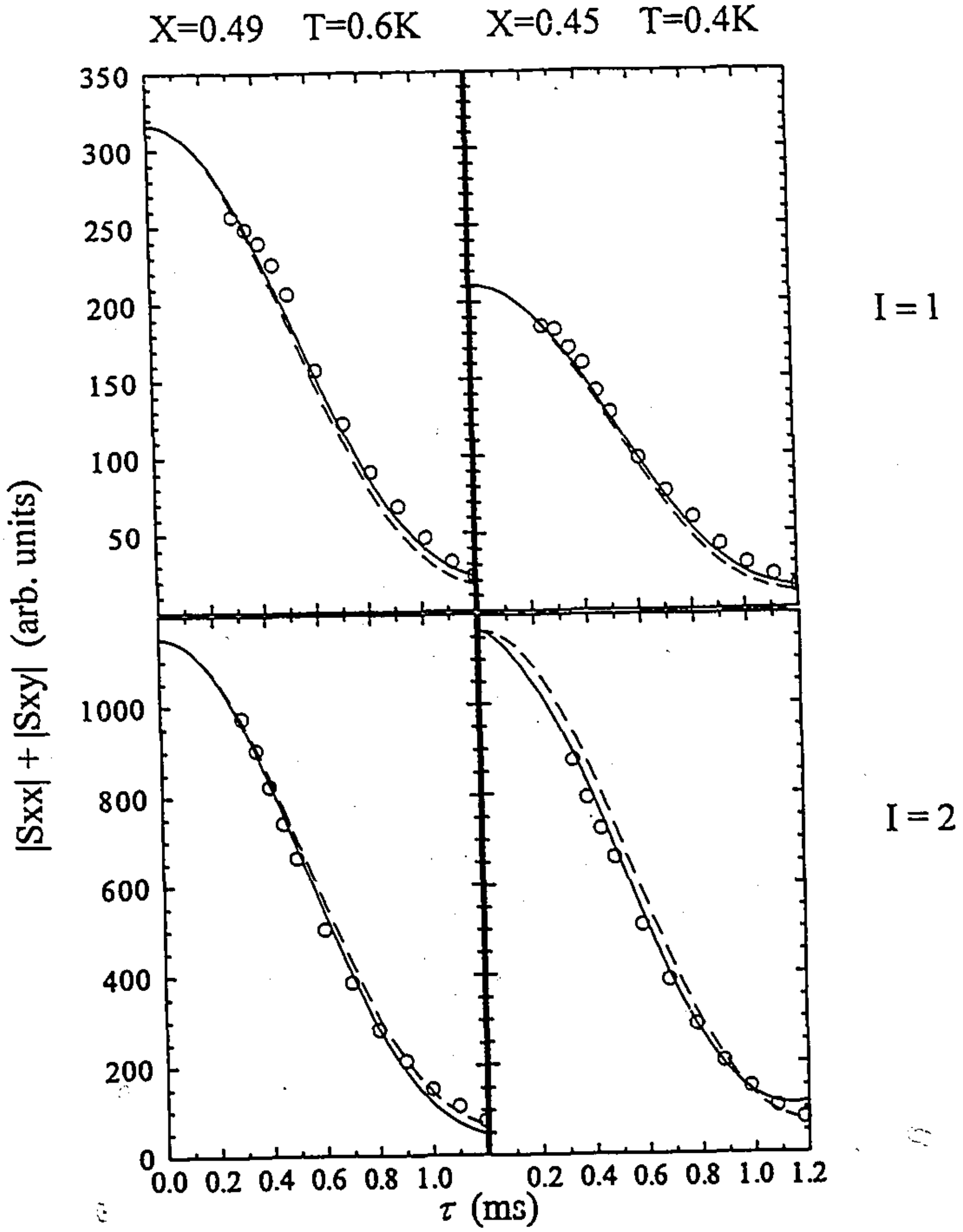

Figure 3.3. Fit of Eq. 28 to the same set of experimental data used in Figure 3.2. The theoretical curves are independent of the inhomogeneous field and show the dependence of the signal amplitude decay on the intermolecular dipole relaxation alone. The results of both the two-parameter and four-parameter representations of the dipolar field are given. The solid curves result from the coupling constants reported in Table 3.2. The broken curves are the result of the two-parameter fit assuming $\overline{\delta_{21}} = \overline{\delta_{11}}$ and $\overline{\delta_{22}} = \overline{\delta_{12}}$ using average values.

| X | T (K) | $\overline{\alpha}(\mathrm{I}=1)$ (Hz) | $\overline{\delta_{11}}$ (Hz) | $\overline{\delta_{12}}$ (Hz) | $\overline{\alpha}(\mathrm{I}=2)$ (Hz) | $\overline{\delta_{21}}$ (Hz) | $\overline{\delta_{22}}$ (Hz) |
|---|---|---|---|---|---|---|---|
| 0.06 | 0.1 | - | - | - | 120 | - | 223 |
| 0.06 | 0.2 | - | - | - | 120 | - | 223 |
| 0.06 | 1.2 | - | - | - | 120 | - | 223 |
| 0.28 | 0.2 | 125 | 64 | 175 | 120 | 64 | 191 |
| 0.30 | 1.2 | 92 | 107 | 199 | 104 | 127 | 203 |
| 0.40 | 0.6 | 95 | 107 | 199 | 107 | 111 | 207 |
| 0.45* | 0.1 | 123 | 130 | 195 | 123 | 115 | 215 |
| 0.45 | 0.4 | 115 | 111 | 191 | 123 | 127 | 199 |
| 0.45 | 1.0 | 115 | 111 | 191 | 123 | 115 | 199 |
| 0.49 | 0.6 | 145 | 119 | 187 | 155 | 135 | 195 |

Table3.2. Summary of the theoretical coupling constants used throughout the analysis. Note that the $X$=0.45 sample at 0.1K (marked by the asterisk) is affected by the additional damping from orientational fluctuations, as described in the text, resulting in larger than expected values for $\overline{\delta_{11}}$ and $\overline{\delta_{12}}$. The observed trend in the magnitudes of the dipolar coupling constants is as expected for the different values of $X$ i.e. $\overline{\delta_{j1}}$ increases and $\overline{\delta_{j2}}$ decreases as $X$ increases. While samples with larger $X$ tend to exhibit larger values of $\overline{\alpha_j}$, there is no reason to expect a correlation between these two quantities.

surprising when one considers the difference in spin magnitudes but perhaps this also hints at the distribution of environments experienced by the *o*-$D_2$ molecules.

The data from these two samples were again used to produce Figure 3.4. The data (open circles) are compared with the curves calculated from [3.2.30] where the values of the inhomogeneous field $\overline{\alpha_j}$ in Table 3.2 have been used. The experimental scatter is exacerbated in this case owing to the fact that the difference in phase of $S_{xx}$ and $S_{xy}$ leads to a subtraction. This operation cancels out the effect of the intermolecular dipole interaction, yet despite this more serious deviation of the theory it is noted that the inhomogeneous field appears to be uncoupled from the intermolecular dipolar field. Again it is apparent that the inhomogeneous field affects each spin in the sample in a uniform fashion and has only a slightly larger effect on the sample with the larger concentration of $I = 1$ spins. While our basic understanding of the $\overline{\delta_{jk}}$'s is good, the origin of the inhomogeneous field is unclear as discussed previously. *(88)*

In Figure 3.5, for a sample with $X = 0.28$ and $T = 0.2$K ( incorrectly labeled $X = 0.24$ in Figure 7 of *(88)* ), the dependence of the signal amplitude on the angle of the second pulse, $\beta$, is presented for four different values of $\tau$ . This set of experiments represents the most demanding examination of the validity of the entire theoretical model, as it incorporates systematic variations of all experimentally significant parameters. The values of the parameters reported in Table 3.2 are the averages of those used to fit all four sets of data and were varied within 10% in order to closely match the experimental points. The increasing deviations from these means generally arise from results with larger values of $\tau$. As previously discussed, given the form of $\overline{\delta_{jk}}$ expressed in [3.2.9], it is tacitly expected that for a spin $j$ coupled to the field generated by surrounding spins $I_k = 1$, $\overline{\delta_{j1}}$ should decrease with decreasing $X$, a trend observed from the results for Figures 3.2, 3.3 and 3.5 shown in Table 3.2. While the reverse should be true for $I_k = 2$, i.e. $\overline{\delta_{j2}}$ should increase with decreasing $X$, the results suggest more efficient coupling to spins $I_k = 2$ in lattices with larger concentrations of $I = 1$ molecules. Despite this apparent contradiction in the expected behaviour of the dipolar field, we do note that the average values of $\overline{\delta_{j1}}$ and $\overline{\delta_{j2}}$ appear to independent of the magnitude of the spin $i$, hence $\overline{\delta_{21}} \approx \overline{\delta_{11}}$ and $\overline{\delta_{22}} \approx \overline{\delta_{12}}$ consistently throughout this analysis as expected. The fit of the theory to the experimental data presented in Figure 3.5 makes use of the four-parameter procedure because here an attempt is made to simultaneously account for the influence of all relevant parameters. There is increasing disparity between the theoretical curves and the experimental evidence for large values of both $\tau$ and $\beta$ , the common cause being the dephasing of the prepared coherences. Apart from the unfavourable S/N typical for low amplitude signals, as the amplitudes decrease with increasing $\tau$ and $\beta$ the effects of imperfect pulse tuning become increasingly important and thus some systematic deviation might be introduced. This heralds the breakdown of the two-parameter model for the dipolar field, as increasingly divergent values of the $\overline{\delta_{jk}}$'s must be used in order to closely match the experimental data for the longer values of $\tau$. However, a relaxation mechanism hitherto unaccounted for may exist. Spin diffusion and the motion of neighbouring atoms or defects should have negligible influences at these temperatures, but it remains possible for cross-relaxation to be effective. This would manifest itself as a zero-quantum ($\Delta M = 0$) exchange of polarization between two spins and might have been neglected due to the strictly secular representation of the intermolecular dipolar interaction.

For the $I = 2$ $S_{xx}$ case, Figure 3.6 shows how these theoretical curves are constituted of the functions $A$, $B$, ..., N defined by [3.2.28] and presented the Appendix. In the absence of an inhomogeneous field, these functions are dependent only upon the pulse terms and have odd symmetry about $\beta = \pi/2$. However, when $\overline{\alpha_j} \neq 0$, those contributions associated with the higher frequency dipole terms ($E$ and $N$ for example) are favoured at larger values of $\beta$, as shown in Figure 3.6 where $\overline{\alpha_i} = 120\text{Hz}$ and $\tau$ = 1.0ms. It should be expected, then, that such high frequency terms are attenuated for increasing values of $\tau$, as evidenced in Figure 3.5.

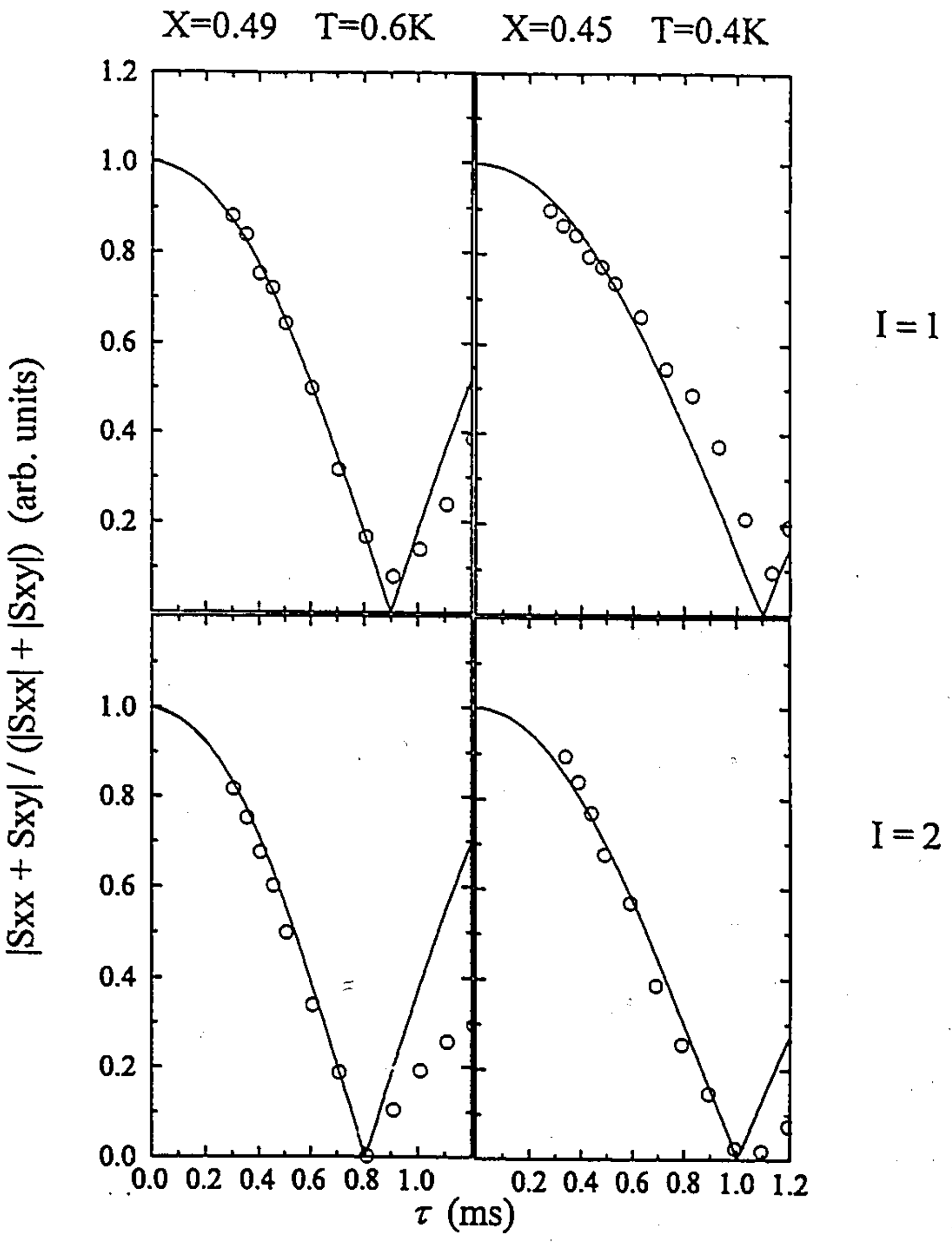

Figure 3.4. Fit of [3.2.30] to the experimental data for samples with $X = 0.49$ at $T = 0.6$K and $X = 0.45$ at 0.4K. The theoretical curve shows the contribution of the inhomogeneous field alone to the signal amplitude decay and its independence on the dipolar field. Fit parameters used are reported in Table 3.2.

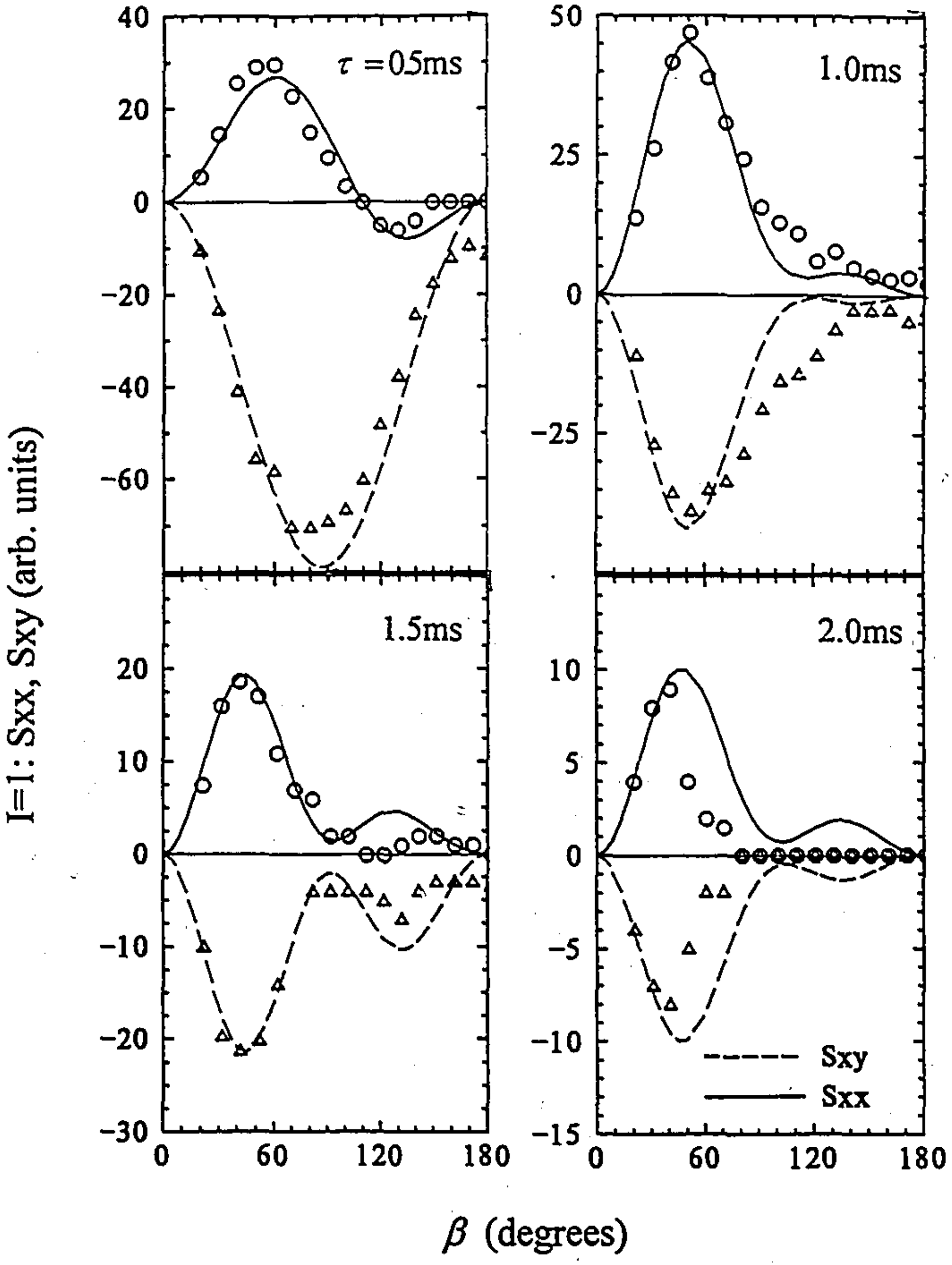

Figure 3.5a. Dependence of the signal amplitude on the angle of the second pulse, $\beta$, for four different values of $\tau$ for a sample with $X = 0.28$ at $T = 0.2$K. The symbols (circles for $S_{xx}$, triangles for $S_{xy}$) mark the experimental data and the solid and broken curves, the best fit of the theory. For $I = 1$ the fit parameters for all four sets of data are: $\overline{\alpha_j} = 120$ Hz, $\overline{\delta_{11}} = 64$ Hz, $\overline{\delta_{12}} = 175$ Hz.

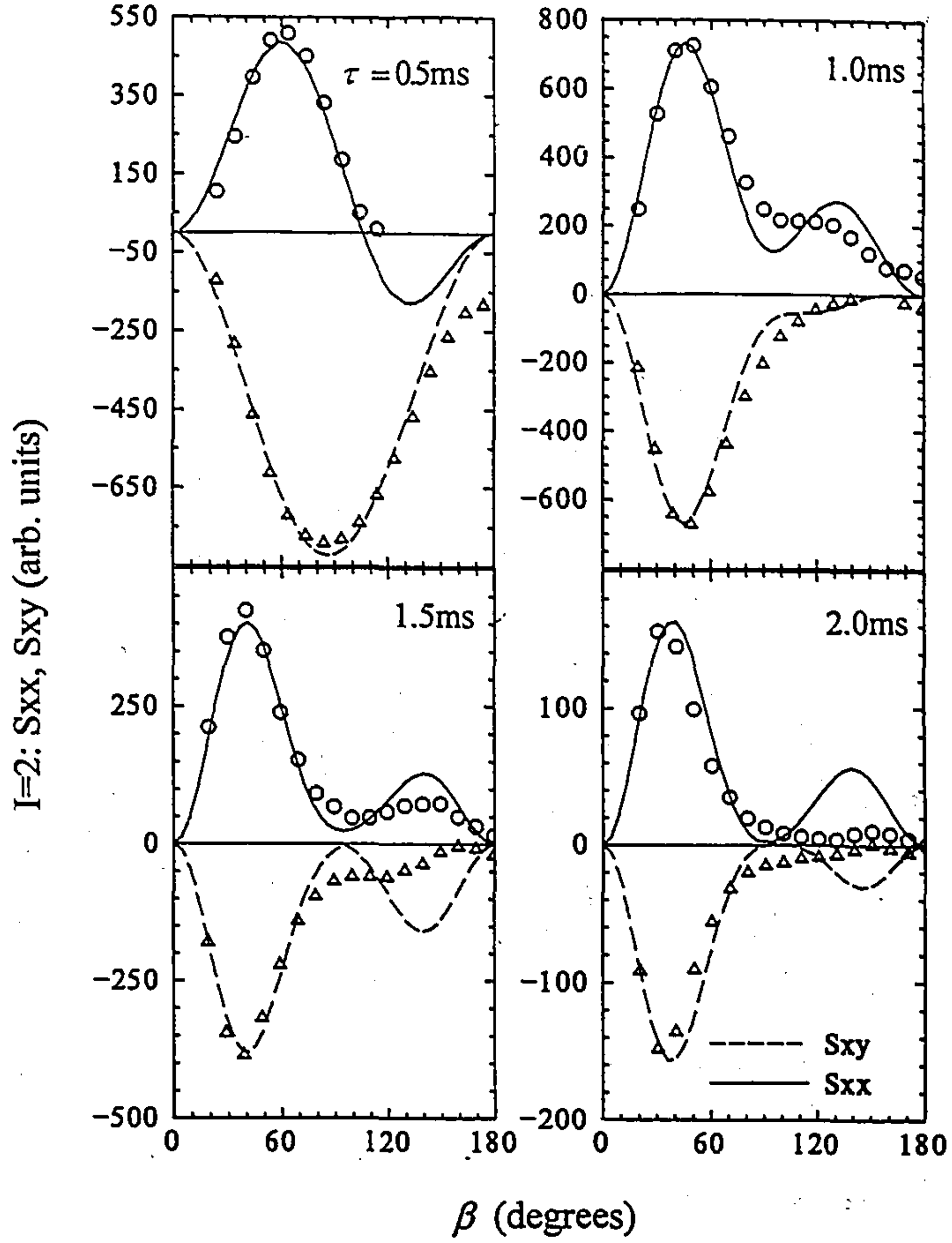

Figure 3.5b. Same as Figure 3.5a for $I$=2: $\overline{\alpha_j}$ = 120 Hz, $\overline{\delta_{22}}$ = 190 Hz, $\overline{\delta_{21}}$ = 64 Hz. In both cases the values of the dipole coupling terms were varied individually to within 10%, with increasing deviation at large values of τ.

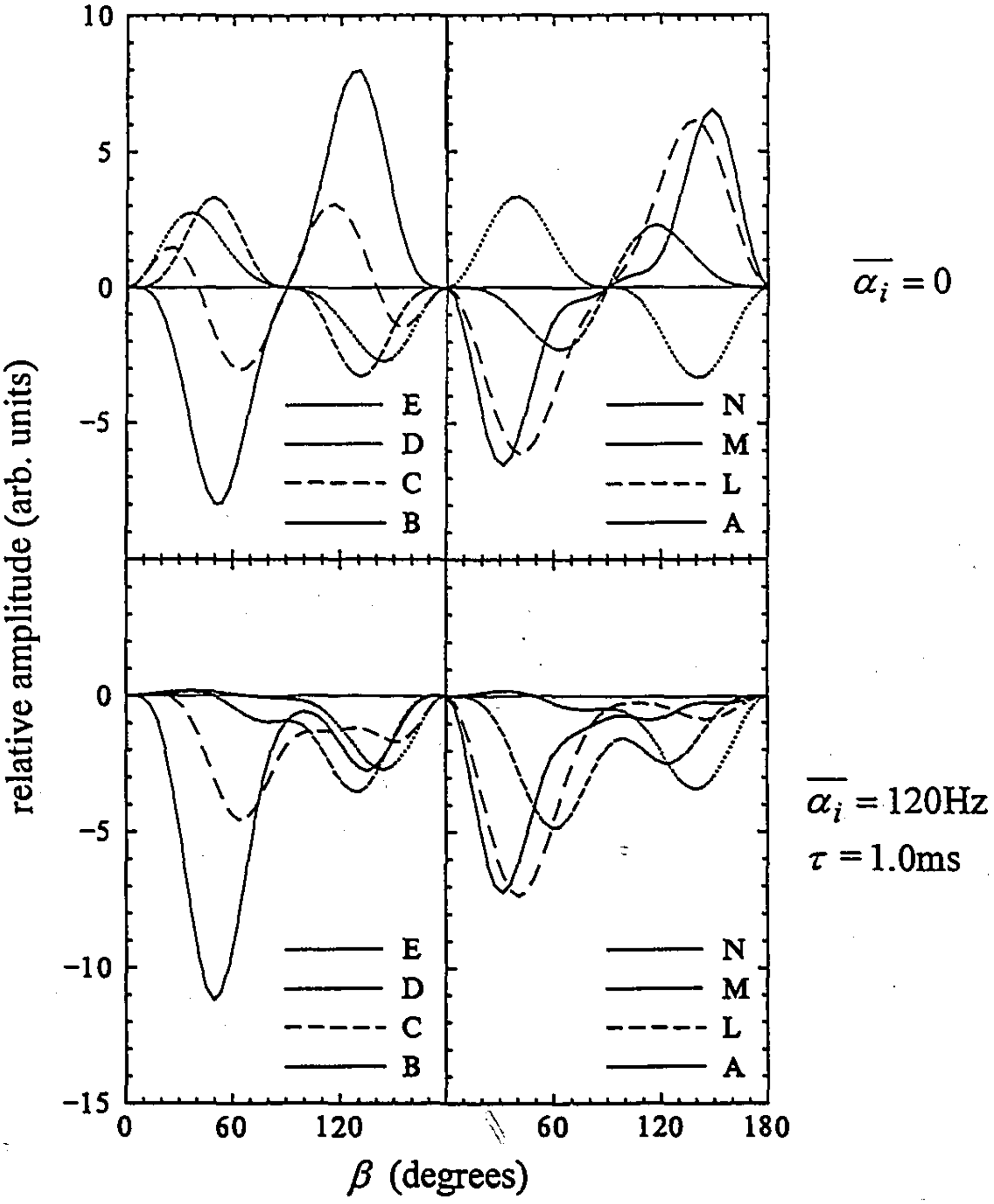

Figure 3.6. Individual amplitudes of the parameters defined in [3.2.28b] and listed in the Appendix, used for the theoretical curves in Fig. 3.5 for the $I$=2, $S_{xx}$ signal amplitudes. Top for $\overline{\alpha_j} = 0$ and bottom for $\overline{\alpha_j} = 120$Hz and $\tau$= 1.0ms.

*Positions of Principal and Satellite Echoes*

| Molecular State $\left\|M_i\right\rangle$ | Eigenvalue |
|---|---|
| $\|2\rangle = \|11\rangle$ | $-2\overline{\alpha_j} + 2a_j + b_j + 2\sum_{k \neq j} \overline{\delta_{jk}} I_{zk}$ |
| $\|1\rangle = \frac{1}{\sqrt{2}}[\|10\rangle + \|01\rangle]$ | $-\overline{\alpha_j} - a_j - b_j/2 + \sum_{k \neq j} \overline{\delta_{jk}} I_{zk}$ |
| $\|x\rangle = \frac{1}{\sqrt{2}}[\|-11\rangle + \|1-1\rangle]$ | $2a_j - b_j$ |
| $\|y\rangle = \|00\rangle$ | $-4a_j$ |
| $\|-1\rangle = \frac{1}{\sqrt{2}}[\|-10\rangle + \|0-1\rangle]$ | $\overline{\alpha_j} - a_j - b_j/2 - \sum_{k \neq j} \overline{\delta_{jk}} I_{zk}$ |
| $\|-2\rangle = \|-1-1\rangle$ | $2\overline{\alpha_j} + 2a_j + b_j - 2\sum_{k \neq j} \overline{\delta_{jk}} I_{zk}$ |

Table 3.3. Energies of the Molecular States for *o*-$D_2$

In order to account for the positions of the principal and satellite echoes for $I = 2$, the frequencies of the relevant coherences must be determined. To summarize, the eigenvalues of the molecular states of total spin $I$ are calculated by considering the intramolecular quadrupole and dipolar energies of the atomic spin states. Table 3.3 shows how these molecular states are constructed and presents the corresponding eigenvalues under the Hamiltonian of [3.2.2]. Note that the states $|x\rangle$ and $|y\rangle$ are linear combinations of the *ortho* $I = 0$ and $I = 2$, $M=0$ states which are mixed through elements in the flip-flop terms of the intramolecular dipole contribution. Assuming that the splitting $6a_j - b_j$ between the $|x\rangle$ and $|y\rangle$ states is large relative to the intermolecular nuclear dipole interaction ( recall $\overline{\delta_{jk}} \approx 100\text{Hz}$ ), the latter is treated as a non-degenerate first order perturbation as these states can be considered to be uncoupled. Table 3.4 shows the frequencies of the single quantum coherences $|M\rangle\langle M'|$ from which four transitions in the frequency domain are expected, namely,

$$\nu - \nu_0 = \pm\left(3a_j + \frac{3b_j}{2}\right) = \pm X_1$$

and [3.3.1].

$$\nu - \nu_0 = \pm\left(3a_j - \frac{b_j}{2}\right) = \pm X_2$$

During the first time interval $\tau$, the spins accumulate a phase $\pm 2\pi X_n \tau$ relative to the Larmor frequency that can be refocussed subsequent to the second pulse, which has the effect of mixing these coherences. Formation of the principal echo is due to those two components that do not change relative phase, subject to the condition $X_n t = X_n \tau$, while two satellite echoes are possible, corresponding to the two coherence changes $X_1 t = X_2 \tau$ and $X_2 t = X_1 \tau$. Using the frequencies of these $\Delta M = \pm 1$ transitions, echoes are expected to be found at $t = k\tau$ where $k = \frac{X_1}{X_2}$, 1, $\frac{X_2}{X_1}$ or

$$k = \frac{t}{\tau} = \frac{1 + {}^{3b_j}\!/_{2a_j}}{1 - {}^{b_j}\!/_{2a_j}},\ 1,\ \frac{1 - {}^{b_j}\!/_{2a_j}}{1 + {}^{3b_j}\!/_{2a_j}} \qquad [3.3.2]$$

which is equivalent to the expression obtained by Volz *et al. (90)* and Conradi *et al. (97)* for $a = 3a_j$, where a different convention for the nuclear quadrupole interaction is used. Note from [3.2.8] that while $a_j$ and $b_j$ are functions of the polarization and the relative orientation of the molecular axis and the external magnetic field, the ratios appearing in [3.3.2] are not. It would be expected, therefore, that the values of $k$ would be independent of the orientational ordering, the mole fraction of $I$=1 spins and the admixture between the $J$=0 and $J$=2 rotational states and would be given by $k$ = 0.845, 1 and 1.183. This exemplifies the fact that $I$ is not a good quantum number for $o$-$D_2$, otherwise we would expect Solomon echoes at $k = 1/3$, 1 and 3. *(98)*

| Operator<br>$\lvert M\rangle\langle M'\rvert$ | Frequency |
|---|---|
| $\lvert 2\rangle\langle 1\rvert$ | $-\overline{\alpha_j}+3a_j+{}^{3b_j}/_{2}+\sum_{k\neq j}\overline{\delta_{jk}}I_{zk}$ |
| $\lvert 1\rangle\langle x\rvert$ | $-\overline{\alpha_j}-3a_j+{}^{b_j}/_{2}+\sum_{k\neq j}\overline{\delta_{jk}}I_{zk}$ |
| $\lvert 1\rangle\langle y\rvert$ | $-\overline{\alpha_j}+3a_j-{}^{b_j}/_{2}+\sum_{k\neq j}\overline{\delta_{jk}}I_{zk}$ |
| $\lvert x\rangle\langle -1\rvert$ | $-\overline{\alpha_j}+3a_j-{}^{b_j}/_{2}+\sum_{k\neq j}\overline{\delta_{jk}}I_{zk}$ |
| $\lvert y\rangle\langle -1\rvert$ | $-\overline{\alpha_j}-3a_j+{}^{b_j}/_{2}+\sum_{k\neq j}\overline{\delta_{jk}}I_{zk}$ |
| $\lvert -1\rangle\langle -2\rvert$ | $-\overline{\alpha_j}-3a_j-{}^{3b_j}/_{2}+\sum_{k\neq j}\overline{\delta_{jk}}I_{zk}$ |

Table 3.4. Frequencies of the Single Quantum Operators for $o$-$D_2$

Whether or not the satellite echoes are observed, however, will depend upon the admixture of the rotational states for in the spherically symmetrical $J$=0 state the values of $a_j$ and $b_j$ both vanish and the frequencies of Table 3.3 collapse to a single degenerate transition. Even given finite values of these coupling terms it is necessary that the broadened NMR lines are well resolved. The *$k\neq 1$* satellite echoes described in *(90)* for HD and $o$-$D_2$ embedded in an amorphous silica substrate, a system with large crystal fields, are not observed in solid $D_2$ (see Figure 3.1). Use of the values $a_j$ = 290Hz and $b_j$ = -70 Hz ( obtained from [3.2.8] for $C_{sr}(X,T) = 0.02$ and $\left(1-3\cos^2\theta_{B,zj}\right) = 1$, corresponding to a weakly oriented system *(99)* ) in [3.3.1] shows that the frequency separation $|X_1|-|X_2|$ is only about 150Hz, which is comparable to the inhomogeneous broadening frequency $\overline{\alpha_j}$ = 130Hz. Given this situation, it is likely that the satellites are not observed because of the weak orientational ordering of the $o$-$D_2$ fraction. The weak polarization indicated by the admixture coefficient $C_{sr}(X,T)$ results in the small observed values of the intramolecular coupling constants $a_j$ and $b_j$. Consequently, the frequencies of the single quantum coherences shown in Table 3.4 become degenerate and only the $k$ = 1 echoes may form. In contrast, the crystal field must have been very large for the experiments on $D_2$ embedded in an amorphous silicon matrix. *(90)* There, the strength of the orientational ordering is already evident from the sharpness of the principal echo, indicating significant NMR line broadening. Under these conditions, $C_{sr}(X,T)$ may well be of the order of unity and therefore $|X_1|-|X_2|$ will be much larger than any small local field inhomogeneity resulting in observable satellite echoes.

# Chapter 4. CONCLUSION

A formal theory for the solid echo amplitude of both the *ortho* and *para* fractions in solid $D_2$ has been presented. The numerical results obtained for the contributions to the spin-pair dipolar field and the inhomogeneous magnetic field are consistent with those obtained from analysis of the experimental line shapes: observed signal amplitude decay is well approximated in terms of our model for dipolar spin relaxation and inhomogeneous line broadening. Similarly, the experimentally observed dependence upon the parameters of the pulse sequence is accounted for as well, in terms of the evolution of the detailed dipole-dipole coupling terms. The magnitude of these terms is consistent with expectations, however, the origin of the inhomogeneous field needs clarification.

While the satellite echoes expected for the $I$=2 fraction of solid $D_2$ have not been observed, we posit that it is a combination of weak crystal fields and the existence of inhomogeneous broadening that contribute to the lack of resolution of the NMR frequency spectrum, resulting in quenching of the satellites.

The deviations from Curie's law for the $I$=1 spins, the origins of the inhomogeneous field as well as the possible existence of unaccounted relaxation mechanisms need further discussion. The phase of the solid hydrogen is primarily determined by the dominant EQQ interactions between $I$=1 molecules. At both low temperatures and higher values of $X$, strong localized orientational ordering would tend to produce the regimes associated with a glassy phase, which would certainly produce inhomogeneities throughout the sample. A mild increase in the magnitude of the inhomogeneous field was generally observed from the theoretical simulations for experiments performed at lower temperatures, but in this case, only a tentative trend in the data can be inferred. These ordering processes would also be more effective at lower temperatures, providing an efficient form of relaxation. As the temperature increases, random motions of the $I$=1 molecules would result in a much shorter correlation time for fluctuations of the EQQ interaction. Thus, fast relaxation mechanisms that occur below the limits of resolution of the NMR experiment could account for the apparent "loss" of $I$=1 spins at low temperatures. Given this development of a more comprehensive theory for the response of the solid deuteriums to two pulse NMR experiments, it is expected that further interest in these concerns will be generated.

## APPENDIX 1.

### Explicit Formulation of the Functions Defined in [3.2.24] of the Text

Evaluation of [3.2.24] subject to the selection rules of [3.2.25-27] was performed with the help of MAPLE to derive [3.2.28]. The MAPLE code also contains a routine for the evaluation of the general form of the rotation matrices of [3.2.15]. Listed below are the terms required to reproduce the theoretical results.

*a*

$$\begin{aligned}&\left(1+2\cos^2\beta\cos^2\varphi-2\cos^2\varphi-\cos^2\beta\right)\left(\tfrac{35}{8}\cos^4\beta+\tfrac{5}{2}\cos^3\beta-\tfrac{9}{4}\cos^2\beta-\tfrac{1}{2}\cos\beta+\tfrac{7}{8}\right)\\&+\left(1-\cos^2\beta\right)\cos\left(2\overline{\alpha_j}\tau\right)\left(\tfrac{35}{8}\cos^4\beta-\tfrac{5}{2}\cos^3\beta-\tfrac{9}{4}\cos^2\beta+\tfrac{1}{2}\cos\beta+\tfrac{7}{8}\right)\end{aligned}$$

*b*

$$\begin{aligned}&\left(1+2\cos^2\beta\cos^2\varphi-2\cos^2\varphi-\cos^2\beta\right)\left(-7\cos^4\beta-2\cos^3\beta+6\cos^2\beta+2\cos\beta+1\right)\\&+\left(1-\cos^2\beta\right)\cos\left(2\overline{\alpha_j}\tau\right)\left(-7\cos^4\beta+2\cos^3\beta+6\cos^2\beta-2\cos\beta+1\right)\end{aligned}$$

*c*

$$\begin{aligned}&\left(1+2\cos^2\beta\cos^2\varphi-2\cos^2\varphi-\cos^2\beta\right)\left(\tfrac{7}{2}\cos^4\beta-2\cos^3\beta-\tfrac{9}{2}\cos^2\beta+\cos\beta+2\right)\\&+\left(1-\cos^2\beta\right)\cos\left(2\overline{\alpha_j}\tau\right)\left(\tfrac{7}{2}\cos^4\beta+2\cos^3\beta-\tfrac{9}{2}\cos^2\beta-\cos\beta+2\right)\end{aligned}$$

*d*

$$\begin{aligned}&\left(1+2\cos^2\beta\cos^2\varphi-2\cos^2\varphi-\cos^2\beta\right)\left(-\cos^4\beta+2\cos^3\beta-2\cos\beta+1\right)\\&+\left(1-\cos^2\beta\right)\cos\left(2\overline{\alpha_j}\tau\right)\left(-\cos^4\beta-2\cos^3\beta+2\cos\beta+1\right)\end{aligned}$$

*e*

$$\begin{aligned}&\left(1+2\cos^2\beta\cos^2\varphi-2\cos^2\varphi-\cos^2\beta\right)\left(\tfrac{1}{8}\cos^4\beta-\tfrac{1}{2}\cos^3\beta+\tfrac{3}{4}\cos^2\beta-\tfrac{1}{2}\cos\beta+\tfrac{1}{8}\right)\\&+\left(1-\cos^2\beta\right)\cos\left(2\overline{\alpha_j}\tau\right)\left(\tfrac{1}{8}\cos^4\beta+\tfrac{1}{2}\cos^3\beta+\tfrac{3}{4}\cos^2\beta+\tfrac{1}{2}\cos\beta+\tfrac{1}{8}\right)\end{aligned}$$

$l$

$$\left(1+2\cos^2\beta\cos^2\varphi-2\cos^2\varphi-\cos^2\beta\right)\left(\tfrac{3}{2}\cos^2\beta+\cos\beta+\tfrac{1}{2}\right)$$
$$+\left(1-\cos^2\beta\right)\cos\left(2\overline{\alpha_j}\tau\right)\left(\tfrac{3}{2}\cos^2\beta-\cos\beta+\tfrac{1}{2}\right)$$

$m$

$$\left(1+2\cos^2\beta\cos^2\varphi-2\cos^2\varphi-\cos^2\beta\right)\left(2-2\cos^2\beta\right)$$
$$+2\left(1-\cos^2\beta\right)^2\cos\left(2\overline{\alpha_j}\tau\right)$$

$n$

$$\left(1+2\cos^2\beta\cos^2\varphi-2\cos^2\varphi-\cos^2\beta\right)\left(\tfrac{1}{2}\cos^2\beta-\cos\beta+\tfrac{1}{2}\right)$$
$$+\left(1-\cos^2\beta\right)\cos\left(2\overline{\alpha_j}\tau\right)\left(\tfrac{1}{2}\cos^2\beta+\cos\beta+\tfrac{1}{2}\right)$$

$A$

$$\left(\tfrac{35}{4}\cos^4\beta+5\cos^3\beta-\tfrac{9}{2}\cos^2\beta-\cos\beta+\tfrac{7}{4}\right)\Big(\cos^2\varphi\cos^4\beta-\tfrac{1}{2}\cos^4\beta$$
$$+2\cos^2\varphi\cos^3\beta-\cos^3\beta-2\cos^2\varphi\cos\beta+\cos\beta-\cos^2\varphi+\tfrac{1}{2}$$
$$+18\cos^2\beta\left(2\cos^2\varphi\cos^2\beta-\cos^2\beta-2\cos^2\varphi+1\right)\Big)$$
$$+\cos\left(2\overline{\alpha_j}\tau\right)\left(\tfrac{35}{8}\cos^4\beta-\tfrac{5}{2}\cos^3\beta-\tfrac{9}{4}\cos^2\beta+\tfrac{1}{2}\cos\beta+\tfrac{7}{8}\right)$$
$$\times\left(1-2\cos\beta+2\cos^3\beta-\cos^4\beta-9\left(\cos^2\beta-1\right)\cos^2\beta\right)$$

$B$

$$\left(-7\cos^4\beta-2\cos^3\beta+6\cos^2\beta+2\cos\beta+1\right)\Big(\cos^2\varphi\cos^4\beta-\tfrac{1}{2}\cos^4\beta$$
$$+2\cos^2\varphi\cos^3\beta-\cos^3\beta-2\cos^2\varphi\cos\beta+\cos\beta-\cos^2\varphi+\tfrac{1}{2}$$
$$+9\cos^2\beta\left(2\cos^2\varphi\cos^2\beta-\cos^2\beta-2\cos^2\varphi+1\right)\Big)$$
$$+\cos\left(2\overline{\alpha_j}\tau\right)\left(-7\cos^4\beta+2\cos^3\beta+6\cos^2\beta-2\cos\beta+1\right)$$
$$\times\left(1-2\cos\beta+2\cos^3\beta-\cos^4\beta-9\left(\cos^2\beta-1\right)\cos^2\beta\right)$$

C

$$\begin{aligned}
&\Bigl(\tfrac{7}{2}\cos^4\beta+2\cos^3\beta-\tfrac{9}{2}\cos^2\beta-\cos\beta+2\Bigr)\Bigl(2\cos^2\varphi\cos^4\beta-\cos^4\beta\\
&+4\cos^2\varphi\cos^3\beta-2\cos^3\beta-4\cos^2\varphi\cos\beta+2\cos\beta-2\cos^2\varphi+1\\
&+9\cos^2\beta\bigl(2\cos^2\varphi\cos^2\beta-\cos^2\beta-2\cos^2\varphi+1\bigr)\Bigr)\\
&+\cos\bigl(2\overline{\alpha_j}\tau\bigr)\Bigl(\tfrac{7}{2}\cos^4\beta-2\cos^3\beta-\tfrac{9}{2}\cos^2\beta+\cos\beta+2\Bigr)\\
&\times\Bigl(1-2\cos\beta+2\cos^3\beta-\cos^4\beta-9\bigl(\cos^2\beta-1\bigr)\cos^2\beta\Bigr)
\end{aligned}$$

D

$$\begin{aligned}
&\Bigl(-\cos^4\beta+2\cos^3\beta-2\cos\beta+1\Bigr)\Bigl(2\cos^2\varphi\cos^4\beta-\cos^4\beta\\
&+4\cos^2\varphi\cos^3\beta-2\cos^3\beta-4\cos^2\varphi\cos\beta+2\cos\beta-2\cos^2\varphi+1\\
&+9\cos^2\beta\bigl(2\cos^2\varphi\cos^2\beta-\cos^2\beta-2\cos^2\varphi+1\bigr)\Bigr)\\
&+\cos\bigl(2\overline{\alpha_j}\tau\bigr)\Bigl(-\cos^4\beta-2\cos^3\beta+2\cos\beta+1\Bigr)\\
&\times\Bigl(1-2\cos\beta+2\cos^3\beta-\cos^4\beta-9\bigl(\cos^2\beta-1\bigr)\cos^2\beta\Bigr)
\end{aligned}$$

E

$$\begin{aligned}
&\Bigl(\tfrac{1}{8}\cos^4\beta-\tfrac{1}{2}\cos^3\beta+\tfrac{3}{4}\cos^2\beta-\tfrac{1}{2}\cos\beta+\tfrac{1}{8}\Bigr)\Bigl(2\cos^2\varphi\cos^4\beta-\cos^4\beta\\
&+4\cos^2\varphi\cos^3\beta-2\cos^3\beta-4\cos^2\varphi\cos\beta+2\cos\beta-2\cos^2\varphi+1\\
&+9\cos^2\beta\bigl(2\cos^2\varphi\cos^2\beta-\cos^2\beta-2\cos^2\varphi+1\bigr)\Bigr)\\
&+\cos\bigl(2\overline{\alpha_j}\tau\bigr)\Bigl(\tfrac{1}{8}\cos^4\beta+\tfrac{1}{2}\cos^3\beta+\tfrac{3}{4}\cos^2\beta+\tfrac{1}{4}\cos\beta+\tfrac{1}{8}\Bigr)\\
&\times\Bigl(1-2\cos\beta+2\cos^3\beta-\cos^4\beta-9\bigl(\cos^2\beta-1\bigr)\cos^2\beta\Bigr)
\end{aligned}$$

$L$

$$\begin{aligned}
&\big(\tfrac{3}{2}\cos^2\beta+\cos\beta+\tfrac{1}{2}\big)\big(2\cos^2\varphi\cos^4\beta-\cos^4\beta\\
&+4\cos^2\varphi\cos^3\beta-2\cos^3\beta-4\cos^2\varphi\cos\beta+2\cos\beta-2\cos^2\varphi+1\\
&+9\cos^2\beta\big(2\cos^2\varphi\cos^2\beta-\cos^2\beta-2\cos^2\varphi+1\big)\big)\\
&+\cos\big(2\overline{\alpha_j}\tau\big)\big(\tfrac{3}{2}\cos^2\beta-\cos\beta+\tfrac{1}{2}\big)\\
&\times\big(1-2\cos\beta+2\cos^3\beta-\cos^4\beta-9\big(\cos^2\beta-1\big)\cos^2\beta\big)
\end{aligned}$$

$M$

$$\begin{aligned}
&\big(2-2\cos\beta\big)\big(2\cos^2\varphi\cos^4\beta-\cos^4\beta\\
&+4\cos^2\varphi\cos^3\beta-2\cos^3\beta-4\cos^2\varphi\cos\beta+2\cos\beta-2\cos^2\varphi+1\\
&+18\cos^2\beta\big(2\cos^2\varphi\cos^2\beta-\cos^2\beta-2\cos^2\varphi+1\big)\big)\\
&+\cos\big(2\overline{\alpha_j}\tau\big)\big(1-\cos\beta\big)\\
&\times\big(2-4\cos\beta+4\cos^3\beta-2\cos^4\beta-18\big(\cos^2\beta-1\big)\cos^2\beta\big)
\end{aligned}$$

$N$

$$\begin{aligned}
&\big(\tfrac{1}{2}-\cos\beta+\tfrac{1}{2}\cos^2\beta\big)\big(2\cos^2\varphi\cos^4\beta-\cos^4\beta\\
&+4\cos^2\varphi\cos^3\beta-2\cos^3\beta-4\cos^2\varphi\cos\beta+2\cos\beta-2\cos^2\varphi+1\\
&+9\cos^2\beta\big(2\cos^2\varphi\cos^2\beta-\cos^2\beta-2\cos^2\varphi+1\big)\big)\\
&+\cos\big(2\overline{\alpha_j}\tau\big)\big(\tfrac{1}{2}+\cos\beta+\tfrac{1}{2}\cos^2\beta\big)\\
&\times\big(1-2\cos\beta+2\cos^3\beta-\cos^4\beta-9\big(\cos^2\beta-1\big)\cos^2\beta\big)
\end{aligned}$$

## APPENDIX 2. MAPLE routine for the evaluation of the Redfield matrix [1.5.20]

```
#       Evaluation of the Redfiled superoperator for general spin mag. si
#       The j symbol as defined in Edmond's Eq. 3.6.10 for the Clebsh-Gordan
#       co-eff and 3.7.3 for the j sumbol defined in terms of the latter
#
#       DINESEN     Nov/93.
#

fac:=proc(n) GAMMA(n+1) end;

j:=proc(m1,m2,m3)
        local s, ss, f;
        if m1+m2+m3 <> o then RETURN (0) fi;
        ss:=0;
        for s from 0 to si+m3 do
                if si-m1-s < 0 or si+m3-s < 0 or 2-si+m1+s <0 then
                        f:=0
                else
        f:=fac(si+m1+s)*fac(2+si-m1-s)/(fac(s)*fac(si-m1-s)*fac(2-si+m1+s)*fac(si+m3-
s)):
                fi;
                        ss:=ss+(-1)**s*f;
                od;
                f:=fac(2)*fac(si-m1)*fac(2-m2)*fac(si-m3)*fac(si+m3)/
        (fac(6)*fac(1)*fac(2)*fac(si+m1)*fac(2+m2)):
        edmonds:=(-1)**(-2*si-m1-m3)*ss*sqrt(f);
end;
#
#       build the redfield matrix element R(alpha,alphap,beta,betap) of Jn's
#
red:=proc(alpha,alphap,beta,betap)
                local i, m, gamm;
                R:=array(1..3,[0,0,0]);
                m:=alphap-betap;
                if abs(m)<=2 then R[abs(m)+1]:=R[abs(m)+1-70*(-1)^(2*si-alpha-betap)
```

```
                *j(-alpha,m,beta)*j(-betap,-m,alphap) fi;
        m:=alpha-beta;
        if abs(m)<=2 then R[abs(m)+1]:=R[abs(m)+1-70*(-1)^(2*si-alpha-betap)
                *j(-alpha,m,beta)*j(-betap,-m,alphap) fi;
        if alphap=betap then
                for i from 0 to 2*si do
                        gamm:=si-i;
                        m:=gamm-beta;
        if abs(m)<=2 then R[abs(m)+1]:=R[abs(m)+1+70*(-1)^(2*si-alpha-betap)
                *j(-gamm,m,beta)*j(-beta,-m,alphap) fi;
                od;
        fi;
        if alpha=beta then
                for i from 0 to 2*si do
                        gamm:=si-i;
                        m:=gamm-betap;
                if abs(m)<=2 then R[abs(m)+1]:=R[abs(m)+1+70*(-1)^(2*si-alpha-
betap)
                *j(-gamm,m,alphap)*j(-betap,-m,gamm)        fi;
                od;
        fi;
end;
```

## REFERENCES

1. H.C. Ohanian, Principles of Quantum Mechanics, New Jersey, Printice Hall (1990).

2. D.A. McQuarrie, Quantum Chemistry, Mill Valley, University Science Books (1983).

3. P.A.M. Dirac, The Principles of Quantum Mechanics 4th ed., Oxford, Claredndon Press (1958).

4. E.U. Condon and G.H. Shortley, The Theory of Atomic Spectra, Cambridge, Cambridge University Press (1951).

5. K. Gottfried, Quantum Mechanics vol. 1, Reading, Addison-Wesley (1966).

6. A.R. Edmonds, Angular Momentum in Quantum Mechanics, Princeton, Princeton University Press (1958).

7. B.G. Wybourne, Classical Groups for Physicists, New York, John Wiley and Sons (1974).

8. B.C. Sanctuary, J. Chem. Phys. 64 4352 (1976).

9. B.L. Silver, Irreducible Tensor Methods, New York, Academic Press (1976).

10. M.D. Rose, Elementary Theory of Angular Momentum, New York, John Wiley (1957).

11. H. Messiah, Quantum Mechanics vol. 2, New York, North Holland Publishing (1962).

12. E.P. Wigner, Group Theory, New York, Academic Press (1959).

13. J. Schwinger in Quantum Theory of Angular Momentum L.C. Biedenharn and H. van Dam eds., New York, Academic Press (1965).

14. L.C. Biedenharn and J.C. Louck, Angular Momentum in Quantum Physics: Theory and Applications, Reading, Addison-Wesley (1981).

15. J.A.R. Coope, R.F. Snider and F.R. McCourt, J. Chem. Phys. 45 2264 (1965).

16. J.A.R. Coope and R.F. Snider, J. Math. Phys. 11 1103 (1970).

17. F.M. Chen, H. Morcal and R.F. Snider, J. Chem. Phys. 57 542 (1972).

18. E.P. Wigner, Z. Physik 43 624 (1927).

19. B.C. Sanctuary, Mol. Phys. 48 1155 (1983).

20. B.C. Sanctuary, J. Chem. Phys. 64 4352 (1976).

21. R.R. Ernst, G. Bodenhausen and A. Wokaun, Principles of Nuclear Magnetic Resonance in One and Two Dimensions, Oxford, Clarendon Press (1987).

22. K. Blum, Density Matrix Theory and Applications, New York, Clarendon Press (1981).

23. R.C. Tolman, The Principles of Statistical Mechanics, Oxford, Clarendon Press (1986).

24. J. von Neumann, Mathematical Foundations of Quantum Mechanics, Princeton, Princeton University Press (1955).

25. B.C. Sanctuary and T.K. Halstead, Bull. Magn. Reson. 11 31 (1984).

26. F.P. Feynman, Quantum Electrodynamics, New York, Benjamin Press (1961).
F.J. Dyson, Phys. Rev. 75 486 (1949).

27. N. Magnus, Commun. Pure Appl. Math. 7 649 (1954).

28. R.M. Wilcox, J. Math. Phys. 8 962 (1967).

29. U. Fano, Rev. Mod. Phys. 29 74 (1957).

30. A. Abragam, Principles of Nuclear Magnetism, Oxford, Clarendon Press (1961).

31. C.P. Slichter, Principles of Magnetic Resonance 3rd ed., Heidelberg, Springer-Verlag (1992).

32. O.W. Sørensen *et al.*, Prog. in NMR Specroscopy 16 163 (1983).

33. G. Campolieti and B.C. Sanctuary, J. Chem. Phys. 91 2108 (1989).

34. B.C. Sanctuary and H.B.R. Cole, J. Magn. Reson. 71 106 (1987).

35. J.H. van Vleck, Phys. Rev. 74 1168 (1948).

36. M. Mehring, Principles of High Resolution NMR in Solids 2nd ed., Berlin, Springer-Verlag (1983).

37. B.C. Sanctuary, T.K. Halstead and P.A. Osment, Mol. Phys. 49 753 (1983).

38. B.C. Sanctuary and G. Campolieti, Can. J. Chem. 65 1746 (1987).

39. W.H. Loisell, Quantum Statistical Properties of Radiation, New York, Wiley (1973).

40. A.G. Redfield, Adv. Magn. Reson. 1 1 (1965).

41. F. Bloch, Phys. Rev. 70 460 (1946).

42. R.C. Lyon, J. Pekar, C.T.W. Moonen and A.C. McLaughlin, Mgn. Reson. in Medicine 18 80 (1991).

43. H.J.C. Berendsen and H.T. Edzes, Annals N.Y. Academy Sci. 204 459 (1973).

44. M. Shporer and M.M. Civan, Biochem. Biophys. Acta 354 291 (1974).

45. M.M. Civan and M. Shporer, Biol. Magn. Reson. 1 1 (1978).

46. G. Jaccard, S. Wimperis and G. Bodenhausen, J. Chem. Phys. 85 6282 (1986).

47. U. Eliav and G. Navon, J. Chem. Phys. 95 7114 (1991).

48. I. Furó, B. Halle, P. Quist and T.C. Wong, J. Phys. Chem. 94 2600 (1990).

49. U. Eliav, H. Shinar and G. Navon, J. Magn. Reson. 98 223 (1992).

50. H. Shinar, T. Knubovets, U. Eliav and G. Navon, Biophys. J. 64 1273 (1993).

51. U. Eliav and G. Navon, J. Magn. Reson. B 103 19 (1994).

52. W.D. Rooney and C. Springer Jr., NMR Biomed. 4 209 (1991).

53. W.D. Rooney and C. Springer Jr., NMR Biomed. 4 227 (1991).

54. W.D. Rooney, T. Barbara and C. Springer Jr., J. Am. Chem. Soc. 110 674 (1988).

55. P.O. Westlund and H. Wennerström, J. Magn. Reson. 50 451 (1982).

56. P.O. Westlund and H. Wennerström, J. Magn. Reson. 81 68 (1989).

57. E. Berggren and P.O Westlund, Biophys. J. 58 167 (1990).

58. U. Eliav, A. Baram and G. Navon, J. Chem. Phys. 89 5584 (1988).

59. A.D. McLaughlin, Proc. R. Soc. London Ser. A 280 271 (1964).

60. P.S. Hubbard, J. Chem. Phys. 53 985 (1970).

61. L.G. Werbelow and A.G. Marshall, J. Magn. Reson. 43 443 (1981).

62. N. Müller, G. Bodenhausen, K. Wüthrich and R.R. Ernst, J. Magn. Reson. 65 531 (1985).

63. J. Pekar and J.S. Leigh Jr., J. Magn. Reson. 69 582 (1986).

64. U. Eliav and G. Navon, J. Magn. Reson. 88 223 (1990).

65. B.C. Sanctuary and T.K. Halstead, Adv. Magn. Optical Reson. 15 79 (1990).

66. B.C. Sanctuary and L. Selwyn, J. Chem. Phys. 74 906 (1981).

67. I. Furó, B. Halle and T.C. Wong, J. Chem. Phys. 89 5382 (1988).

68. I. Furó and B. Halle, J. Chem. Phys. 91 42 (1989).

69. B.C. Sanctuary, J. Chem. Phys. 73 1048 (1980).

70. C. Chung and S. Wimperis, J. Magn. Reson. 88 440 (1990).

71. M.D. Schnall, K. Yoishizaki, B. Chance and L.S. Leigh, Magn. Reson. in Medicine 6 15 (1988).

72. J.S. Tauskela, T.R.J. Dinesen and E.A. Shoubridge, unpublished results.

73. W.S. Price, N.H. Ge and L.P Hwang, J. Magn. Reson. 98 134 (1992).

74. N.H. Ge, W.S. Price, L.Z. Hong and L.P Hwang, J. Magn. Reson. 97 656 (1992).

75. I. Furó and B. Halle, Mol. Phys. 76 1169 (1992).

76. L. Brunschweiler, G. Bodenhausen and R.R. Ernst, Mol. Phys. 48 535 (1983).

77. G. Bodenhausen, H. Kogler, and R.R. Ernst, J. Magn. Reson. 58 370 (1984).

78. A. Ben-Reuven, Physical Rev. 145 7 (1966). *ibid* 141 34 (1966).

79. I.F. Silvera, Rev. Mod. Phys. 52 393 (1980).

80. A.B. Harris and H. Meyer, Can. J. Phys. 63 3 (1985).

81. N.S. Sullivan, C.M. Edwards, Y. Lin and D. Zhou, Can. J. Phys. 65 1463 (1987).

82. J. Van Kranendonk, *Solid Hydrogen* (Plenum Press, New York, 1983).

83. A.B. Harris, S. Washburn and H. Meyer, J. Low Temp. Phys. 50 152 (1983).

S. Washburn and H. Meyer, J. Low Temp. Phys. 57 31 (1984) on $H_2$ and references therein.

84. M. Calkins, R. Banke, X. Li and H. Meyer, J. Low Temp. Phys. 65 47 (1986) and *ibid.* 65 90 (1986) on $D_2$ and references therein.

85. A.B. Harris, Phys. Rev. B 2 3495 (1970).

86. I. Yu, S. Washburn and H. Meyer, J. Low. Temp. Phys. 51 369 (1983).

87. I. Yu, S. Washburn, M. Calkins and H. Meyer, J. Low Temp. Phys. 51 401 (1983).

88. D. Clarkson, X. Qin and H. Meyer, J. Low Temp. Phys. 91 119 (1993).

89. X. Qin, D. Clarkson and H. Meyer, J. Low Temp. Phys. 91 153 (1993).

90. M.P. Volz, P. Santos-Filho, M.S. Conradi, P.A. Fedders and R.E. Norberg, Phys. Rev. Lett. 63 2582 (1989).

91. N.F. Ramsey, *Molecular Beams*, (Oxford, London, 1956).

92. A.B. Harris, private communication.

93. N.S. Sullivan, M. Devoret, B.P. Cowan and C. Urbina, Phys. Rev. 17 5016 (1978).

94. S. Lacelle and L. Tremblay, J. Chem. Phys. 102 947 (1995).

D.A. Drabold and P.A. Fedders, Phys. Rev. A 135 715 (1988).

95. A.B. Harris, H. Meyer and X.Qin, Phys. Rev. B 49 3844 (1994).

96. X. Qin and H. Meyer, Phys. Rev. B 49 3857 (1994).

97. M.S. Conradi, P.A. Fedders and R.E. Norberg in *Pulsed Magnetic Resonance, A Recognition of E.L. Hahn*, D.M.S. Bagguley Ed. (Clarendon Press, Oxford, 1992) p. 238.

98. I. Solomon, Phys. Rev. 110 61 (1958).

99. R. Banke, X. Li, D. Clarkson and H. Meyer, J. Low Temp. Phys. 72 99 (1988).

# CONTRIBUTIONS TO ORIGINAL KNOWLEDGE

PART 2. The analytical evolution matrices for the single and double quantum manifolds for $I = 3/2$ subject to a residual quadrupole splitting and relaxation modeled by Redfield theory, are new. These can be used to simulate the response to an arbitrary pulse sequence applied to systems for which the Redfield theory may be applied. Specific solutions for the DQF experiment, derived from the new theory, are discussed in terms of the residual quadrupole coupling and compared to experimental results obtained from Na in human red blood cells. As an appendix, a MAPLE routine is supplied that evaluates the Redfield matrices for general $I$.

PART 3. The theoretical formulation for the NMR of $D_2$ has not been assembled before. This treatment accounts for both the $I$=1 and $I$=2 contributions, where previously, the dynamics of the latter were assumed to match the theory available for $H_2$. A model for the spin pair dipolar field and inhomogeneous field is developed to account for the solid echo decay. To this end, formal solutions to the two pulse solid echo experiment were produced, showing that the intermolecular interactions can be accounted for by the spin pair dipolar model. Dependence of the signal amplitude to all relevant experimental and theoretical parameters is dicussed in detail and comparison with the experiment is good. A discussion of the absence of the expected satellite echoes is also given.

## SUGGESTIONS FOR FUTURE WORK

PART 2. Recently, investigators have begun examining the dynamics of $I$=5/2 nuclei in similar biological conditions. While the individual components of the resonant line of these nuclei is generally not as well resolved as the $I$=3/2 case, it would be worthwhile to evaluate the Redfield matrix for such a system and examine the effect of a residual quadrupole splitting on the results of relevant experiments. It is unlikely that analytical solutions for such a treatment would be readily obtained, given the higher dimensionality of the spin space and the resulting higher order differential equations requiring solution. However, numerical solutions could be found.

PART 3. Given the future production of more NMR experiments on solid $D_2$, the general theory provided here can be further applied to account for behaviour unobserved in the simple two pulse experiment. There does exist some data for the stimulated echo resulting from a three pulse sequence as well as a number of off-resonance experiments, which should be amenable to such a treatment. Perhaps the most intriguing quality of the solid hydrogens is the source of the inhomogeneous field and the observed deviations from Curie's law. While it is not likely that either of these issues will be satisfactorily addressed by NMR methods alone, given the poor resolution of the signal, a more detailed statistical description of this EQQ ordered glass phase would certainly provide much needed insight.